ATMOSPHERIC GRAVITY WAVES, AN OBSERVATIONAL AND NUMERICAL STUDY

by

GEORGE J. BOER

B.Sc., University of British Columbia
(1963)

M.A., University of Toronto
(1965)

SUBMITTED IN PARTIAL FULFILLMENT OF THE

REQUIREMENTS FOR THE DEGREE OF

DOCTOR OF PHILOSOPHY

at the

MASSACHUSETTS INSTITUTE OF TECHNOLOGY

June 22, 1970

Signature of Author .....
Department of Meteorology, 22 June 1970

Certified by .....
Thesis Supervisor

Accepted by .....
Chairman, Departmental Committee on Graduate Students

ATMOSPHERIC GRAVITY WAVES, AN OBSERVATIONAL AND NUMERICAL STUDY

by

GEORGE J. BOER

Submitted to the Department of Meteorology on June 22, 1970 in partial fulfillment of the requirements for the degree of Doctor of Philosophy.

ABSTRACT

Two topics concerning gravity wave motions in the atmosphere are discussed. The first topic concerns the propagation of the waves through regions of varying wind shear and the second topic concerns the detection and measurement of gravity wave motions in the upper atmosphere.

The linear theory of gravity wave motions for a two dimensional, non-rotating, inviscid, adiabatically moving hydrostatic atmosphere is reviewed. A numerical model for the equations is obtained and integrated as an initial and boundary value problem for wave motions with a fixed horizontal wavelength. The behavior of the wave motions for different distributions of the mean wind for which a critical level exists is obtained.

The non-linear approach to the equations of motion in terms of the perturbation equations is discussed and it is shown that no resonant interactions between simple waves is possible in the atmosphere unlike the case for internal waves in the ocean.

The numerical model is extended to include directly the interaction of the wave motions and the mean flow. It is found that the region of accelerated mean flow depends on the initial profile of the mean flow and that a shearing region is produced in the mean flow which descends with time and for which the magnitude of the shear increases until the Richardson stability condition is violated. The behavior of the wave motions at a critical level becomes quite different from that deduced from linear theory as time goes on.

The observational aspect of the study involves the detection and measurement of gravity wave motions in the atmosphere in the 30-60km region. Data obtained by the ROBIN falling sphere method and the smoke trail method are analysed. The ROBIN experiment permitted the evaluation of the errors involved in the measurements as each falling sphere was tracked separately by two radars. The data is reduced by a method which gives a uniform response with height unlike the usual reduction procedure. The spectrum of the velocity profile in the vertical is obtained and found to be similar to that obtained for motions at lower levels. The experiment also permits an estimate of the horizontal and time scales to be made so that the motions may be compared with simple gravity wave theory.

The smoke trail experiment has not been previously used in the 30-60 km region. Despite difficulties in the data reduction it is possible to obtain velocity profiles and to estimate the error involved. The method offers promise if the observational conditions can be optimized. The spectra of the velocity profiles in the vertical are obtained and are found to differ from those obtained in the ROBIN experiment. The horizontal scale of the motions is also estimated.

Thesis Supervisor: Reginald E. Newell

Title: Professor of Meteorology

Table of Contents

List of Figures

List of Tables

Acknowledgements

The author is grateful to his advisor, Professor Reginald E. Newell, and to Professor Norman A. Phillips for their advice on this thesis.

The research was supported, in part, by the Air Force Cambridge Research Laboratories under contract AF19628-69-C-0039. The manuscript was efficiently typed by Mrs. Marie L. Gabbe and Miss Isabelle Kole drafted some of the figures.

The author would also like to thank his wife for her fiscal and emotional aid during this time.

1.0 Introduction

In recent years, a great deal of interest has been shown in those modes of atmospheric motion known as internal gravity waves. This interest is the result of the realization that the smaller scales of motion, which have been observed with increasing accuracy and frequency, can be more meaningfully explained as gravity waves than simply as "turbulence".

These wave motions arise in stratified fluids as a consequence of the buoyancy forces which come into play if a fluid parcel is displaced. They are observed to exist throughout the oceans and atmosphere and are characterized by frequencies, in the atmosphere, of from about five minutes to several hours. For periods of more than about three hours the effect of the earth's rotation becomes of increasing importance and the waves are termed inertial-gravity waves. If the effect of the compressibility of the atmosphere is considered the waves are termed acoustic-gravity waves.

These motions are generated by a great many processes and can transmit energy from one region of the atmosphere to another and from one scale of motion to another. They are important in the understanding of a large number of atmospheric processes particularly in the upper regions of the atmosphere.

Complete understanding of the role of gravity waves in atmospheric processes would require a quantitative knowledge of gravity-wave sources, of the propagation characteristics of the waves, of

the interaction of the waves with themselves and with larger scale flows, and of the dissipation processes which dispose of the waves. With this knowledge, the importance of energy transmission due to the waves could be evaluated and subsidiary effects such as trace substance transport could be investigated. Observational data of sufficient accuracy and resolution would be required to determine the parameters involved and to verify the predicitons of theory.

The sources of gravity wave motions in the atmosphere have been given relatively little study. Possible sources include the flow of an air stream across rough terrain, areas of instability in the atmosphere, fronts, squall lines, pressure jumps, jet streams in the troposphere and stratosphere, weather systems, nuclear explosions, earthquakes, volcanic ruptures, large amplitude oceanic tides and, in the upper atmosphere, auroral-zone currents and the differential heating due to the shadow of the moon during a solar eclipse. The work on natural sources of gravity waves includes the effect of auroral-zone currents (e.g. Chimonais, 1968, Flock and Humsucker, 1968), observational results of pressure fluctuations at the ground inferred to be related to waves generated by the jet stream (Madden and Claerbout, 1968), an attempt by Hines (1968) to relate observed waves in noctilucent clouds to fronts and jet streams in the troposphere, and an older paper by Gossard (1962) presenting the computation of gravity wave energy flux out of the troposphere inferred from observations of surface pressure spectra.

The natural source which appears to offer a reasonable possib-

ility of quantitative treatment is that of flow over surface features. The general topic of mountain waves is reviewed by Krishnamurti(1964) and Queney et al (1960) and recent results include those of Foldvik and Wurtele (1967) and Bretherton (1969). Standing waves extending to conciderable heights may be induced by steady flow over surface features while propagating waves will result from changes in the flow with time.

The propagation characteristics of the waves have been given considerable and fruitful study. Some of the first studies were instigated by observations of travelling ionospheric disturbances (TID'S) observed in the ionospheric F region. The observed properties of the TID'S, notably their propagation over large horizontal distances without appreciable attenuation, led Martyn (1950) to suggest that the disturbances were gravity waves ducted between the ground and some reflecting layer above the ionospheric region of observation. The existence of such a reflection layer did not appear plausible to Hines (1960) who re-awakened interest in the problem by reconsidering the conditions for reflection and ducting of the waves. Subsequently, the propagation and reflection of gravity wave motions, generally in terms of linearized normal mode theory, was investigated by a number of authors including Hines (1963), Hines and Reddy (1967), Pitteway and Hines (1963,1965), Friedman (1966), Pierce (1963,1965), Press and Harkrider (1962), and others. A good collection of recent results in gravity wave theory and observation is given by Georges (1968), and the NCAR Technical Note, Internal Gravity and Acoustic

Waves - A Colloquium (1969). These collections of papers give a very good cross-section of the recent work as well as referencing the past work of importance.

Important results of a theoretical and practical nature grew out of the investigation of the propagation of waves through regions of changing background velocity. It was shown that in a region of wind shear the energy of the wave motions would be absorbed by the mean flow for waves whose phase velocity matched that of the mean flow. This phenomenon has been investigated by Bretherton (1966), Booker and Bretherton (1967), Bretherton and Garrett (1968), Bretherton (1969) and Breeding (1970). These investigations showed that, among other things, the momentum flux associated with the waves would be antennuated by a factor of $\exp\{-2\pi(Ri-\frac{1}{4})^{1/2}\}$ for $Ri > \frac{1}{4}$, where Ri is the Richardson number across the critical level in an inviscid, adiabatically moving atmosphere. For $Ri < \frac{1}{4}$ Jones (1969) found that partial reflection of an incident wave occurred at a critical level and that reducing Ri further led to total reflection and then over-reflection where the energy reflected exceeded that of the energy incident on the critical level. Jones (1969) also investigated the stability of the flow numerically for several cases for $Ri < \frac{1}{4}$.

Houghton and Jones (1968) integrated the linearized equations of motion for acoustic-gravity waves numerically to obtain the time dependent behavior of the waves at a critical level. Breeding (1970) investigated the time dependent non-linear behavior at the critical

level for short periods of time for a numerical model with rather crude horizontal resolution. Breeding's results agreed with those of Hazel (1967) in his conclusion that the effect of viscosity and conduction is unimportant for the critical level phenomena.

Interactions between waves may be studied analytically in simple cases. Such interactions have been studied mainly in terms of incompressible Boussinesq fluids with attention devoted to the implications for internal ocean waves. Phillips (1966) reviews this topic in his book and other papers of note are those of Thorpe (1966) and Craik (1968) among others. It does not seem that the results can be carried over directly to the case of flow that admits compressibility.

The dissipation of the wave motions can be accomplished by viscous and thermal effects which will have their greatest importance in regions above 80 km. This problem has been discussed by Hines (1960), Pitteway and Hines (1963), and by Midgley and Lemohn (1966), Wickersham (1968) and others and permits calculation of the height of maximum amplitude of the waves before dissipation becomes important and the heights at which waves of a given wavelength are removed from the spectrum of upward propagating waves. Bretherton (1969) has discussed the implications of the dissipation of the waves due to an encounter with strong turbulent motions.

Considerable effort has also gone into the theory and observation of the effects of gravity waves in the ionosphere and the upper

atmosphere. These studies have been facilitated and encouraged by methods of remote sensing of the ionospheric motions together with the restricted spectrum of waves which are capable of propagating to high altitudes. Georges (1967) reviews this area and Georges (1968) includes a collection of recent papers on the subject.

The theoretical treatment of the characteristics of gravity wave motions has been given a great deal of attention since Hines began his investigations. Certain areas of the problem are in reasonably satisfactory condition at present, namely those concerning the propagation of the waves through regions of varying background temperature. The identification of the sources of the wave motions is in its infancy however and the propagation of the waves through regions of wind shear has many unexplored implications as does the general problem of nonlinear interaction of waves and of waves with the mean flow. The consequences of energy transport due to gravity waves, (Hines, 1965), is also in unsatisfactory condition from lack of observations of sufficient length and density to permit any but crude estimates.

The observational aspect of the gravity wave problem remains one of considerable complexity. There exist a number of methods of measuring motions in the upper atmosphere each with its characteristic region of applicability and each with its strengths and weaknesses. Craig (1965) discusses many of them. The measurement of gravity wave parameters requires close attention to the time and

space resolution of the measurement techniques – something that has been lacking in most experiments. In fact the nature of gravity waves – a large possible range of frequencies and wavelengths existing simultaneously – makes even the detection of gravity wave motions extremely difficult. The only reasonably good identification of such waves has been in conjunction with nuclear explosions, e.g. Hines (1967), Harkrider (1964). The other main comparison of observation and theory is in the comparison of the minimum theoretical values for vertical wavelength of waves capable of propagating to high altitudes (Hines, 1964). These regions are investigated by rocket-released vapor trails which are observed photographically, as by Zimmerman (1964), Kochanski (1964), Rosenberg and Edwards (1964). Other techniques for measuring small scale motions in the atmosphere include noctilucent cloud measurements, (Witt 1962), which are particularly indicative, meteor trail measurements, e.g. Liller and Whipple (1964), Greenhow and Neufield (1959), Revah (1969), and a complicated array of methods dependent on the sensing of the ionization of the upper atmosphere. One of the impetuses for the study of gravity waves has been the explanation of TID's observed by Munro (1950) and subsequently by many others as was mentioned above.

At lower levels in the atmosphere, below 80 km, data has been obtained from the rocket-balloon sounding system (e.g. Engler (1965), Mahoney and Boer (1967), Boer and Mahoney (1968)) and from a variety of rocket launched sensors which are tracked by high precision radar such as radar chaff, parachute sondes and balloon-parachute sondes.

Despite the large number of methods which are available to measure atmospheric motions, the nature of gravity waves make measurement extremely difficult. The short period of the waves and the large horizontal space scale demands that measurements of the motions be made frequently in time and over a considerable horizontal area. Many of the measurement techniques give good resolution in time and in the vertical but lack a measurement of horizontal scale (these are usually the remote sensing techniques) while other techniques which permit the direct measurement of the motions become complicated and expensive to perform with sufficient time and horizontal resolution.

The purpose of this thesis is to investigate two different aspects of the gravity wave problem. The theoretical aspect of the study will deal with the propagation of gravity waves through regions of wind shear and with the meteorological consequences of non-linear interactions, especially of the waves and the mean flow at a critical level. The second aspect of the problem will deal with the detection and measurement of gravity wave motions in the 30-60 km region. Two measurement techniques, one of which has not been used in this region before, will be investigated and the resulting observations interpreted in terms of gravity wave motions.

The two aspects of the gravity wave problem are not directly connected in the sense that the observations verify the theory for, indeed, such observational results are impossible at present. It is hoped, however, that by discussing these two topics the goal of designing an experiment to identify results predicted by theory will become a little more possible.

2.0 Theoretical and numerical results for the hydrostatic gravity wave

In the previous section, a review of the work done in the field of gravity wave motions has been given together with some indication of the situations in which gravity wave motions may be important in understanding the behavior of the atmosphere. In this section the simple theory of gravity wave motion will be given and new results will be presented concerning the behavior of these waves.

2.1 The equations of motion and results for linear theory

The equations of motion for a fluid in a rotating coordinate system are

$$\begin{aligned}
&\frac{d\vec{u}}{dt} + 2\vec{\Omega}\times\vec{u} + \frac{1}{\rho}\nabla p + \nabla\phi = \vec{F} \\
&\frac{d\rho}{dt} + \rho\nabla\cdot\vec{u} = 0 \\
&\rho\frac{de}{dt} + p\nabla\cdot\vec{u} = \rho\dot{Q} \\
&p = \rho RT \\
&e = C_v T \\
&\frac{d}{dt} = \frac{\partial}{\partial t} + \vec{u}\cdot\nabla
\end{aligned} \qquad (1)$$

where $\vec{u}$ is the velocity vector (u, v, w)

$\vec{\Omega}$ the angular velocity of the earth

p the pressure

ρ the density

e the internal energy/unit mass

$\dot{Q}$ the heating/unit mass/unit time

R the gas constant

C_v the specific heat at constant volume

$\vec{F}$ the resultant of all other forces

$\phi = gz$ the geopotential, g the local value of the acceleration of gravity

T the Kelvin temperature

2.1.0 Approximations to the equations

There exist many approximate formulations of the equations which may be used to simplify the form of the equations while retaining the motions of interest in a particular case. A common approximation is the hydrostatic assumption $\frac{\partial p}{\partial z} = -g\rho$. The assumption is valid when the horizontal space scale of the motions is much greater than the vertical space scale, Lamb (1932).

A second approximation in common use is the tangent plane approximation which treats the equations of motion in a rectilinear coordinate system where the x-axis is taken toward the east, the y-axis toward the north and the z-axis in the direction of the local vertical. The x-y plane is then tangent to the geopotential surface. This eliminates the use of spherical coordinates in the equations of motion and results in considerable simplification. The approximation is valid when the horizontal extent of the motions is much smaller than the radius of the earth.

A third approximation involves the ratio of the frequency of the motions to the coriolis frequency. If the ratio is sufficiently small, the rotation of the earth may be ignored to good accuracy.

The assumption of an inviscid adiabatically moving atmosphere is often invoked, especially in theoretical studies, at which time it becomes an idealization of the atmosphere. The effect of internal friction on the motions is, in general, poorly known. Various approximate methods may be used to simulate this effect including a simple linear viscosity $-\alpha \vec{u}$ in place of $\vec{F}$ or $\vec{F} = K \frac{\partial^2 \vec{u}}{\partial z^2}$ where K is an eddy viscosity coefficient. The adiabatic assumption ignores such effects as heat conduction, latent heat release, surface heating, and radiation effects in the atmosphere. The importance of these effects depends on the time and space scales of the motions involved and differs in different regions of the atmosphere. This effect may also be approximated by a linear or other conduction term.

In this work all the approximations mentioned above will be made with a linear friction and conduction term being used for some purposes.

2.1.1 The energy equations

The kinetic, potential and internal energies per unit mass for a perfect gas are defined respectively as $k = 1/2\ \vec{u} \cdot \vec{u}$, $\phi = gz$, $e = C_v T$. The energy equations are obtained from the equations of motion (1) as

$$\frac{dk}{dt} + \frac{1}{\rho}\vec{u}\cdot\nabla p + g w = \vec{u}\cdot\vec{F}$$

$$\frac{d\phi}{dt} = g w$$

$$\rho\frac{de}{dt} + p\nabla\cdot\vec{u} = \rho\dot{\phi}$$

which are combined to give

$$\rho\frac{d}{dt}(k+\phi+e) = -\nabla\cdot p\vec{u} + \rho\vec{u}\cdot\vec{F} + \rho\dot{\phi}$$

or

$$\frac{\partial}{\partial t}\rho(k+\phi+e) + \nabla\cdot(\rho(k+\phi+e)+p)\vec{u} = \rho\vec{u}\cdot\vec{F} + \rho\dot{\phi}$$

where $E = k+\phi+e$ is called the energy density and

$\vec{J} = (\rho E + p)\vec{u}$ the energy flux vector. For hydrostatic motion the energy equation has the same form if the kinetic energy is redefined to exclude the vertical velocity.

2.1.2 The equations in z coordinates

The assumption of hydrostatic balance allows a reformulation of the equations of motion in terms of the new variable

$z = -\ln(p/p_o)$ where p_o is the standard sea level pressure and z is a scaled vertical coordinate. The equations become, using the traditional approximation for the coriolis term;

$$\frac{d\vec{u}}{dt} + f\,\vec{k}\times\vec{u} + \nabla\phi = \vec{F}$$

$$\omega_z - \omega + \nabla\cdot\vec{u} = 0$$

$$\frac{d\phi_z}{dt} + \kappa\omega\phi_z = \kappa\dot{Q}$$

$$\phi_z = RT$$

where now

$\vec{u} = (u, v)$ is the horizontal velocity vector

ϕ the geopotential

$\omega = \frac{dz}{dt}$ the 'vertical velocity' in this coordinate system

$\frac{d}{dt} = \frac{\partial}{\partial t} + \vec{u}\cdot\nabla + \omega\frac{\partial}{\partial z}$ (where $\frac{\partial}{\partial t}, \frac{\partial}{\partial x}, \frac{\partial}{\partial y}$ are evaluated at constant Z)

$\nabla = \hat{i}\frac{\partial}{\partial x} + \hat{j}\frac{\partial}{\partial y}$ the horizontal ∇ operator

f the coriolis parameter

$\vec{F}$ the resultant of all other forces

$\kappa\dot{Q}$ the heating term

$\kappa = R/C_p$

The relation between the geopotential and the geometrical vertical velocity w is given as $\frac{d\phi}{dt} = gw$.

The kinetic energy equation, consistent with the hydrostatic

approximation, involves only the energy of the horizontal motions and is given by,

$$\frac{dk}{dt} + \vec{u}\cdot\nabla\phi = \vec{u}\cdot\vec{F}$$

or

$$\frac{\partial k}{\partial t} + \nabla\cdot(k+\phi)\vec{u} + \frac{\partial}{\partial z}(k+\phi)\omega - (k+\phi)\omega = \phi_z\omega + \vec{u}\cdot\vec{F}$$

The equation gives the kinetic energy change per unit mass in terms of the divergence of advective and work terms and the transformation between potential and kinetic energy expressed in the term $\phi_z\omega$. The form of the vertical derivative reflects the exponential variation of mass with z. The element of mass in this coordinate system

is $$dm = \rho dx dy dz = dx dy(\rho dz) = dx dy\left(-\frac{dp}{g}\right) = dx dy\left(\frac{p\,dz}{g}\right)$$

This may be written as

$$dm = p\,dx dy\frac{dz}{g}\ ,\quad p = p_0 e^{-z}$$

The kinetic energy equation per unit 'volume' in this coordinate system is then

$$\frac{\partial pk}{\partial t} + \nabla\cdot p(k+\phi)\vec{u} + \frac{\partial}{\partial z}p(k+\phi)\omega = p\omega\phi_z + p\vec{u}\cdot\vec{F}$$

The total energy equation is somewhat different in form in this coordinate system as the new vertical coordinate bears a different relationship to the potential energy than the usual z coordinate.

The thermodynamic equation may be transformed into

$$\frac{dC_pT}{dt} = -\omega\phi_z + \dot{Q}$$

Then together with the kinetic energy equation

$$\frac{d}{dt}(k + C_pT + \phi) = \phi_t + \vec{u}\cdot\vec{F} + \dot{Q}$$

This may be compared to the form of the energy equation in x, y, z coordinates given by Hess (1959) as

$$\frac{d}{dt}\left(k + \frac{p}{\rho} + \phi + C_vT\right) = \frac{1}{\rho}\frac{\partial p}{\partial t} + \vec{u}\cdot\vec{F} + \dot{Q}$$

to which it corresponds. The equation for the total energy per unit volume in the z coordinate system is, for $E = k + C_vT + \phi$

$$\frac{\partial \rho E}{\partial t} + \nabla\cdot\rho(E+\phi_z)\vec{u} + \frac{\partial}{\partial z}\rho\{(E+\phi_z)\omega + \phi_t\} = \rho\vec{u}\cdot\vec{F} + \rho\dot{Q} \qquad (2)$$

The energy flux vectors are

$$\vec{J}_H = \rho(E+\phi_z)\vec{u} \qquad J_z = \rho(E+\phi_z)\omega + \rho\phi_t \qquad (3)$$

The horizontal energy flux is composed of the advective and work terms as before while the vertical energy flux has an additional component $\rho\phi_t$ which is the rate of change of potential energy due to the variation of the geopotential at the height z.

2.1.3 The perturbation equations

The perturbation equations are obtained by expanding the dependent variables in terms of a small parameter

$$\vec{u} = \vec{u}_0 + \epsilon \vec{u}_1 + \epsilon^2 \vec{u}_2 + \cdots$$

$$\omega = \omega_0 + \epsilon \omega_1 + \epsilon^2 \omega_2 + \cdots$$

$$\phi = \phi_0 + \epsilon \phi_1 + \epsilon^2 \phi_2 + \cdots$$

and equating the terms of like order in the perturbation parameter. The zero order equations are

$$\begin{aligned} &\vec{u}_{0t} + \vec{u}_0 \cdot \nabla \vec{u}_0 + \omega_0 \frac{\partial \vec{u}_0}{\partial z} + f \vec{k} \times \vec{u}_0 + \nabla \phi_0 = \vec{F}_0 \\ &\omega_{0z} - \omega_0 + \nabla \cdot \vec{u}_0 = 0 \\ &\phi_{0zt} + \vec{u}_0 \cdot \nabla \phi_{0z} + \omega_0 (\phi_{0zz} + \kappa \phi_{0z}) = \kappa \dot{Q}_0 \end{aligned} \tag{4}$$

The first order equations are

$$\begin{aligned} &\vec{u}_{1t} + \vec{u}_0 \cdot \nabla \vec{u}_1 + \vec{u}_1 \cdot \nabla \vec{u}_0 + \omega_0 \frac{\partial \vec{u}_1}{\partial z} + \omega_1 \frac{\partial \vec{u}_0}{\partial z} \\ &\qquad + f \vec{k} \times \vec{u}_1 + \nabla \phi_1 = \vec{F}_1 \\ &\omega_{1z} - \omega_1 + \nabla \cdot \vec{u}_1 = 0 \\ &\phi_{1zt} + \vec{u}_0 \cdot \nabla \phi_{1z} + \vec{u}_1 \cdot \nabla \phi_{0z} + \omega_0 (\phi_{1zz} + \kappa \phi_{1z}) \\ &\qquad + \omega_1 (\phi_{0zz} + \kappa \phi_{0z}) = \kappa \dot{Q}_1 \end{aligned} \tag{5}$$

The second order equations are

$$\begin{aligned} &\vec{u}_{2t} + \vec{u}_0 \cdot \nabla \vec{u}_2 + \vec{u}_2 \cdot \nabla \vec{u}_0 + \omega_0 \frac{\partial \vec{u}_2}{\partial z} + \omega_2 \frac{\partial \vec{u}_0}{\partial z} + f \vec{k} \times \vec{u}_2 + \nabla \phi_2 \\ &\qquad = -\vec{u}_1 \cdot \nabla \vec{u}_1 - \omega_1 \frac{\partial \vec{u}_1}{\partial z} + \vec{F}_2 \\ &\omega_{2z} - \omega_2 + \nabla \cdot \vec{u}_2 = 0 \\ &\phi_{2zt} + \vec{u}_0 \cdot \nabla \phi_{2z} + \vec{u}_2 \cdot \nabla \phi_{0z} + \omega_0 (\phi_{2zz} + \kappa \phi_{2z}) \\ &\qquad + \omega_2 (\phi_{0zz} + \kappa \phi_{0z}) = -\vec{u}_1 \cdot \nabla \phi_{1z} - \omega_1 (\phi_{1zz} + \kappa \phi_{1z}) + \kappa \dot{Q}_2 \end{aligned} \tag{6}$$

and so on. The zero order equations are non-linear but the remaining

equations are linear and can be solved in order with the higher order equations being forced by lower order terms. The vast majority of results concerning gravity wave motions in the atmosphere have made use of the first order equations only.

The usual form of the first order equations involves the choice of simple solutions to the zero order equations. A typical choice for zero order terms is

$$\vec{u}_0 = \vec{u}_0(z), \quad \omega_0 = 0, \quad \phi_0 = \phi_0(z)$$

for the non-rotating case.

2.1.4 The conservation of energy for perturbation equations

Consider the energy equation

$$\frac{\partial \rho E}{\partial z} + \nabla \cdot \rho (E+\phi_z)\vec{u} + \frac{\partial}{\partial z}\rho\{(E+\phi_z)\omega + \phi_t\} = 0$$

and expand in terms of a small parameter as before. The resultant energy equations are;

For zero order

$$\frac{\partial \rho E_0}{\partial t} + \nabla \cdot \rho (E_0+\phi_{0z})\vec{u}_0 + \frac{\partial}{\partial z}\rho\{(E_0+\phi_{0z})\omega_0 + \phi_{0t}\} = 0 \tag{7}$$

For first order

$$\frac{\partial \rho E_1}{\partial t} + \nabla \cdot \rho\{(E_0+\phi_{0z})\vec{u}_1 + (E_1+\phi_{1z})\vec{u}_0\} + \frac{\partial}{\partial z}\rho\{(E_0+\phi_{0z})\omega_1 + (E_1+\phi_{1z})\omega_1 + \phi_{1t}\} = 0 \tag{8}$$

For second order

$$\frac{\partial \rho E_2}{\partial t} + \nabla \cdot \rho \left\{ (E_0+\phi_{0z})\vec{u}_2 + (E_1+\phi_{1z})\vec{u}_1 + (E_2+\phi_{zz})\vec{u}_0 \right\} \tag{9}$$
$$+ \frac{\partial}{\partial z} \rho \left\{ (E_0+\phi_{0z})\omega_2 + (E_1+\phi_{1z})\omega_1 + (E_2+\phi_{2z})\omega_0 + \phi_{zt} \right\} = 0$$

where
$$E_0 = \frac{\vec{u}_0 \cdot \vec{u}_0}{2} + C_v T_0 + \phi_0$$
$$E_1 = \vec{u}_0 \cdot \vec{u}_1 + C_v T_1 + \phi_1 \tag{10}$$
$$E_2 = \frac{\vec{u}_1 \cdot \vec{u}_1}{2} + \vec{u}_0 \cdot \vec{u}_2 + C_v T_2 + \phi_2$$

Similar equations can be obtained for higher orders.

The form of these energy equations presents a problem in that it is desirable both to preserve the appearance of the kinetic energy in the second order energy equation but to be able to derive the energy relation involving only terms of the first order equations. While the second order equation involves the kinetic energy of the first order it also involves terms of the second order. Eckart (1960) points out that this leaves the choice of giving up the idea of treating the first order equations separately from those of higher order, giving up the kinetic energy concept or devising some way of using the kinetic energy concept which involves the terms of the first order only.

The usual course is to form an energy quadratic using only the terms of desired order. The first order equations, for zero order terms given by $u_0 = u_0(z)$, $w_0 = 0$, $\phi_0 = \phi_0(z)$ for a two-dimensional, non-rotating, non-viscous, adiabatically moving atmosphere on

the tangent plane are, in these coordinates

$$u_t + u_o u_x + w u_{oz} + \phi_x = 0$$

$$w_z - w + u_x = 0 \qquad (11)$$

$$\phi_{zt} + u_o \phi_{zx} + w S_o = 0 \quad , S_o = \phi_{ozz} + k\phi_{oz}$$

Multiplying the first and third equations by u and ϕ_z / S_o gives

$$\left(\frac{u^2}{2}\right)_t + \left(u_o \frac{u^2}{2}\right)_x + w u u_{oz} + u\phi_x = 0$$

$$\left(\frac{\phi_z^2}{2S_o}\right)_t + \left(u_o \frac{\phi_z^2}{2S_o}\right)_x + w\phi_z = 0$$

which is combined to give the energy equation

$$\frac{\partial \rho E}{\partial t} + \frac{\partial}{\partial x} \rho \left(E u_o + u\phi\right) + \frac{\partial}{\partial z} \rho w \phi = - u_{oz} \rho u w \qquad (12)$$

$$E = \frac{u^2}{2} + \frac{\phi_z^2}{2S_o}$$

The energy so defined consists of the kinetic energy of the first order flow and a term proportional to the variance of temperature and which is apparently that of an 'available potential energy' in the sense of Lorenz (1967). The time variation of the energy is a function of the flux of energy plus the term $u_{oz} \rho u w$ which is interpreted as the interaction of the perturbation with the mean flow.

2.1.5 Simple plane wave solutions

The simplest form of gravity wave solutions to the equations of motion are reviewed in this section. Consider the simple form of the equations (5) for a non-rotating atmosphere where u_0, S_0 are taken to be constant. Solutions of the form $(u,w,\phi) = Re\,(\hat{u},\hat{w},\hat{\phi})\,e^{z/2}\,e^{i(\vec{k}\cdot\vec{x}-\nu t)}$ $\vec{k}=(k,m)$, are introduced to give, for $\sigma = \nu - k u_0$

$$\begin{pmatrix} -i\sigma & 0 & ik \\ ik & im-1/2 & 0 \\ 0 & S_0 & -i\sigma(im+1/2) \end{pmatrix} \begin{pmatrix} \hat{u} \\ \hat{w} \\ \hat{\phi} \end{pmatrix} = 0 \qquad (13)$$

The equation for the complex amplitudes can be solved if and only if the determinant of the matrix is zero, i.e., for

$$\sigma^2 = \frac{k^2 S_0}{m^2 + 1/4} \qquad (14)$$

This is the frequency relation for simple plane hydrostatic wave motion. Two of the amplitudes may be expressed in terms of a third or they may be expressed in terms of a constant; for instance

$$\begin{aligned} \hat{u} &= ikM\ell \\ \hat{w} &= k^2\ell \qquad M = im - 1/2 \\ \hat{\phi} &= i\sigma M\ell \end{aligned} \qquad (15)$$

For given ν and k real, $m = \pm\sqrt{\frac{k^2 S_0}{\sigma^2} - 1/4}$ and solutions are of the form

$$(u,w,\phi) = Re\,(\hat{u},\hat{w},\hat{\phi})\,e^{z/2}\,e^{i(kx \pm |m| z - \nu t)} \qquad (16)$$

for $\frac{k^2 S_0}{\sigma^2} - \frac{1}{4} > 0$. For $\frac{k^2 S_0}{\sigma^2} - \frac{1}{4} < 0$ solutions are of the form $(u, w, \phi) = Re(\hat{u}, \hat{w}, \hat{\phi})\, e^{z/2}\, e^{\pm imz}\, e^{i(kx - \nu t)}$ and are termed evanescent.

The phase of a simple wave is $\psi = kx + mz - \nu t$. The velocities of points moving horizontally and vertically with constant phase are respectively $C_{px} = \nu/k$, $C_{pz} = \nu/m$ These are the trace velocities. The term $C_{px} = \nu/k$ is referred to as the horizontal phase velocity in cases where the dependence of the phase on z is not given explicitly as is common usage.

The group velocity is defined as $\vec{C}_g = \left(\frac{\partial \nu}{\partial k}, \frac{\partial \nu}{\partial m} \right)$ which may be evaluated from the frequency equation. Specifically

$$C_{gx} = u_0 + \frac{k S_0}{\sigma (m^2 + 1/4)} = u_0 + \frac{\sigma}{k} = \frac{\nu}{k} = C_{px} \qquad (18)$$

$$C_{gz} = \frac{-m\sigma}{m^2 + 1/4} = \frac{-m\sigma^3}{k^2 S_0} = \frac{-m k S_0^{1/2}}{(m^2 + 1/4)^{3/2}} = \pm \frac{\sigma^3}{k^2 S_0} \sqrt{\frac{k^2 S_0}{\sigma^2} - \frac{1}{4}}$$

The energy flux terms as expressed by equation (12) are

$$J_x = p(E u_0 + u\phi) \qquad J_z = p w \phi$$

If the solutions (16) are introduced into these expressions and they are then averaged over a wavelength in the x-direction (indicated by a bar $\overline{(\ )}$, they take the form

$$J_x = \bar{E}\, C_{gx} \qquad J_z = \bar{E}\, C_{gz}$$

where (19)

$$\bar{E} = \tfrac{1}{2} p_0 \left\{ \frac{|\hat{u}|^2}{2} + \frac{|\hat{w}|^2 S_0}{2\sigma^2} \right\}$$

$$J_x = u_0 \bar{E} + \tfrac{1}{2} p_0 \langle \hat{u}^* \hat{\phi} \rangle$$

$$J_z = \tfrac{1}{2} p_0 \langle \hat{w}^* \hat{\phi} \rangle$$

are expressed in terms of the complex wave amplitudes and $\langle\ \rangle$ means "the real part of". The energy of the wave motion is thus transmitted with the group velocities for the energy terms defined by equation (12).

The vertical flux of energy depends on the sign of m and σ as is seen from $C_{gz} = \frac{-m\sigma}{m^2+1/4}$. The group velocity and trace velocity $C_{pz} = \nu/m$ have opposite signs for $\sigma = (\nu - ku_0) > 0$ and the same signs for $\sigma < 0$.

2.1.6 Variable background conditions

The behavior of gravity waves which propagate through regions of variable wind and temperature may be investigated by several methods. The effect of slow variations of the wind and temperature on the wave motions may be investigated by ray tracing as in Eckhart (1960), Bretherton (1966), Jones (1969).

Consider the linearized equations in the general form

$$u_t + u_0 u_x + v_0 u_y + w_0 u_z + u u_{0x} + v u_{0y} + w u_{0z} + \phi_x = 0$$

$$v_t + u_0 v_x + v_0 v_y + w_0 v_z + u v_{0x} + v v_{0y} + w v_{0z} + \phi_y = 0$$

$$w_z - w + u_x + v_y = 0$$

$$\phi_{zt} + u_0 \phi_{zx} + v_0 \phi_{zy} + w_0 S + u \phi_{0zx} + v \phi_{0zy} + w S_0 = 0$$

One assumes the variables are of the form

$$u = Re\ \hat{u}(x,y,z,t)\, e^{z/2} e^{i\psi(x,y,z,t)}$$

whence

$$\frac{\partial u}{\partial x} = Re\left\{ \frac{\partial \hat{u}}{\partial x} e^{z/2} e^{i\psi} + i\frac{\partial \psi}{\partial x}\, \hat{u}\, e^{z/2} e^{i\psi} \right\}$$

The other variables are treated similarly. The further assumption is made that the phase ψ varies much more rapidly than the amplitude $\hat{u}$. With these assumptions the equations become

$$(i\psi_t + u_o i\psi_x + v_o i\psi_y + \omega_o i\psi_z)\hat{u} + \hat{u}u_{ox} + \hat{v}u_{oy} + \hat{\omega}u_{oz} + i\psi_x\hat{\phi} = 0$$

$$(i\psi_t + u_o i\psi_x + v_o i\psi_y + \omega_o i\psi_z)\hat{v} + \hat{u}v_{ox} + \hat{v}v_{oy} + \hat{\omega}v_{oz} + i\psi_y\hat{\phi} = 0$$

$$(i\psi_z - 1/2)\hat{\omega} + i\psi_x\hat{u} + i\psi_y\hat{v} = 0$$

$$(i\psi_z + 1/2)(i\psi_t + u_o i\psi_x + v_o i\psi_y + \omega_o i\psi_z)\hat{\phi} + \omega_o i\psi_z k\hat{\phi} + \hat{u}\phi_{oz x} + \hat{v}\phi_{oz y} + \hat{\omega}S_o = 0$$

Now assuming further:

i. $\omega_o = 0$

ii. The spatial variation of the background winds is small compared to the phase variation.

iii. The horizontal variation of the background geopotential is small compared to the phase variation and the vertical variation of the background geopotential.

The resulting equations can be written as

$$\begin{pmatrix} -i\sigma & 0 & 0 & ik \\ 0 & -i\sigma & 0 & il \\ ik & il & im - 1/2 & 0 \\ 0 & 0 & S_o & -i\sigma(im + 1/2) \end{pmatrix} \begin{pmatrix} \hat{u} \\ \hat{v} \\ \hat{\omega} \\ \hat{\phi} \end{pmatrix} = 0$$

where $k = \psi_x$, $l = \psi_y$, $m = \psi_z$, $\nu = -\psi_t$, $\sigma = \nu - k u_0 - l v_0$

and the frequency and wave numbers are functions of the coordinates.

The frequency relation is obtained as before to give

$$\sigma^2 = \frac{(k^2+l^2) S_0}{(m^2+1/4)} \tag{21}$$

The group velocities are

$$\begin{aligned} C_{gx} &= \frac{dx}{dt} = u_0 + \frac{k\sigma}{(k^2+l^2)} \\ C_{gx} &= \frac{dy}{dt} = v_0 + \frac{l\sigma}{(k^2+l^2)} \\ C_{gz} &= \frac{dz}{dt} = -\frac{m\sigma^3}{(k^2+l^2) S_0} \end{aligned} \tag{22}$$

which also defined the equations of the rays. Then for

$\nu = \Omega(k, l, m; x, y, z, t)$ the equations of the wave numbers

and the frequency may be written

$$\begin{aligned} \frac{dk}{dt} &= -k u_{0x} - l v_{0x} + \frac{\sigma S_{0x}}{2 S_0} \\ \frac{dl}{dt} &= -k u_{0y} - l v_{0y} + \frac{\sigma S_{0y}}{2 S_0} \\ \frac{dm}{dt} &= -k u_{0z} - l v_{0z} + \frac{\sigma S_{0z}}{2 S_0} \\ \frac{d\nu}{dt} &= k u_{0t} + l v_{0t} - \frac{\sigma S_{0t}}{2 S_0} \end{aligned} \tag{23}$$

where

$$\frac{d}{dt} = \frac{dx}{dt}\frac{\partial}{\partial x} + \frac{dy}{dt}\frac{\partial}{\partial y} + \frac{dz}{dt}\frac{\partial}{\partial z} + \frac{\partial}{\partial t} = \frac{\partial}{\partial t} + C_{gx}\frac{\partial}{\partial x} + C_{gy}\frac{\partial}{\partial y} + C_{gz}\frac{\partial}{\partial z}$$

Bretherton (1966) investigated the behavior of a wave in a background flow

$$u_0 = u_0(z)$$

$$v_0 = w_0 = 0$$

with S_0 = constant. The equation of the phase is

$$(\psi_t + u_0\psi_x)^2(\psi_z^2 + 1/4) - (\psi_x^2 + \psi_y^2)S_0 = 0$$

The simplest form of ψ which satisfies the equation is

$\psi = kx - \nu t + \Theta(z)$, k, ν, constant. Then

$(\Theta_z)^2 = m^2 = \frac{k^2 S_0}{\sigma^2} - 1/4$ and the vertical equation of the ray is

$$\frac{dz}{dt} = c_{gz} = \frac{-m\sigma^3}{k^2 S_0} \sim k\frac{(c_{px} - u_0(z))^2}{S_0^{1/2}}$$

For $u_0 = a z$, integration gives

$$z = \frac{c_{px}}{a}\left[1 - 1/\left(1 + c_{px}\frac{a k t}{S_0^{1/2}}\right)\right]$$

which shows that the wave packet approaches the "critical level" $\sigma = k(c_{px} - u_0(z)) = 0$ asymptotically with time. The vertical wave number m goes to ∞ at the critical level and the wave is incident but not reflected from this level.

Jones (1969) considered a stratified incompressible fluid and obtained equations of a form very similar to those of equations (22,23) and pointed out that for constant S_0 and for constant linear background velocities the first two of equations (23) form a system with constant coefficients. Solutions have the form

$$\begin{pmatrix} k \\ l \end{pmatrix} = A \begin{pmatrix} e^{\alpha_1 t} \\ e^{\alpha_2 t} \end{pmatrix} \qquad (24)$$

where A is a 2x2 matrix of constants and where α_1, α_2 are roots of the equation

$$\alpha^2 + \alpha(u_{ox} + v_{oy}) + u_{ox}v_{oy} - u_{oy}v_{ox} = 0$$

But in this case it was assumed that $\omega_o = 0$ so that the mean flow is non-divergent and

$$\alpha^2 + u_{ox}v_{oy} - u_{oy}v_{ox} = 0 \qquad (25)$$

The wavenumbers may have exponential behavior in time (implying critical level behavior or reflection) or sinusoidal variation depending on the sign of $u_{ox}v_{oy} - u_{oy}v_{ox}$.

Some additional results may be deduced from this formulation. Consider the case for $u_o = u_o(z,t)$, $v_o = \omega_o = 0$. The background wind changes with time. In this case both m and ν depend on t and z. An equation for the local variation of $\sigma = \nu - k u_o$, the intrinsic frequency and the parameter which specifies the critical level may be derived from the last of equations (23). Thus for S_o = constant

$$\nu_t - k u_{ot} + c_{gz}(\nu_z - k u_{oz}) + c_{gz} k u_{oz} = 0$$

$$\sigma_t + c_{gz}(\sigma_z + k u_{oz}) = 0$$

The group velocity is approximately

$$c_{gz} \sim \sigma^2 / k S_o^{1/2}$$

whence

$$\sigma_t + \frac{\sigma^2}{k S_o^{1/2}}(\sigma_z + k u_{oz}) = 0 \qquad (26)$$

This is an explicit formula for the intrinsic frequency and shows that the critical level $\sigma = 0$ is a nonlinear function of z and t. If the shear u_{oz} of the wind changes with time, the critical level will vary with time and the critical level phenomena will occur in a distributed region rather than at a particular level.

Another phenomena which should be pointed out is the possibility of ducting the wave packet in the horizontal. This may be illustrated for the simple case $u_o = u_o(y)$. The group velocity in the y-direction is

$$c_{gy} = \frac{a^2}{\sigma}\sqrt{\frac{\sigma^2}{a^2} - k^2} \quad , \quad a^2 = \frac{S_o}{m^2 + 1/4}$$

Here $c_{gy} = 0$ for $\sigma^2 \to k^2 a^2$. Taking $u_o = by$ the equation of the ray with time is

$$y = \frac{\nu}{kb} - \frac{a}{kb}\sqrt{(A - kbt)^2 + k^2}$$

, A an integral constant. This shows a change in direction. It is thus possible for the wave packet to be trapped in the horizontal in a region of a minimum of the background wind. (A more formal treatment could be given in terms of a "turning point" in WKB theory as discussed in Morse and Feschback (1953)). Other simple background wind fields give similar results.

There is another interesting relation which may be derived. The equations of the zero order flow are

$$u_{ot} + u_o u_{ox} + v_o u_{oy} + \phi_{ox} = 0$$

$$v_{ot} + u_o v_{ox} + v_o v_{oy} + \phi_{oy} = 0 \qquad (27)$$

For the assumption that the flow is non-divergent the equations may be manipulated to give

$$u_{ox} v_{oy} - v_{ox} u_{oy} = \tfrac{1}{2} \nabla^2 \phi_o$$

Thus for constant linear background velocities or for gradients small enough so that (24) is a reasonable approximation to the solution for the horizontal wave numbers, the behavior of the solution as given by (25) depends on the sign of the horizontal Laplacian of the geopotential.

A more precise investigation into the behavior of gravity waves in a region of vertical wind shear can be made using the linear equations (11). Assuming the variables have the form

$$(u, \omega, \phi) = Re(\hat{u}(z), \hat{\omega}(z), \hat{\phi}(z))\, e^{z/2} e^{i(kx - \nu t)}$$

the equations may be written in any of the three forms

$$\frac{d^2\hat{\omega}}{dz^2} + \hat{\omega}\left[\frac{k^2 S_o}{\sigma^2} + \frac{k}{\sigma}(u_{oz} + u_{ozz}) - \frac{1}{4}\right] = 0 \qquad (28)$$

$$\frac{d}{dz}\begin{pmatrix} \frac{\hat{\omega}}{-i\sigma} \\ \phi_{oz}\frac{\hat{\omega}}{-i\sigma} + \hat{\phi} \end{pmatrix} = \begin{pmatrix} \frac{1}{2} - \frac{k^2}{\sigma^2}\phi_{oz} & \frac{k^2}{\sigma^2} \\ -\phi_{oz}\left(\frac{k^2}{\sigma^2}\phi_{oz} + k - 1\right) & -\left(\frac{1}{2} - \frac{k^2}{\sigma^2}\phi_{oz}\right) \end{pmatrix} \begin{pmatrix} \frac{\hat{\omega}}{-i\sigma} \\ \phi_{oz}\frac{\hat{\omega}}{-i\sigma} + \hat{\phi} \end{pmatrix}$$

$$\frac{d}{dz}\begin{pmatrix} \frac{\hat{\omega}}{-i\sigma} \\ \hat{\phi} \end{pmatrix} = \begin{pmatrix} \frac{1}{2} & \frac{k^2}{\sigma^2} \\ -S_o & -\frac{1}{2} \end{pmatrix} \begin{pmatrix} \frac{\hat{\omega}}{-i\sigma} \\ \hat{\phi} \end{pmatrix}$$

The second of these equations is in a form suitable for calculations where the atmosphere is divided into layers with constant temperature and background wind as the components of the matrix are constant and the variables are continuous across an interface.

The u equation of motion

$$u_t + uu_x + \omega u_z + \phi_x = 0$$

can be put in the form

$$(pu)_t + (puu + p\phi)_x + (pu\omega)_z = 0$$

and defines the horizontal and vertical momentum fluxes. The vertical momentum flux $F = pu\omega$ averaged over a wavelength in the horizontal can be obtained from equations (28) quite generally as

$$\overline{F} = \overline{pu\omega} = p\frac{k}{\sigma}\overline{\omega\phi} = \frac{1}{2}R_e p_0 \hat{u}\hat{\omega}^* = \frac{1}{2}R_e p_0 \frac{k}{\sigma}\hat{\omega}^*\hat{\phi}$$

and using the third equation it can be shown that

$$\frac{d}{dz}\overline{F} = \frac{d}{dz}p\overline{u\omega} = \frac{d}{dz}p\frac{k}{\sigma}\overline{\omega\phi} = 0$$

That is, the momentum flux is constant with height except possibly at $\sigma = 0$. Booker and Bretherton (1967) investigated the behavior of the solutions to the first of equations (28) for a Boussinesq fluid near the critical level $\sigma = 0$ and obtained solutions of the form

$$\hat{\omega} = A(z - i\beta)^{1/2 + i\mu} + B(z - i\beta)^{1/2 - i\mu}$$

$$\mu = \sqrt{\frac{S_0}{U_{0z}^2} - \frac{1}{4}}\ , \quad \beta = \frac{\alpha}{kU_{0z}}$$

where $\alpha \to 0$ for on inviscid fluid. They matched the solutions across the critical level and showed:

i) The terms $A(z-i\beta)^{1/2+i\mu}$, $B(z-i\beta)^{1/2-i\mu}$ may be identified with waves carrying energy upwards and downwards.

ii) The momentum flux is constant above and below the critical level but decreases by the factor $e^{-2\pi\mu}$ across the critical level and changes sign.

iii) This divergence of the momentum flux implies an acceleration of the mean flow.

iv) The amplitudes of the formal solutions vary as

$$\hat{\omega} \sim z^{1/2}, \quad \hat{u} \sim z^{-1/2}, \quad \hat{\phi} \sim z^{1/2}$$

near a critical level at $z = 0$.

The result that $\hat{u} \to \infty$ at a critical level is obviously physically unrealistic and arises as a consequence of the implicit assumptions that the interaction has been occurring for infinite time, the mean flow is constant, and no non-linear interactions are important. The more realistic results which follow if these restrictions are removed are investigated in what follows.

2.2. A linear numerical model

The design of a numerical model for a set of partial differential equations demands consideration of the accuracy, stability and convergence, initial and boundary conditions, and the amount of computation which must be done.

The equations used were

$$
\begin{aligned}
&u_t + u_0 u_x + w u_{0z} + \phi_x = -\alpha u \\
&w_z - w + u_x = 0 \\
&\phi_{zt} + u_0 \phi_{zx} + w S_0 = -\alpha \phi_z \\
&\phi_t + u_0 \phi_x + w \phi_{0z} = g w \quad \text{at } z = 0
\end{aligned}
\tag{29}
$$

which include linear dissipation terms and the boundary condition at the bottom boundary relating the geopotential to the geometric vertical velocity w there. As the time step necessary for stability is expected to be small and the horizontal phase speed of the waves is large a calculation using the equations in the present form would require a great deal of effort. A much simpler scheme is obtained by specializing the horizontal variation of the variables as a sinusoid. The substitution

$$
(u, w, \phi) = (\hat{u}(z,t), \hat{w}(z,t), \hat{\phi}(z,t))\, e^{z/2}\, e^{ikx} \tag{30}
$$

is made. The equations then take the form

$$
\begin{aligned}
&\hat{u}_t + iku_0\hat{u} + \hat{w} u_{0z} + ik\hat{\phi} = -\alpha\hat{u} \\
&\hat{w}_z - \frac{\hat{w}}{2} + ik\hat{u} = 0 \\
&\left(\hat{\phi}_z + \frac{\hat{\phi}}{2}\right)_t + iku_0\left(\hat{\phi}_z + \frac{\hat{\phi}}{2}\right) + \hat{w} S_0 = -\alpha\left(\hat{\phi}_z + \frac{\hat{\phi}}{2}\right) \\
&\hat{\phi}_t + iku_0\hat{\phi} + \hat{w}\phi_{0z} = g\hat{w} \quad \text{at } z = 0
\end{aligned}
\tag{31}
$$

where the real part of (30) specifies the physically meaningful results. The equations are independent of x and require calculation over a two-dimensional grid. The variables are scaled with $e^{-z/2}$.

which has the desirable effect of removing the growth of the amplitude of the solutions with z.

The scheme chosen here is a modified leapfrog scheme and is of the second order in truncation error. The stability of the scheme is tested by making use of the von Neumann necessary stability condition (Richtmyer and Morton, 1967). The stability of a nonlinear system of equations cannot be tested directly. The usual procedure is to test the linearized form of the equations and such a calculation will provide a guide to stability for the nonlinear equations as well. The von Neumann stability condition is a necessary condition for the stability of the Fourier modes of the solution — it gives no information on the stability of other modes which may be necessary to satisfy the boundary conditions. Unfortunately, the theory of stability for mixed initial-boundary value problems is complicated to apply in practice and less than fully informative when applied. The complications of non-Fourier modes caused considerable difficulty in this study when, as a first step, a linear leapfrog scheme with no background wind or any other complicating factors was used where the variables were evaluated at every grid point and where forward differences were used in the boundary conditions. The scheme proved to be unstable even though the von Neumann stability condition was well satisfied. In attempting to resolve this difficulty it was found that the sufficient condition for stability of the Fourier modes was also satisfied and it became apparent that the instability was due to the form of the boundary conditions.

A stable scheme, correct to second order in the truncation error, can be obtained however. The finite difference scheme is designed to make the best use of the form of the equations. The finite difference grid for the linearized equations is shown in Fig. (2.1). The variables in the delimited squares in the figure are all labeled with the grid values shown.

The finite difference form of the equations of motion are;

$$\frac{\hat{u}_j^{\tau+1}-\hat{u}_j^{\tau}}{\Delta t}+(iku_0+\alpha_j)\left(\frac{\hat{u}_j^{\tau+1}+\hat{u}_j^{\tau}}{2}\right)+\frac{1}{4}\left(\hat{\omega}_{j+1}^{\tau+1}+\hat{\omega}_j^{\tau+1}+\hat{\omega}_{j+1}^{\tau}+\hat{\omega}_j^{\tau}\right)u_{0z}+ik\hat{\phi}_j^{\tau}=0$$

$$\frac{\hat{\omega}_{j+1}^{\tau+1}-\hat{\omega}_j^{\tau+1}}{\Delta z}-\frac{1}{4}\left(\hat{\omega}_{j+1}^{\tau+1}+\hat{\omega}_j^{\tau+1}\right)+ik\hat{u}_j^{\tau+1}=0$$

$$\frac{\hat{\phi}_{j+1}^{\tau+1}-\hat{\phi}_{j+1}^{\tau}-\left(\hat{\phi}_j^{\tau+1}-\hat{\phi}_j^{\tau}\right)}{\Delta t\,\Delta z}+\frac{\hat{\phi}_{j+1}^{\tau+1}-\hat{\phi}_{j+1}^{\tau}+\hat{\phi}_j^{\tau+1}-\hat{\phi}_j^{\tau}}{4\,\Delta t} \qquad (32)$$

$$+(iku_0+\alpha_j)\left(\frac{\hat{\phi}_{j+1}^{\tau+1}+\hat{\phi}_{j+1}^{\tau}-\left(\hat{\phi}_j^{\tau+1}+\hat{\phi}_j^{\tau}\right)}{2\Delta z}+\frac{1}{8}\left(\hat{\phi}_{j+1}^{\tau+1}+\hat{\phi}_{j+1}^{\tau}+\hat{\phi}_j^{\tau+1}+\hat{\phi}_j^{\tau}\right)\right)$$

$$+\hat{\omega}_{j+1}^{\tau+1}S_0=0$$

$$\frac{\hat{\phi}_1^{\tau+1}-\hat{\phi}_1^{\tau}}{\Delta t}+iku_0\left(\frac{\hat{\phi}_1^{\tau+1}+\hat{\phi}_1^{\tau}}{2}\right)+\phi_{0z}\left(\frac{\hat{\omega}_2^{\tau+1}+ik\hat{u}_1^{\tau+1}\Delta z/2}{1+\Delta z/4}\right)$$

$$=g\hat{\omega} \quad \text{at } z=0$$

The value of ω_1 in the lower boundary condition is obtained, correct to the second order in truncation error, by expanding in Taylor series and using the continuity equation.

The equations are solved by assuming $\hat{\omega}=0$ at the upper boundary and solving the $\hat{u}$ and $\hat{\omega}$ equations simultaneously from top to bottom. The equation for $\hat{\phi}$ is then solved from the bottom

Figure 2.1

Finite difference grid for the linearized equations

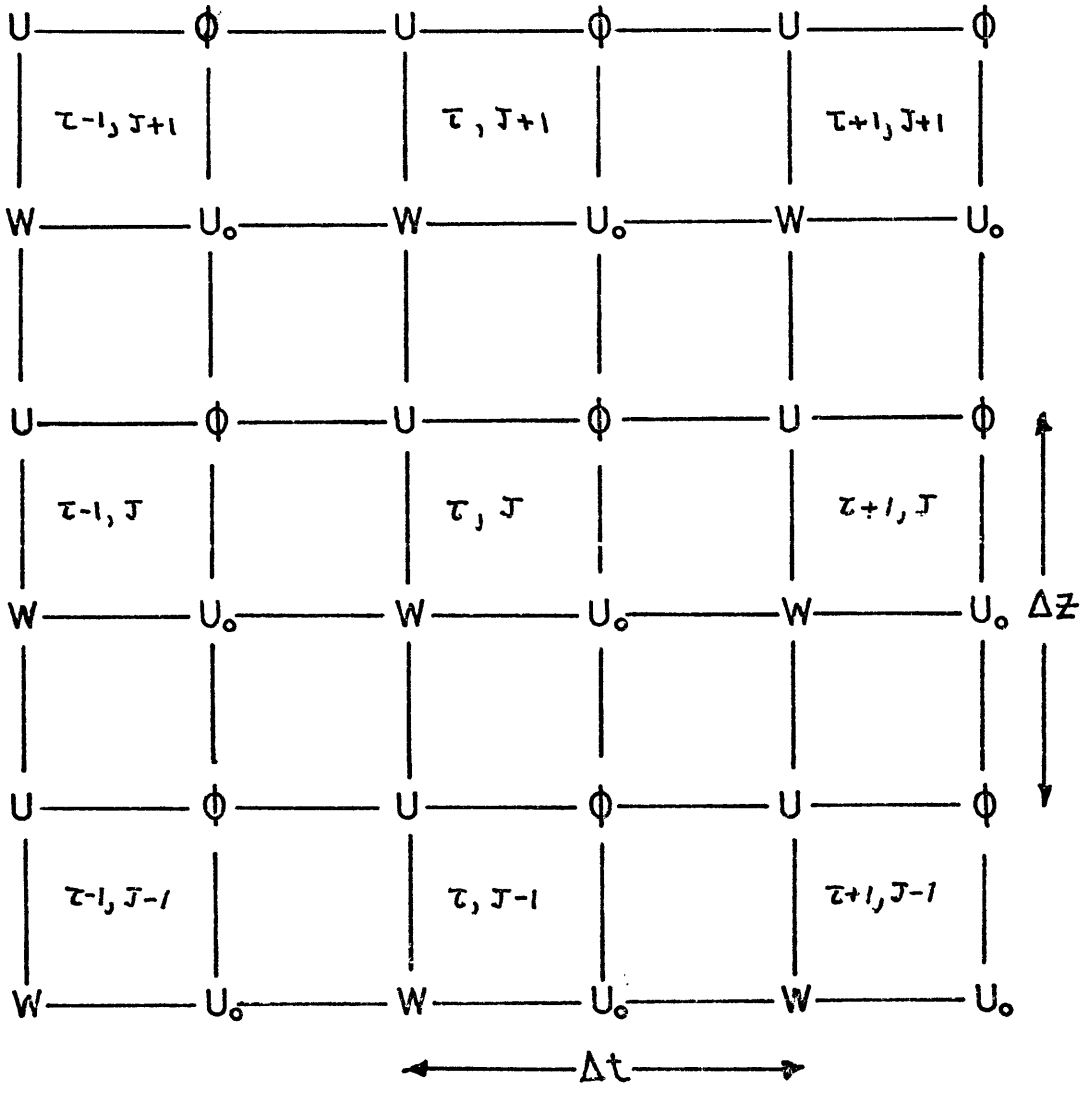

The variables at the corners of the squares are all labeled with the values of τ and J shown in the interior.

to the top of the grid after making use of the bottom boundary condition.

The motions are forced at the lower boundary and dissipated by means of the linear dissipation terms in the upper part of the region of integration. The upper boundary condition is, therefore, not a reflection condition for the waves and radiation of the waves to higher regions or dissipation by some mechanism is simulated.

Assuming the spatial variation of the variables is of the form e^{ipj}, $j = z/\Delta z$, $p = z\pi\Delta z/L_z$ the finite difference equations may be written as $F x^{\tau+1} = G x^{\tau}$ where $x^{\tau} = \begin{pmatrix} \hat{u}^{\tau} \\ \hat{w}^{\tau} \\ \hat{\phi}^{\tau} \end{pmatrix}$ and where, for $a = \sin\frac{p}{2}$, $b = \cos\frac{p}{2}$

$$F = \begin{pmatrix} 1 + (iku_0 + \alpha)\Delta t/2 & b\Delta t\, u_{0z}/2 & 0 \\ ik\Delta z & 2ia - b\Delta z/2 & 0 \\ 0 & \Delta t\Delta z S_0 & (2ia + \frac{b\Delta z}{2})(1 + (iku_0 + \alpha)\frac{\Delta t}{2}) \end{pmatrix}$$

$$G = \begin{pmatrix} 1 - (iku_0 + \alpha)\Delta t/2 & -b\Delta t\, u_{0z}/2 & -ik\Delta t \\ 0 & 0 & 0 \\ 0 & 0 & (2ia + \frac{b\Delta z}{2})(1 - (iku_0 + \alpha)\frac{\Delta t}{2}) \end{pmatrix}$$

Thus $x^{\tau+1} = F^{-1}G\, x^{\tau}$ where $F^{-1}G$ is the amplification matrix for the finite difference scheme. To satisfy the von Neumann stability condition the eigenvalues of the matrix must satisfy

$$|\lambda| \leq 1 + O(\Delta t)$$

The equation for the eigenvalues can be written

$$\left\{\lambda(1+i\delta+\beta)-(1-i\delta-\beta)\right\}^2+\frac{k^2\Delta t^2 S_0\lambda}{|\gamma|^2}=0$$

for

$$\gamma=\frac{2\alpha i}{\Delta z}+\frac{b}{2}$$

$$|\gamma|^2=\frac{1}{4}\left\{1+\left(\left(\frac{4}{\Delta z}\right)^2-1\right)\sin^2\frac{p}{2}\right\}$$

$$\beta=\frac{ik\Delta t\,u_{0z}}{4|\gamma|^2}\left\{\cos^2\frac{p}{2}-4i\frac{\sin p}{\Delta z}\right\}$$

$$\delta=ku_0\Delta t/2$$

For $\alpha=u_{0z}=0$, the equation becomes

$$\left\{\lambda(1+i\delta)-(1-i\delta)\right\}^2+\frac{k^2\Delta t^2 S_0\lambda}{|\gamma|^2}=0$$

and $|\lambda|=1$ if

$$k^2\Delta t^2\left\{\frac{S_0}{1+\left(\left(\frac{4}{\Delta z}\right)^2-1\right)\sin^2\frac{p}{2}}-\frac{u_0^2}{4}\right\}\leq 1$$

For any reasonable choice of Δz for the scaled vertical coordinate,

$\left(\frac{4}{\Delta z}\right)^2-1>0$ and the worst choice for $\sin^2\frac{p}{2}$ is zero.

This gives the stability condition $\Delta t^2 k^2\left(S_0-\frac{u_0^2}{4}\right)\leq 1$.

For this case the choice of Δt is governed by the value for which $u_0=0$. A non-zero mean wind actually increases the permissible time-step.

An approximate stability condition can be obtained for the case $u_0\neq 0, u_{0z}\neq 0, \alpha=0$ by assuming $p=0$ is the worst choice as in the previous case. This gives

$$\Delta t^2 k^2 \left\{ \frac{(S_o - u_o u_{oz}/4)^2}{(S_o + u_{oz}^2/4)} - \frac{u_o^2}{4} \right\} \leq 1$$

for the stability condition.

For $\alpha \neq 0$, $u_o = u_{oz} = 0$ the condition is

$$\Delta t^2 \left\{ k^2 S_o + \alpha^2/4 \right\} \leq 1$$

By considering the effect of each of these terms a reasonable estimate of the permissible time-step can be made.

2.2.1 Results of calculation for the linear model

The calculations performed for the linear model are similar in many respects to these of Houghton and Jones (1968) which came to light after this study was begun. Many aspects of their model are the same as the model used here but a basic difference is the assumption of hydrostatic motions made here. The hydrostatic model allows a simplified set of equations to be used and permits a time step to at least thirty times that required for stability by their model. This saving in computation time permits the extension of the numerical model to include non-linear effects which are discussed in the next section.

The integration of the equations was carried out for $S_o = 2.05 \times 10^4$ m^2/sec^2 corresponding to a constant temperature of 250^oK. The horizontal wavelength used was 100 km which is of the

order of magnitude of that deduced from observations reported in a later section. This gives the wavenumber $k = 2\pi \times 10^{-5}$ m^{-1}. The initial conditions in each case were $\hat{u} = \hat{\omega} = \hat{\phi} = 0$, $u_0 = u_0(z)$ a specified function of height. The motions were forced at the lower boundary by $g\hat{\omega}_0 e^{-i\Gamma t}$ where $\hat{\omega}_0$ = 1.0 m/sec and $\Gamma = 2\pi / (1.8 \times 10^3$ sec). The forcing period of thirty minutes is the smallest convenient fraction of an hour which is consistent with the hydrostatic assumptions. The time for the wave to propagate one wavelength in the vertical can be shown from the group velocity to be proportional to the period. The qualitative nature of the results will not depend on the period chosen.

The motions were dissipated in the upper portion of the region, $z > z_0$ by the linear friction terms where

$$\alpha = \begin{cases} \alpha_0 \left(e^{\beta(z - z_0)} - 1 \right), & z > z_0 \\ 0, & z < z_0 \end{cases}$$

where, in general, $\alpha_0 = 0.002$ sec^{-1}, max $\beta(z - z_0) = 2.5$.

Case I: No mean wind.

This simple case for $u_0 = 0$ serves as a check on the numerical scheme. The integration used Δt = 60 sec, Δz corresponding to 250 m. The total region of integration was 60 km in the vertical with the upper 15 km acting as a damping region.

The solution for $\omega = Re\, \hat{\omega}(z,t) e^{z/2} e^{ikx}$ can be displayed in a number of ways. The real and complex parts of $\hat{\omega}$ could be

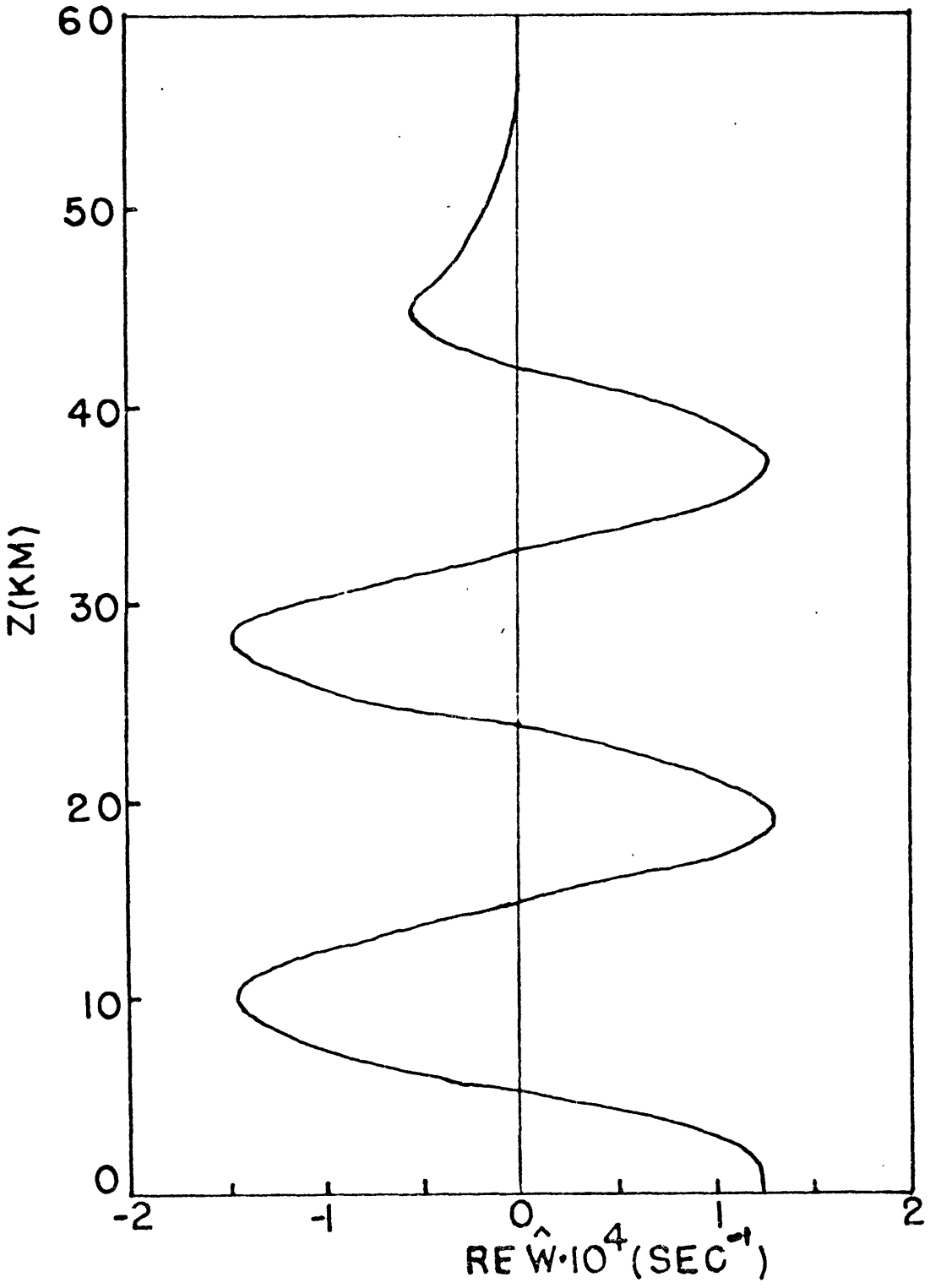

Figure 2.2: The vertical profile of $R_e\hat{\omega}$ after three hours.

plotted, the amplitude $|\hat{\omega}|$ and phase from $\hat{\omega} = |\hat{\omega}| e^{i\theta}$ could be presented, or the value of $\omega = Re\, \hat{\omega} e^{z/2} e^{ikx}$ could be shown for a given value of x. For simple cases the value of the variables at x = 0 will be presented $(Re\,\hat{\omega})$. Such plots display the variables in a manner which shows the vertical structure in a straightforward form and which resemble the type of profiles typically obtained in measurements as shown in sections (3.0). In more complicated cases the complex part of the variables $(Im\,\hat{\omega})$ can be displayed. The amplitude variation $e^{z/2}$ is scaled out in all cases.

Fig. (2.2) shows the value of ω at $x = 0$ after three hours. The vertical wavelength can be checked from the dispersion relation $m^2 = \frac{k^2 S_0}{\sigma^2} - 1/4$ which gives a value corresponding to 18.3 km. This is in good agreement with the calculated value. The maximum amplitude of ω can also be checked with the value obtained from linear theory,

$$Re\,\hat{\omega} = Re\, \frac{g\hat{\omega} k^2 e^{-imz}}{\sigma^2 \left(\frac{k^2 \phi_{0z}}{\sigma^2} - \frac{1}{2} - im\right)}$$

This gives a value of 13.9×10^{-5} sec^{-1} in good agreement with the calculated values.

The simple model does produce the expected gravity wave motions. The damping terms are successful in removing wave energy and simulating the propagation of the waves out of the region.

Case II: Linear wind shear with a critical level.

This calculation has been presented by Houghton and Jones for their model. The hydrostatic calculation is presented here for completeness and for comparison with later non-linear calculations.

The numerical parameters used in this case, were $\Delta t = 30$ sec, Δz corresponding to 500 m, $u_o = 13.5\, z$ m/sec for $z < z_o$, $u_o = 74.2$ m/sec for $z > z_o$. Here z_o at 45 km is the lower boundary of the damping region. A critical level for the forced wave motion exists at 30 km where $u_o = 55.5$ m/sec. The graphs of u at x = 0 and the term $\frac{1}{2} \rho_o \hat{u} \hat{w}^*$ which is proportional to the momentum flux are presented in Figs. (2.3, 2.4) at various times.

The transmission of wave energy can be followed from the form of the momentum flux with time. The region of decrease in momentum flux moves upward more slowly as it approaches the critical level in agreement with the decrease in group velocity given by simple theory. Very little flux occurs across the critical level and the momentum flux discontinuity at the critical level is becoming established. The small scale features in the momentum flux are the result of transient motions caused by the impulsive start of the forcing at t = 0. As time goes on the flux approaches a constant value below the critical level.

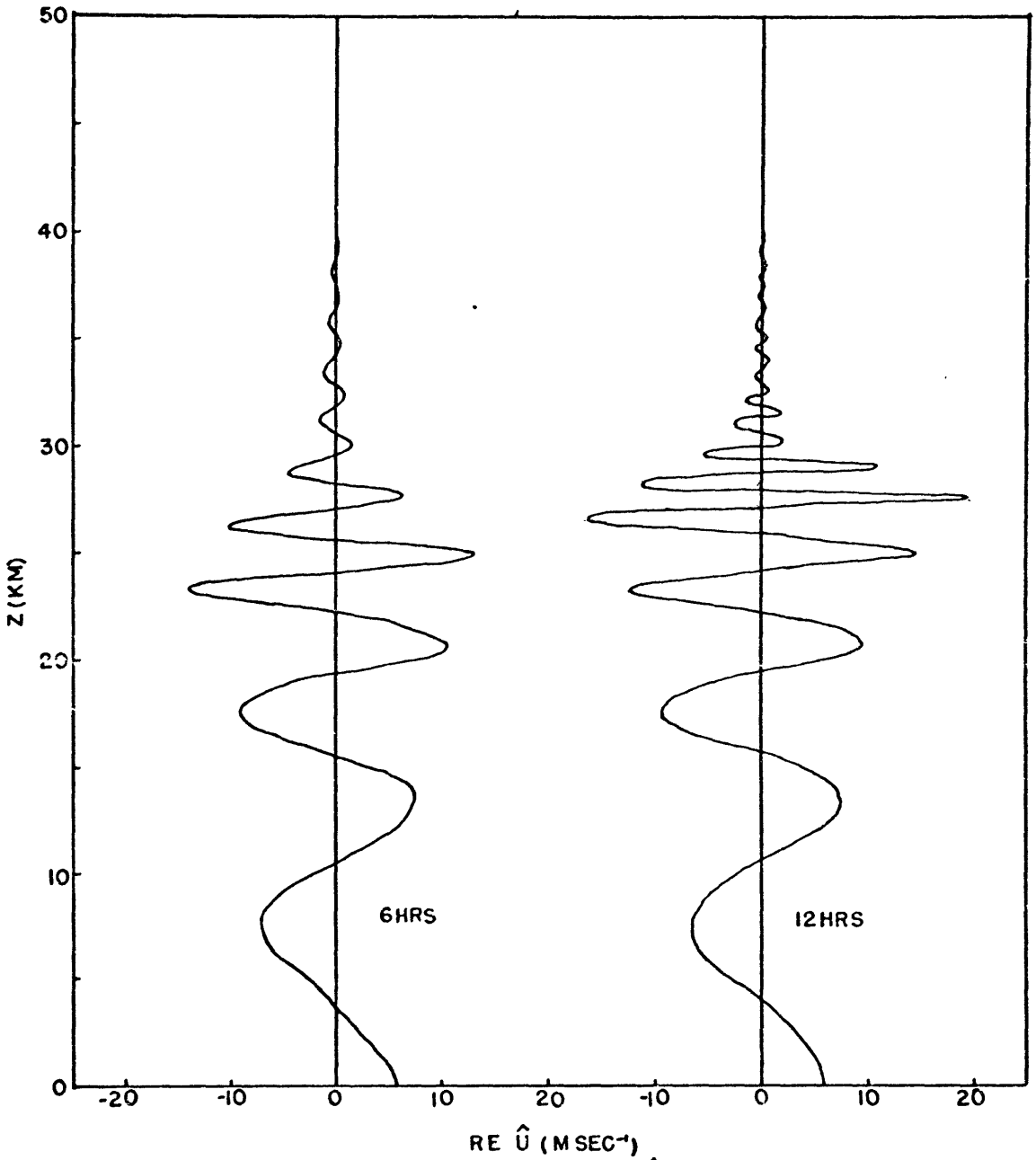

Figure 2.3: The vertical profile of $Re\,\hat{u}$ at 6 and 12 hours for wave motions propagating through a mean wind field which increases linearly with height. A critical level for the wave motions exists at 30 km.

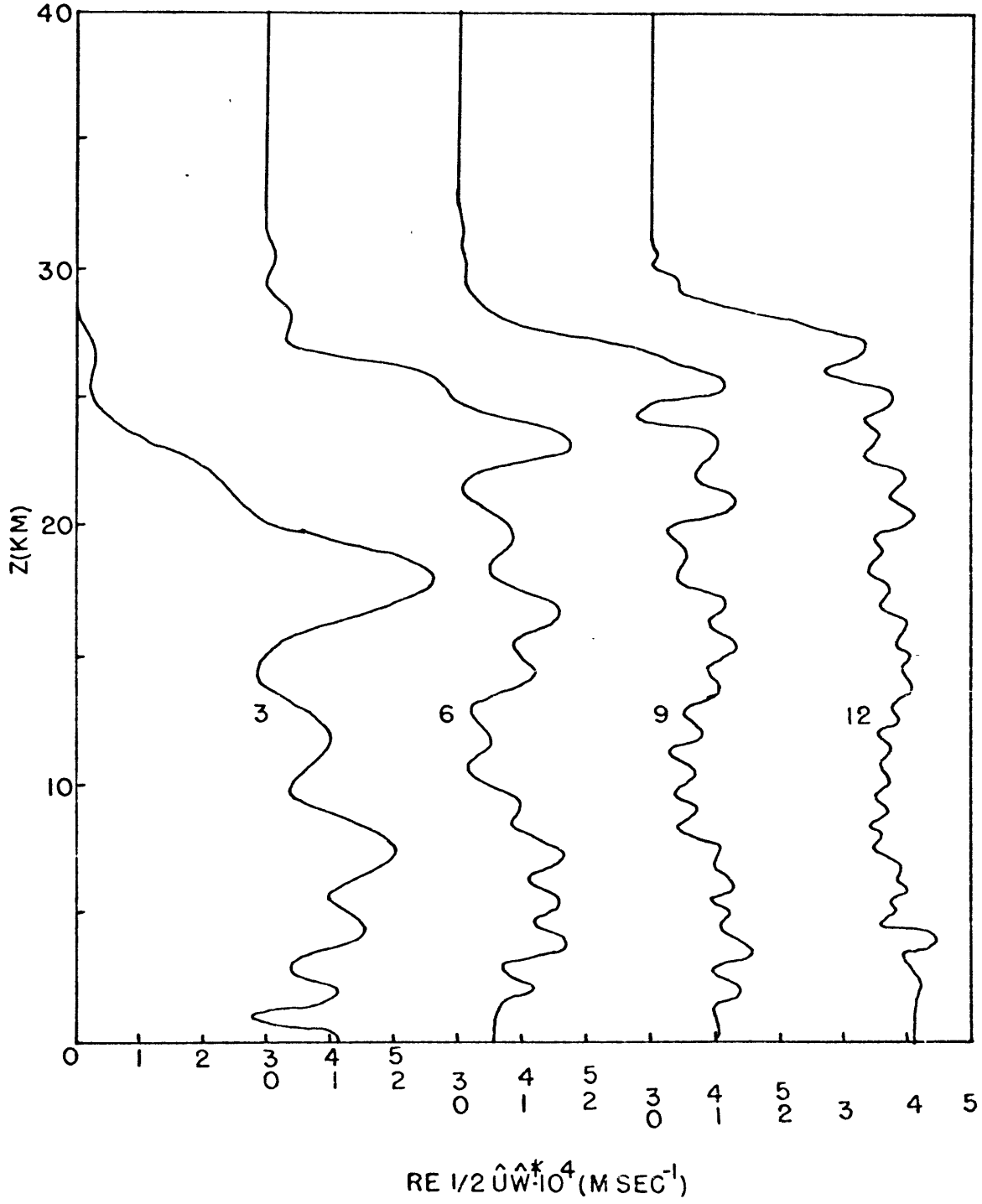

Figure 2.4: The distribution of the term $R_e\frac{1}{2}\hat{u}\hat{w}^*$, which is proportional to the momentum flux, at three hour intervals from 3 to 12 hours for wave motions propagating through a mean wind field which increases linearly with height. A critical level for the wave motions exists at 30 km.

The graphs of u show the decrease of vertical wavelength as the waves propagate through the region of positive wind shear and the growth of the magnitude of the motions near the critical level. Very little motion occurs above the critical level.

Case III: Time dependent mean flow

This case has also been treated by Houghton and Jones (1968) in a somewhat different manner. The novel feature presented here is the integration of equation (26) for the local value of $\sigma = \nu - k u_0$.

The calculation proceeds exactly as in the previous case for six hours. From six to nine hours the vertical gradient of the mean wind is increased uniformly until the critical level, originally at 30 km, is lowered to 20 km. The calculation is continued for a further nine hours. The resulting values of the momentum flux and the u component of velocity are shown in Figs. (2.5a,2.5b).

The wave motions shown in the figures can be most easily understood by considering the time dependent behavior of the local value of the intrinsic frequency $\sigma = \nu - k u_0$. The local frequency ν is a function of z and t as is $u_0(z,t)$ in this case. Fig. (2.6) shows the value of σ for the six hours following the beginning of the acceleration of the mean flow. Before the acceleration of the mean flow, the waves could not penetrate the level where $u_0 = 55.5$ m/sec. . The acceleration

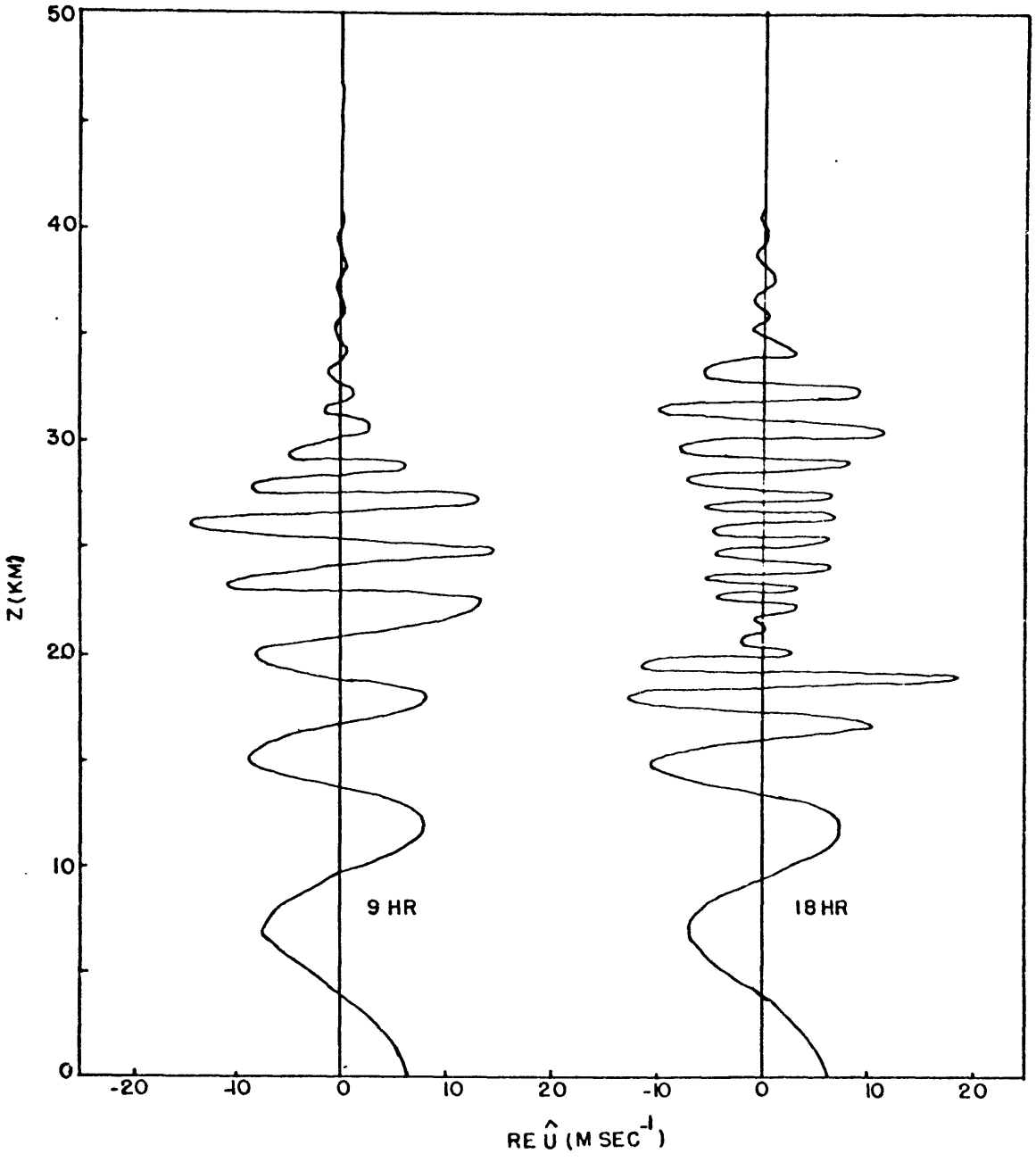

Figure 2.5a: The vertical profile of $Re\hat{u}$ at 9 and 18 hours for the case of a time dependent mean wind.

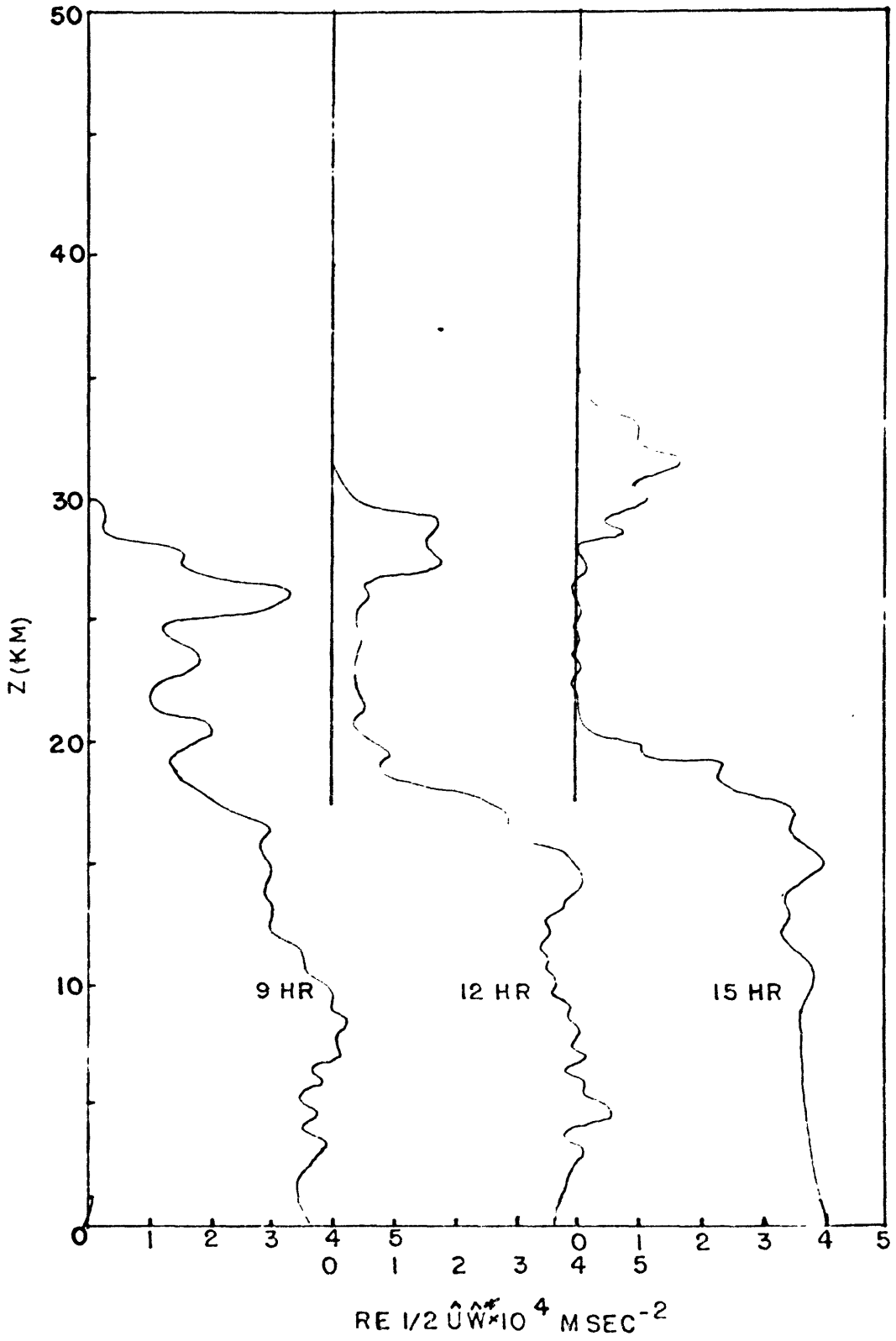

Figure 2.5b: The vertical distribution of the term $Re\,\frac{1}{2}\hat{u}\hat{w}^*$, which is proportional to the momentum flux of the waves, at 9, 12 and 18 hours for the case of a time dependent mean wind.

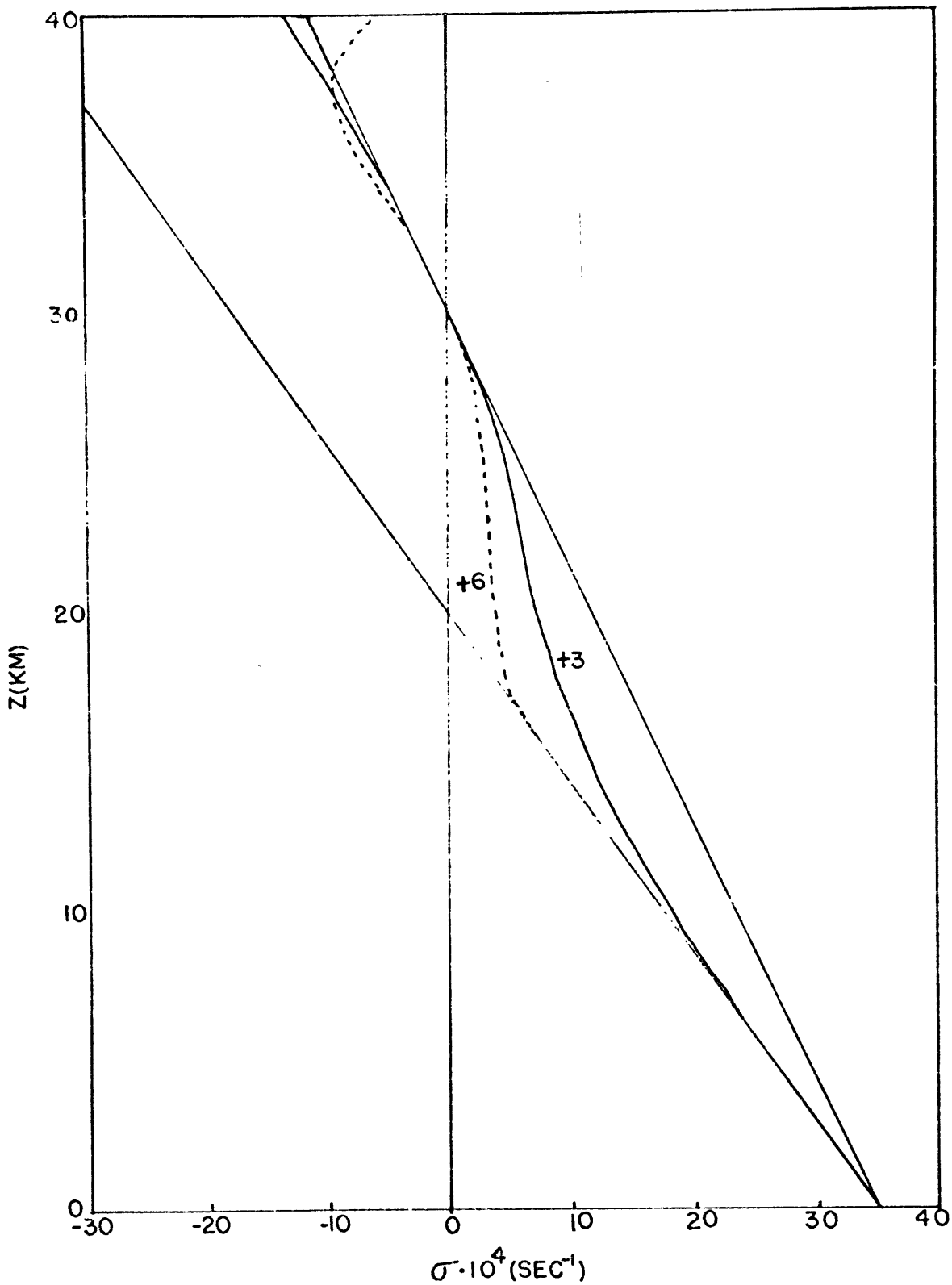

Figure 2.6: Time dependent behaviour of the local value of σ for the case of the mean wind changing with time. The straight lines give the distribution of σ appropriate to a constant mean wind which increased linearly with height with a critical level at 30 and at 20 km. The curves show the behaviour of σ as the mean wind changes with timefor 3 and 6 hours after the beginning of the change.

of the mean flow alters the local value of the frequency of the waves and waves now exist in the region where $u_0 > 55.5$ m/sec. The waves will continue to propagate upward towards the critical levels defined by their altered frequencies. The critical levels so defined will differ depending on the value of the frequency when the acceleration of the mean flow was begun. No one critical level exists and a critical region is more correctly referred to.

The behavior of the momentum flux and the u component of wave motion shows this effect. There is a continued propagation of energy into the regions above the original critical level at 30 km. The new critical level at 20 km, for motions forced at the lower boundary, prevents propagation of energy past this level and the motions are separated into two regions.

Case IV: Shearing region.

The mean wind in this case has a shearing level as shown in Fig. (2.7a). A critical level exists where $u_0 = 55.5$ m/sec. The integration is done with $\Delta t = 30$ sec, Δz corresponding to 125 m, and the amplitude of the forcing term at the lower boundary proportional to $(1 - e^{-\delta t})$, $\delta = (1 \text{ hr})^{-1}$. The resulting momentum flux and horizontal wave velocity is shown in Figs. (2.7a, 2.7b) for 12 hours.

In this case the effects of the wind shear and the critical level on the wave motions are confined to a relatively small region in the vertical. The discontinuity in the momentum flux at the critical

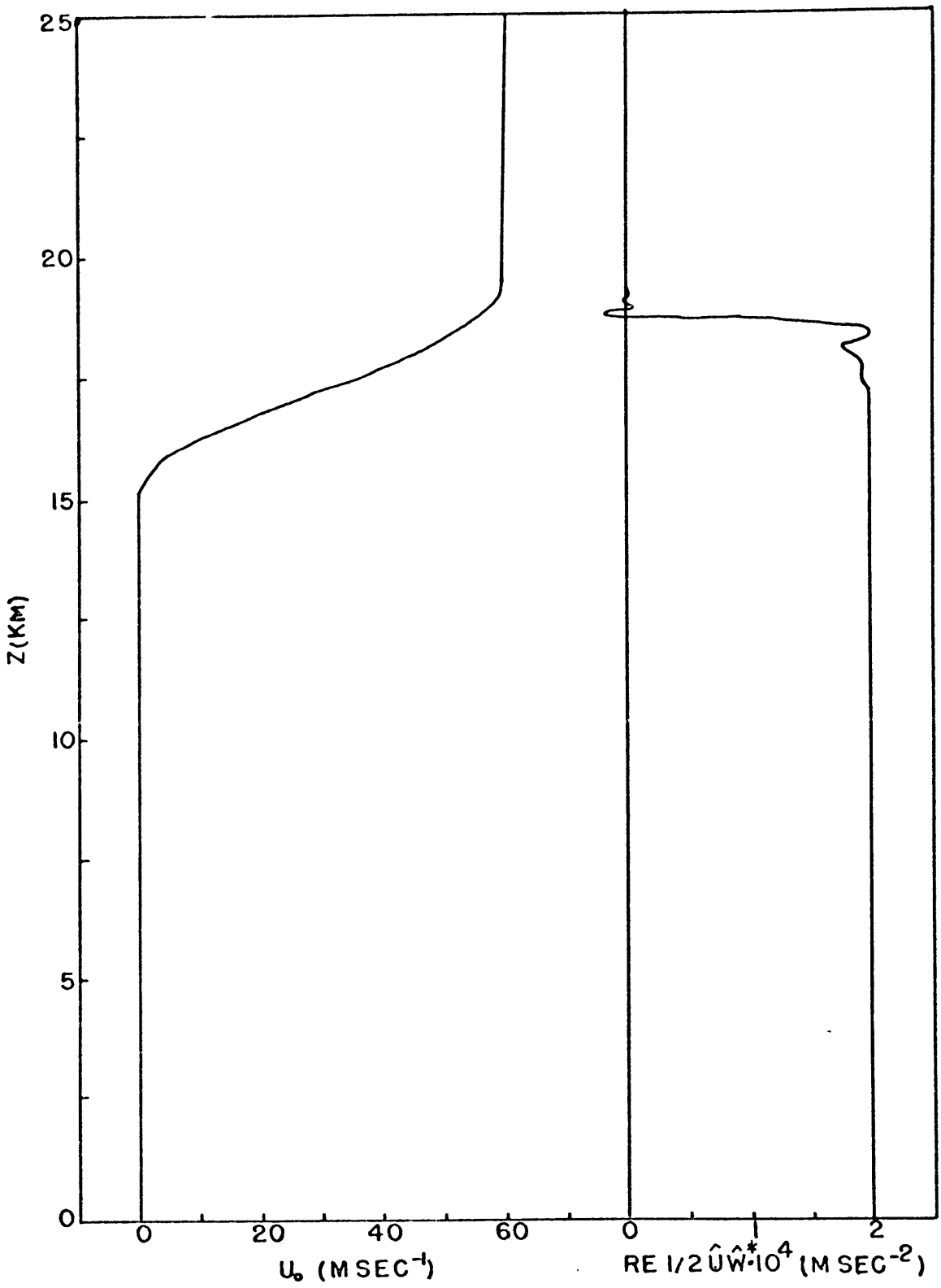

Figure 2.7a: The vertical profile of the mean wind u_o and of the momentum flux term $\rho_a \frac{1}{2}\hat{u}\hat{w}^*$ showing the sharp decrease of the flux across the critical level where u_o =55.5m/sec after 12 hours.

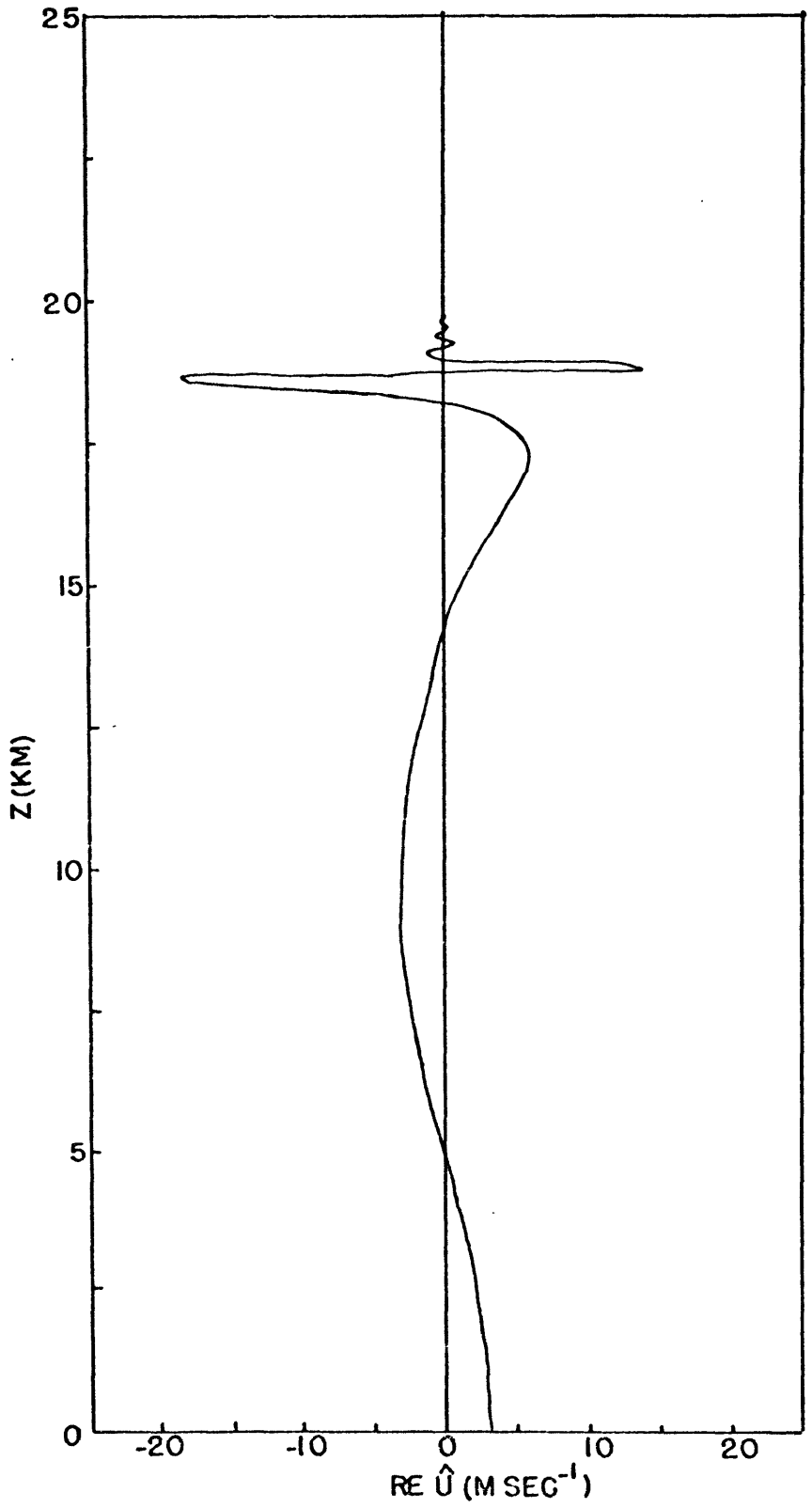

Figure 2.7b: The vertical profile of $Re\,\hat{u}$ after 12 hours for wave motions propagating through a mean wind field with a shearing region containing a critical level.

level is established much more rapidly than for the case with a linear wind profile. The momentum flux below the critical level has none of the small scale variation seen in previous cases where the forcing was begun impulsively. The gradual growth of the amplitude of the forcing produces less transient motion in the calculation. The reduction in the vertical wavelength as the waves propagate through the region of wind shear is not as obvious as in previous cases and is confined to the region near the critical level.

Shear regions in the atmosphere are considered a possible source of gravity wave motions and are also sinks for motions for which a critical level exists. The two processes are intimately related as the critical level interaction may accelerate the mean flow and produce shears which violate the Richardson stability condition. The production of small scale motions and turbulence in a region of wind shear may thus depend to an extent on the propagation of gravity waves into the region. This behavior would be difficult to detect observationally if it resembled the motions modeled here. Away from the shear zone the wavemotions have relatively small amplitude and large vertical wavelength and such motions would not be observationally obvious

Case V: Over-reflection.

Jones (1969) investigated the effect of a critical level for which $R_i < 1/4$ and for which the Booker and Bretherton analysis is

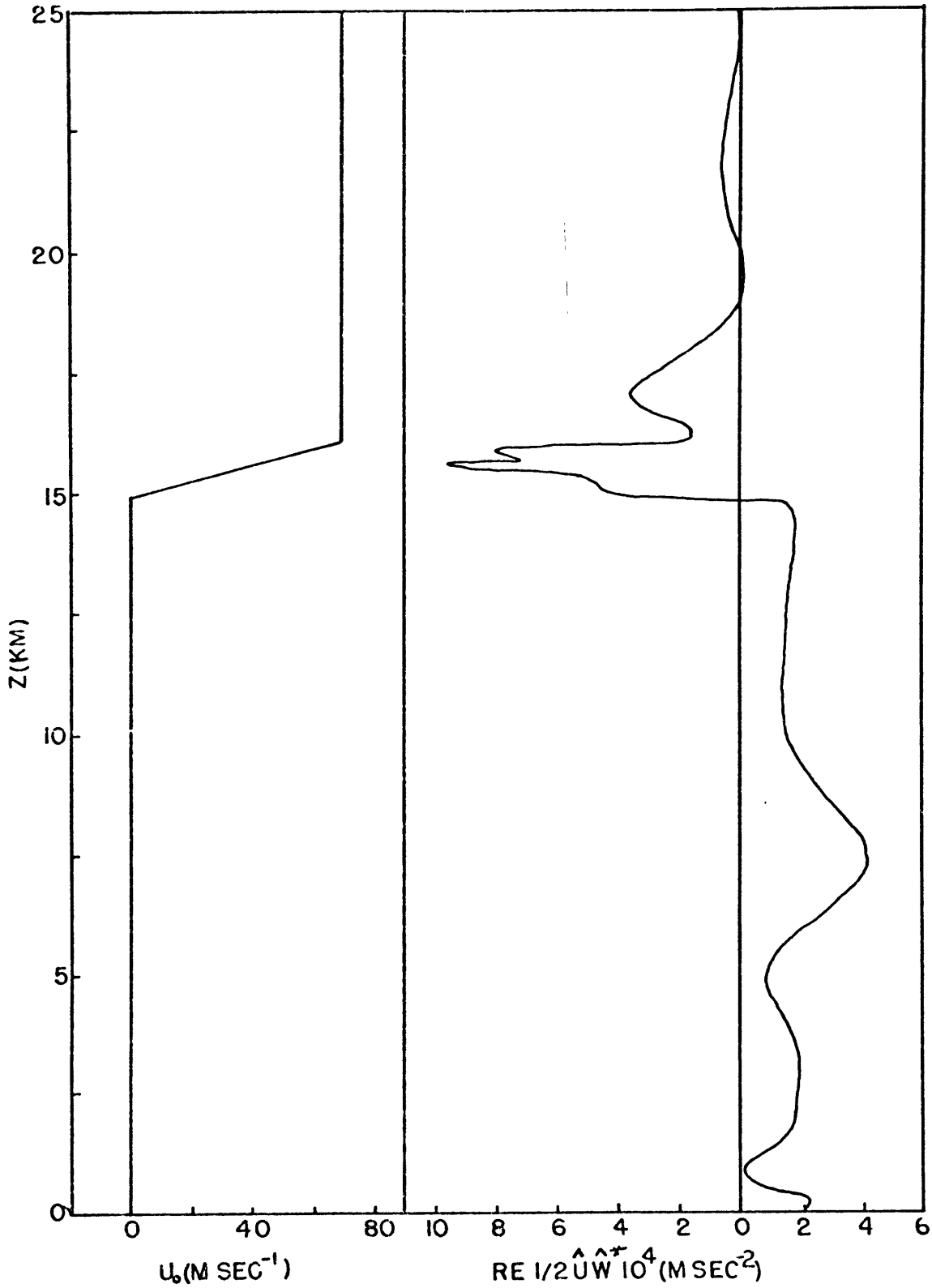

Figure 2.8a: The vertical profile of the mean wind u_o and of the momentum flux term $Re\frac{1}{2}\hat{u}\hat{w}^*$ at 3 hours. A critical level for the wave motions exists where u_o =55.5m/sec. The critical level is embedded in the shear zone for which Ri=0.125.

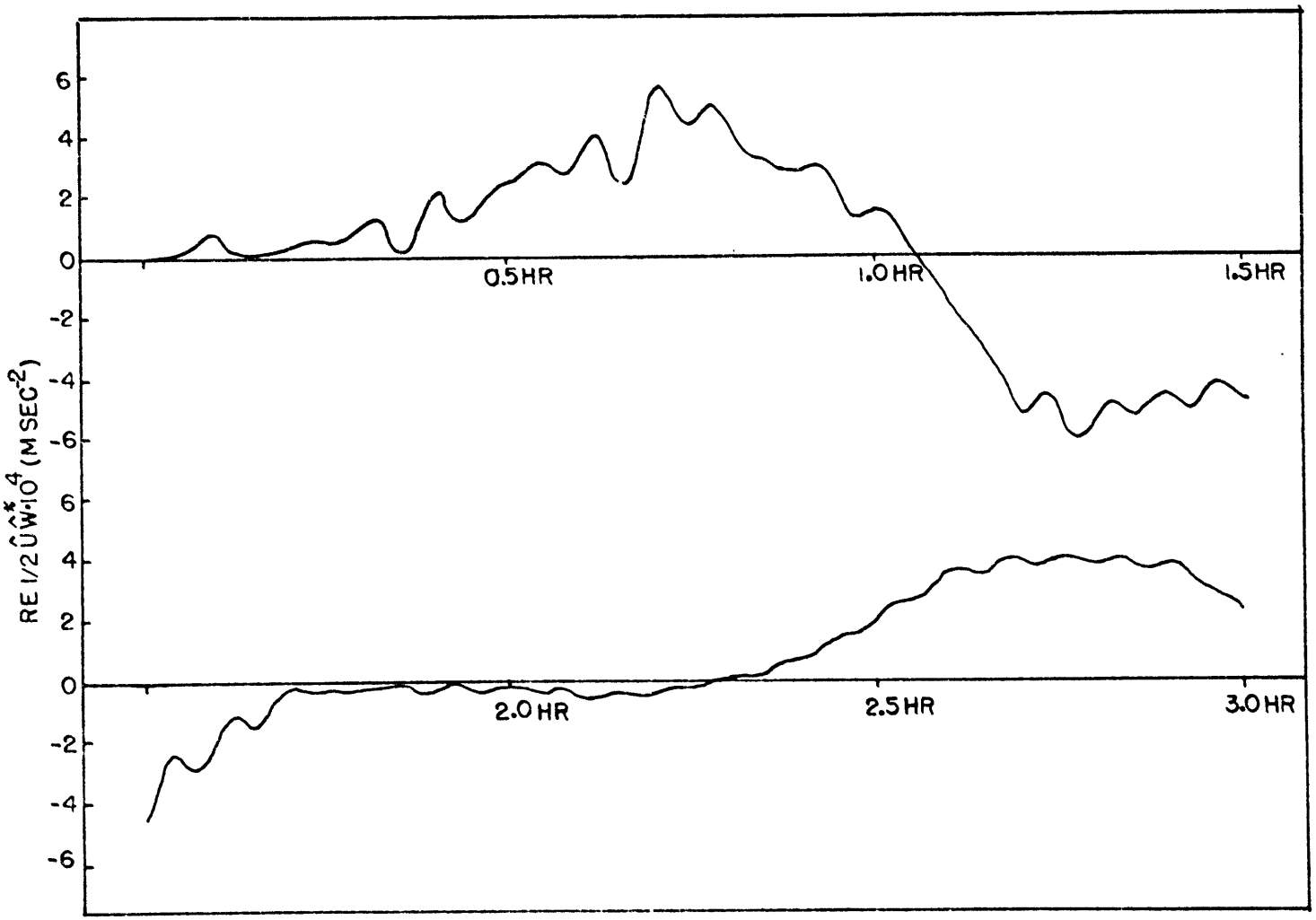

Figure 2.8b: The momentum flux term $\rho_e \frac{1}{2} \hat{u}\hat{w}^*$ at 9.5km showing the oscillatory behaviour of the flux with time.

not applicable. His work consisted of the integration of the equivalent of the first of equations (28) and he found that, for R_i small enough, the reflected wave had greater energy than the incident wave. This was termed over-reflection.

The time dependent behavior in such a case can be investigated by the numerical model. The conditions are exactly those of the shearing layer calculation except the mean wind has the shear zone shown in Fig. (2.8a) for which $R_i = 0.125$ and the amplitude of the forcing term depends on $(1 - e^{-\beta t})$, $\beta = 3/\text{hr}$.

Fig. (2.8b) gives the value of the momentum flux term at 9.5 km with time. The flux does not approach the constant value which would be expected if the wave energy penetrated, was absorbed by, or was partially or totally reflected by the critical level. This is completely different behavior than that of the previous case for which $R_i > 1/4$. The momentum flux as a function of z at 3 hours is given in Fig. (2.8a) and is quite different from that of Fig. (2.7a).

The wave motions are being over reflected at the critical level. The reflected waves carry momentum downward and this effect together with the continued forcing at the lower boundary result in an oscillatory momentum flux. The momentum flux above the critical level shows appreciable flux of negative momentum in this region which is a quite different result than that for the case $R_i > 1/4$. Thus for R_i sufficiently small the behavior at a critical level

changes markedly with appreciable momentum flux above the critical level and non-steady flux in the region below the critical level.

Summary

In this section a numerical model for the calculation of hydrostatic gravity-wave motions has been presented. The model has second order accuracy in truncation error and is stable for time steps of the order of 30 sec. Results have been obtained demonstrating the linear time dependent behavior of wave motions for several cases.

These examples give the behavior of the wave motions at a critical level for the cases of constant wind shear, time dependent wind shear, a shearing region, and a shearing region for which over-reflection occurs. The results point out the profound effects of a critical level on the wave motions and give insight into the mechanisms that will be involved when the acceleration of the mean flow is included directly in the calculations. Thus, the propagation of wave motions through a region of wind shear containing a critical level will reduce the vertical wavelength of the motions. The discontinuity of the momentum flux at a critical level will accelerate the mean flow and alter the intrinsic frequency of the waves permitting further vertical propagation. The acceleration of the mean flow will give rise to a shearing region in the mean wind which may violate the Richardson stability condition and lead to the production of wave motions or may cause the over-reflection of incident wave motions with the resulting oscillatory behavior of the momentum flux.

2.3 Non-linear effects

The linear theory of gravity wave motions has been extremely fruitful in explaining the behavior of the waves and retains its validity for a surprising array of conditions. The real atmosphere is not linear however and there are several reasons to begin the study of the non-linear characteristics of gravity waves. In the simplest case, the solutions to the gravity wave equations have a growth of amplitude with height of the form $e^{z/2}$. Non-linear effects will ultimately become important for waves capable of propagating to great heights. The behavior of a wave at a critical level demands that the resultant acceleration of the flow be taken into effect. Other topics such as the resonant interaction of waves and the correct specification of the energy of linearized motions require non-linear treatment.

2.3.1 The perturbation approach

One approach to the non-linear behavior of wave motions is in terms of the perturbation equations (6). Such methods have been used extensively for treatment of surface and internal waves in the ocean (e.g. Phillips, 1966) where the incompressible Bousinessq equations are used. Spizzichino (1969) has considered the interaction between a tidal and a gravity wave by this approach. Einaudi (1968) used a different perturbation expansion to show the non-linear steepening of the wave slopes with height which is a consequence of the $e^{z/2}$ growth of the wave amplitudes. Hines (1969)

discussed the form of the energy equation to second order in perturbation amplitude for the non-hydrostatic equations (equation (9) in this formulation).

Consider first the interaction of simple plane waves. The equations for inviscid, adiabatic motions with no rotation can be written in the form

$$\frac{\partial^2}{\partial t^2}(\omega_{zz} - \omega_z) + S_0 \nabla^2 \omega = F \tag{34}$$

where

$$F = \frac{\partial}{\partial t}\frac{\partial}{\partial z}\nabla_0 \cdot \left\{(\vec{u}\cdot\nabla + \omega\frac{\partial}{\partial z})\vec{u}\right\} - \nabla^2\left\{\vec{u}\cdot\nabla\phi_z + \omega(\phi_{zz}+k\phi_z)\right\} \tag{35}$$

The geopotential has been written as $\phi_0(z) + \phi(x,y,z,t)$ and ϕ_{0z} is taken to be constant. The linear equation of motion for $\vec{u}_0 = \omega_0 = 0$ is obtained by setting F = 0. Plane wave solutions of the form

$$\omega = Re\,\hat{\omega}\, e^{z/2} e^{i(\vec{K}\cdot\vec{x} - \nu t)}$$

$$\vec{K} = (k, m), \quad \vec{x} = (x, z)$$

give the usual frequency relation

$$\nu^2 = k^2 S_0 / (m^2 + 1/4)$$

The equation, to second order in perturbation magnitude, may be used to investigate the interaction between the simple first order wave solutions. The expression for F to second order involves only products of first order terms. If two plane wave solutions to the linearized equations are substituted into F the resulting expression will

have the form

$$
\begin{aligned}
& a e^{z} e^{i\{(\vec{K}_1+\vec{K}_2)\cdot\vec{x}-(\nu_1+\nu_2)t\}} \\
+\ & b e^{z} e^{i\{(\vec{K}_1-\vec{K}_2)\cdot\vec{x}-(\nu_1-\nu_2)t\}} \\
+\ & c e^{z} e^{2i\{\vec{K}_1\cdot\vec{x}-\nu_1 t\}} \\
+\ & d e^{z} e^{2i\{\vec{K}_2\cdot\vec{x}-\nu_2 t\}}
\end{aligned}
\tag{36}
$$

where the real part of this expression is to be taken.

Solutions to the second order equations will then have the form

$$
\begin{aligned}
\omega = \mathrm{Re}\Bigg\{ & \frac{a e^{z} e^{i\{(\vec{K}_1+\vec{K}_2)\cdot\vec{x}-(\nu_1+\nu_2)t\}}}{(\nu_1+\nu_2)^2\left[(m_1+m_2)^2-i(m_1+m_2)\right]-(k_1+k_2)^2 S_0} \\
& + \frac{b e^{z} e^{i\{(\vec{K}_1-\vec{K}_2)\cdot\vec{x}-(\nu_1-\nu_2)t\}}}{(\nu_1-\nu_2)^2\left[(m_1-m_2)^2-i(m_1-m_2)\right]-(k_1-k_2)^2 S_0} \\
& + \frac{c e^{z} e^{2i\{\vec{K}_1\cdot\vec{x}-\nu_1 t\}}}{(2\nu_1)^2\left[(2m_1)^2-i2m_1\right]-(2k_1)^2 S_0} \\
& + \frac{d e^{z} e^{2i\{\vec{K}_2\cdot\vec{x}-\nu_2 t\}}}{(2\nu_2)^2\left[(2m_2)^2-i2m_2\right]-(2k_2)^2 S_0} \Bigg\}
\end{aligned}
\tag{37}
$$

These solutions are second order forced motions and will be unimportant unless:

i) The denominators of the terms are zero, i.e. unless resonance can occur.

ii) The wave motions extend over a considerable vertical region so that the e^{z} dependence of the forced motions results in appreciable amplitude.

These solutions for motions forced by second order interactions of simple first order plane wave motions differ greatly from those appropriate to internal wave motions in the ocean. The wave solutions obtained using the Bousinessq approximation for the ocean satisfy the non-linear equations of motion and can thus be of finite amplitude. No forced solutions of the form $e^{2i(\vec{k}_1\cdot\vec{x}-\nu_1 t)}$, $e^{2i(\vec{k}_2\cdot\vec{x}-\nu_2 t)}$ occur. Furthermore it is possible to find combinations with real frequencies and wave numbers of first order waves which satisfy the resonance condition. This is not possible for simple waves in the atmosphere as can be seen from equation (37) except possibly in special cases such as $(\nu_1\pm\nu_2)=(k_1\pm k_2)=0$ For such cases it can be shown that the amplitudes in equation (37) are zero so that the forced solution does not arise.

One case for which the resonance condition can be approximately satisfied is the case for m_1, m_2 large. Then

$$(\nu_1\pm\nu_2)^2(m_1\pm m_2)^2-(k_1\pm k_2)^2 S_0\sim 0$$

can be satisfied for an appropriate choice of

$$\nu_1^2\sim\frac{k_1^2 S_0}{m_1^2}\quad,\quad \nu_2^2\sim\frac{k_2^2 S_0}{m_2^2}$$

The resonance condition is $\dfrac{(k_1\pm k_2)}{(m_1\pm m_2)}=\pm\dfrac{k_1}{m_1}\pm\dfrac{k_2}{m_2}$

much like that of internal waves in the ocean, (e.g. Phillips, 1966).

This case implies small vertical wavelength so that the effect of the $e^{z/2}$ amplitude dependence of the first order solutions is small. It is the effect of this amplitude dependence on height which alters the resonance condition for atmospheric waves. It is interesting to speculate that the introduction dissipation into the equations would allow a choice of complex wave numbers which would satisfy a resonance condition but there does not seem to be any simple example of this.

The energy equation for the perturbation equations of motion is of note. For the first order equations of motion the usual energy equation was obtained in the form

$$\frac{\partial \rho \mathcal{E}}{\partial t} + \frac{\partial}{\partial x} \rho \left(u_0 \mathcal{E} + u_1 \phi_1 \right) + \frac{\partial}{\partial z} \rho w_1 \phi_1 = -u_{0z} \rho u_1 w_1$$

$$\text{where } \mathcal{E} = \frac{u_1^2}{2} + \frac{\phi_{1z}^2}{2 S_0} \tag{38}$$

The equation involves the product of terms of first order in perturbation magnitude. The equation is not the total energy equation correct to the second order in perturbation magnitude however. The corresponding second order energy equation is

$$\frac{\partial \rho E_2}{\partial t} + \frac{\partial}{\partial x} \rho \left\{ (E_0 + \phi_{0z}) u_2 + (E_1 + \phi_{1z}) u_1 + (E_2 + \phi_{2z}) u_0 \right\}$$
$$+ \frac{\partial}{\partial z} \rho \left\{ (E_0 + \phi_{0z} w_2 + (E_1 + \phi_{1z}) w_1 + \phi_{2t} \right\} = 0 \tag{39}$$

$$E_0 = \frac{u_0^2}{2} + C_v T_0 + \phi_0$$

$$E_1 = u_0 u_1 + C_v T_1 + \phi_1$$

$$E_2 = u_0 u_2 + \frac{u_1^2}{2} + C_v T_2 + \phi_2$$

This equation can only be evaluated if the second order motions u_2, w_2, ϕ_2 are known as opposed to equation (38) which involves only the first order terms.

Hines (1969) obtained the second order energy equation for simple non-hydrostatic motions by solving the second order equations and evaluating the terms. It is worth doing this for the hydrostatic equations as the results have a much simpler and clearer form.

The simple case considered here is that for u_0 = constant. The simple plane wave solutions for the first order equations have been given in section (2.15). The second order perturbation equations with u_0 = constant are;

$$\begin{aligned} &u_{2t} + u_0 u_{2x} + \phi_{2x} = -\{u_1 u_{1x} + w_1 u_{1z}\} \\ &w_{2z} - w_2 + u_{2x} = 0 \\ &\phi_{2zt} + u_0 \phi_{2zx} + w_2 S_0 = -\{u_1 \phi_{1zx} + w_1(\phi_{1zz} + k\phi_{1z})\} \end{aligned} \tag{40}$$

The first order plane wave solutions are substituted into the R.H.S. of the equations. These terms can be shown to have the form

$$Re\, a\, e^{z}\, e^{2i(kx + mz - \nu t)}$$

The second order solutions will thus have the same form and no second order steady motions are included.

If the energy equations are averaged over a wavelength in the x-coordinate, indicated by a bar $\overline{(\ )}$, they become

$$\frac{\partial}{\partial t} p\bar{E} + \frac{\partial}{\partial z} p\overline{w_1 \phi_1} = 0$$

$$\frac{\partial}{\partial t} p\bar{E}_2 + \frac{\partial}{\partial z} p\left\{ \overline{(E_0 + \phi_{0z})w_2} + \overline{(E_1 + \phi_{1z})w} + \overline{\phi_{2t}} \right\} = 0$$

The energy density and vertical energy flux terms so defined can be evaluated in terms of the complex wave amplitudes of the solutions of the form

$$(u_1, \omega_1, \phi_1) = Re\,(\hat{u}_1, \hat{\omega}_1, \hat{\phi}_1)\, e^{z/2} e^{i(kx+mz-\nu t)}$$

$$(u_2, \omega_2, \phi_2) = Re\,(\hat{u}_2, \hat{\omega}_2, \hat{\phi}_2)\, e^{z} e^{2i(kx+mz-\nu t)}$$

The resulting equations are

$$\frac{\partial}{\partial t} \rho_0 \left\{ \frac{|\hat{u}_1|^2}{2} + \frac{|\hat{\phi}_{1z}|^2}{2S_0} \right\} + \frac{\partial}{\partial z} \rho_0 \left\{ \hat{\omega}_1^* \hat{\phi}_1 \right\} = 0$$

$$\frac{\partial}{\partial t} \rho_0 \left\{ \frac{|\hat{u}_1|^2}{2} \right\} + \frac{\partial}{\partial z} \rho_0 \left\{ u_0 \hat{u}_1 \hat{\omega}_1^* + \hat{\omega}_1^* \hat{\phi}_1 \right\} = 0$$

The vertical energy flux associated with the usual energy equation in this simple case differs from the "total" vertical energy flux to second order as does the energy density. For more complicated cases such as $u_0 = u_0(z)$ the second order solutions are not easily obtained but the identification of the $\overline{\omega\phi}$ term with the "total" vertical energy flux is certainly incorrect. There does not appear to be any way of obtaining the correct second order energy result using only the first order equations of motion. The results obtained in terms of the "usual" linear energy equations must always be considered in this light. In the following section, calculations involving the interaction of a gravity wave with the mean flow are presented. The energy equation which arises is a more general form of the second order "total" energy equation.

2.3.2 A numerical approach to non-linear wave motions

In this section some numerical results will be presented which are obtained by solving the non-linear equations of motion for a truncated Fourier expansion of the variables. The purpose of the calculations is to gain insight into the meteorological consequences of the interaction of gravity waves with the mean flow at a critical level.

Assuming the motions have an exact periodicity in x they may be expanded in Fourier series. The expansion has the form

$$\xi(x,z,t) = \sum_{n=-\infty}^{\infty} E(n,z,t)\, e^{iNx}, \quad N = 2\pi n/L$$

$$E(n,z,t) = \frac{1}{L}\int_0^L \xi(x,z,t)\, e^{-iNx}$$

$$E(n,z,t) = E^*(-n,z,t)$$

$$\frac{1}{L}\int_0^L \xi(x,z,t)\, f(x,z,t)\, e^{-iNx}dx = \sum_{m=-\infty}^{\infty} E(n-m)\,\bar{F}(m)$$

The equations of motion may be put in the following form in terms of the complex Fourier coefficients

$$\frac{\partial u(n)}{\partial t} + \sum_{m=-\infty}^{\infty}\left\{ iM\,u(m)u(n-m) + w(n-m)\frac{\partial}{\partial z}u(m)\right\} + iN\phi(n) = -\alpha\left(u(n) - u(n,t=0)\right)$$

$$\frac{\partial w(n)}{\partial z} - w(n) + iN u(n) = 0 \qquad (41)$$

$$\frac{\partial^2}{\partial t\,\partial z}\phi(n) + \sum_{m=-\infty}^{\infty}\left\{ u(n-m)\, iM\frac{\partial \phi(m)}{\partial z} + w(n-m)\frac{\partial}{\partial z}\left(\frac{\partial \phi(m)}{\partial z} + k\phi(m)\right)\right\} = -\alpha\frac{\partial}{\partial z}\left(\phi(n) - \phi(n,t=0)\right)$$

$$\frac{\partial \phi(n)}{\partial t} + \sum_{m=-\infty}^{\infty} \left\{ u(n-m)\, i M \phi(m) + w(n-m) \frac{\partial}{\partial z} \phi(n) \right\} = g\, w(n) \quad \text{at } z=0$$

The non-linear solutions to the equations of motion can be calculated to arbitrary accuracy by the retention of a sufficient number of terms in the Fourier expansion.

2.3.3 The interaction of the mean flow and one Fourier component

The simplest set of equations which retains the interaction of the mean flow with the wave motion is obtained by keeping only the mean and first Fourier component in the expansion. In terms of the complex Fourier amplitudes the equations are:

$$\begin{aligned}
&u_{1t} + ikU_0 u_1 + w_1 U_{0z} + ik\phi_1 = -\alpha (u_1 - u_1(t=0)) \\
&w_{1z} - w_1 + iku_1 = 0 \\
&\phi_{1zt} + ikU_0 \phi_{1z} + w_1 S_0 = -\alpha (\phi_{1z} - \phi_{1z}(t=0)) \\
&\phi_{1t} + ikU_0 \phi_1 + w_1 \phi_{0z} = g w_1 \quad \text{at } z=0 \qquad (42) \\
&U_{0t} + w_1^* u_{1z} + w_1 u_{1z}^* = -\alpha (U_0 - U_0(t=0)) \\
&\phi_{0zt} + ik \{ u_1^* \phi_{1z} + u_1 \phi_{1z}^* \} + w_1^* S_1 + w_1 S_1^* = 0 \\
&\phi_{0t} + ik \{ u_1^* \phi_1 - u_1 \phi_1^* \} + \{ w_1^* \phi_{1z} + w_1 \phi_{1z}^* \} = 0 \quad \text{at } z=0
\end{aligned}$$

where

$$S_0 = \frac{\partial}{\partial z} (\phi_{0z} + k\phi_0)$$

$$S_1 = \frac{\partial}{\partial z} (\phi_{1z} + k\phi_1)$$

$$k = 2\pi / L$$

The total energy averaged over the fundamental period is

$$\frac{1}{L}\int_0^L E\,dx = \sum_{n=-\infty}^{\infty} \frac{|u_n|^2}{2} + C_v T_0 + \phi_0$$

and the averaged energy equation is

$$\frac{\partial}{\partial t} p\left\{ \sum_{n=-\infty}^{\infty} \frac{|u_n|^2}{2} + C_v T_0 + \phi_0 \right\}$$
$$+\frac{\partial}{\partial z} p\left\{ \sum_{n=-\infty}^{\infty} \omega_n^* \left(\frac{\phi_{nz}}{K} + \phi_n \right) + \frac{1}{2} \sum_{m=-\infty}^{\infty} u_m \sum_{n=-\infty}^{\infty} u_{n-m}\, \omega_n + \phi_{0\epsilon} \right\} = 0$$

For one Fourier component this becomes

$$\frac{\partial}{\partial t} p\left\{ \frac{u_0^2}{2} + |u_1|^2 + C_v T_0 + \phi_0 \right\} \qquad (44)$$
$$+2\,\mathrm{Re}\,\frac{\partial}{\partial z} p\left\{ u_0 u_1 \omega_1^* + \frac{\omega_1^* \phi_{1z}}{K} + \omega_1^* \phi_1 + \frac{\phi_{0\epsilon}}{2} \right\} = 0$$

This equation can be obtained directly from the equations (42).

The equation for ϕ_{0z} can be written as

$$(p\phi_{0z})_t + \left(\frac{\partial}{\partial z} + K\right) p\left(\omega_1^* \phi_{1z} + \omega_1 \phi_{1z}^*\right) = -\alpha p\left(\phi_0 - \phi_{0(t=0)}\right)$$

For motions which are sinusoidal in time the term $\omega_1^* \phi_{1z} + \omega_1 \phi_{1z}^*$ is zero. As the motions are forced sinusoidally at the lower boundary, the calculated value of this term will be negligible. The assumption is made that the mean value of the geopotential is constant in time.

2.3.4 Results of calculations for one Fourier component

The amplitudes of the first Fourier component in equations (42) were scaled by $e^{-z/2}$, (i.e., $\hat{u}_1 = e^{-z/2} u_1$) to remove this growth of amplitude with height for the calculated values. The finite difference grid used for the calculation is given in Fig. (2.1) and the finite difference equation used were; (dropping the subscript for the first Fourier component),

$$\frac{\hat{u}_j^{\tau+1} - \hat{u}_j^{\tau}}{\Delta t} + \left(\frac{ik}{2}\left(u_{0j+1}^{\tau} + u_{0j}^{\tau}\right) + \alpha_j \right)\left(\frac{\hat{u}_j^{\tau+1} + \hat{u}_j^{\tau}}{2} \right)$$
$$+ \frac{1}{4}\left(\hat{\omega}_{j+1}^{\tau+1} + \hat{\omega}_j^{\tau+1} + \hat{\omega}_{j+1}^{\tau} + \hat{\omega}_j^{\tau}\right)\left(\frac{u_{0j+1}^{\tau} - u_{0j}^{\tau}}{\Delta z}\right) + ik\hat{\phi}_j^{\tau} = 0$$

$$\frac{\hat{\omega}_{j+1}^{\tau+1} - \hat{\omega}_j^{\tau+1}}{\Delta z} - \frac{1}{4}\left(\hat{\omega}_{j+1}^{\tau+1} + \hat{\omega}_j^{\tau+1}\right) + ik\hat{u}_j^{\tau+1} = 0$$

$$\frac{\hat{\phi}_{j+1}^{\tau+1} - \hat{\phi}_{j+1}^{\tau} - \left(\hat{\phi}_j^{\tau+1} - \hat{\phi}_j^{\tau}\right)}{\Delta t \Delta z} + \frac{\hat{\phi}_{j+1}^{\tau+1} - \hat{\phi}_{j+1}^{\tau} + \hat{\phi}_j^{\tau+1} - \hat{\phi}_j^{\tau}}{4\Delta t}$$
$$+ \left\{ \frac{ik}{2}\left(u_{0j}^{\tau+1} + u_{0j}^{\tau}\right) + \alpha_j \right\}\left\{ \frac{\hat{\phi}_{j+1}^{\tau+1} + \hat{\phi}_{j+1}^{\tau} - \left(\hat{\phi}_j^{\tau+1} + \hat{\phi}_j^{\tau}\right)}{2\Delta z} + \frac{1}{8}\left(\hat{\phi}_{j+1}^{\tau+1} + \hat{\phi}_{j+1}^{\tau} + \hat{\phi}_j^{\tau+1} + \hat{\phi}_j^{\tau}\right) \right\}$$
$$+ \hat{\omega}_{j+1}^{\tau+1} S_0 = 0$$

$$\frac{u_{0j}^{\tau+1} - u_{0j}^{\tau}}{\Delta t} + e^{\Delta z j}\left\{ \hat{\omega}_j^{*\tau+1}\left(\frac{\hat{u}_j^{\tau+1} - \hat{u}_{j-1}^{\tau+1}}{\Delta z} \right) + \hat{\omega}_j^{\tau+1}\left(\frac{\hat{u}_j^{*\tau+1} - \hat{u}_{j-1}^{\tau+1}}{\Delta z} \right) \right\} = -\alpha_j \left[u_{0j}^{\tau} - u_{0j}^{\tau=0} \right)$$

$$\frac{\hat{\phi}_1^{\tau+1} - \hat{\phi}_1^{\tau}}{\Delta t} + \frac{ik}{2}\left(u_{01}^{\tau+1} + u_{01}^{\tau}\right)\left(\frac{\hat{\phi}_1^{\tau+1} + \hat{\phi}_1^{\tau}}{2}\right) + \phi_{0z}\left(\frac{\hat{\omega}_2^{\tau+1} + ik\hat{u}_1^{\tau+1}\Delta z/2}{(1+\Delta z/4)} \right) = g\hat{\omega} \quad \text{at } z=0$$

The calculation proceeds in a manner similar to that of the linear case. The initial values of all variables are zero except for u_0 and ϕ_0 which are specified functions of height. The value of ϕ_0 is $\phi_0 = RT_0 z$ in each case corresponding to a constant temperature of 250°K. The motions are dissipated in the upper portion of the region of integration as was done in the linear case.

The motions are forced at the lower boundary exactly as in the linear case except that the amplitude of the forcing term is reduced to w = 0.1 m/sec. The time step used in each case is Δt = 30 sec and Δz corresponds to 125 m unless otherwise noted.

Case I, $u_0 = 0$ initially

In this case u_0 is initially zero everywhere. The region of integration is 60 km in the vertical and the motions were dissipated in the upper 20 km of the region $z > z_0$ i.e.,

$$\alpha = \begin{cases} 0.002\left(-1 + e^{0.87(z-z_0)}\right), & z > z_0 \\ 0, & z < z_0 \end{cases}$$

The forcing was begun impulsively at t = 0 and Δz corresponded to 250 m for this case.

As in the linear case the values presented are the solutions at x = 0 unless otherwise specified and are scaled with $e^{-z/2}$. Thus for $w = 2 Re\, \hat{w}_1 e^{z/2} e^{ikx}$ the graph of $Re\, \hat{w}_1$ is presented in Figure (2.9) together with the value of u_0 after three hours. The points of note are;

i) The graph of ω shows the appropriate wavelike behavior with a vertical wavelength which agrees with that given by the frequency relation (14). The motions are damped out in the dissipative region and do not reach the upper boundary.

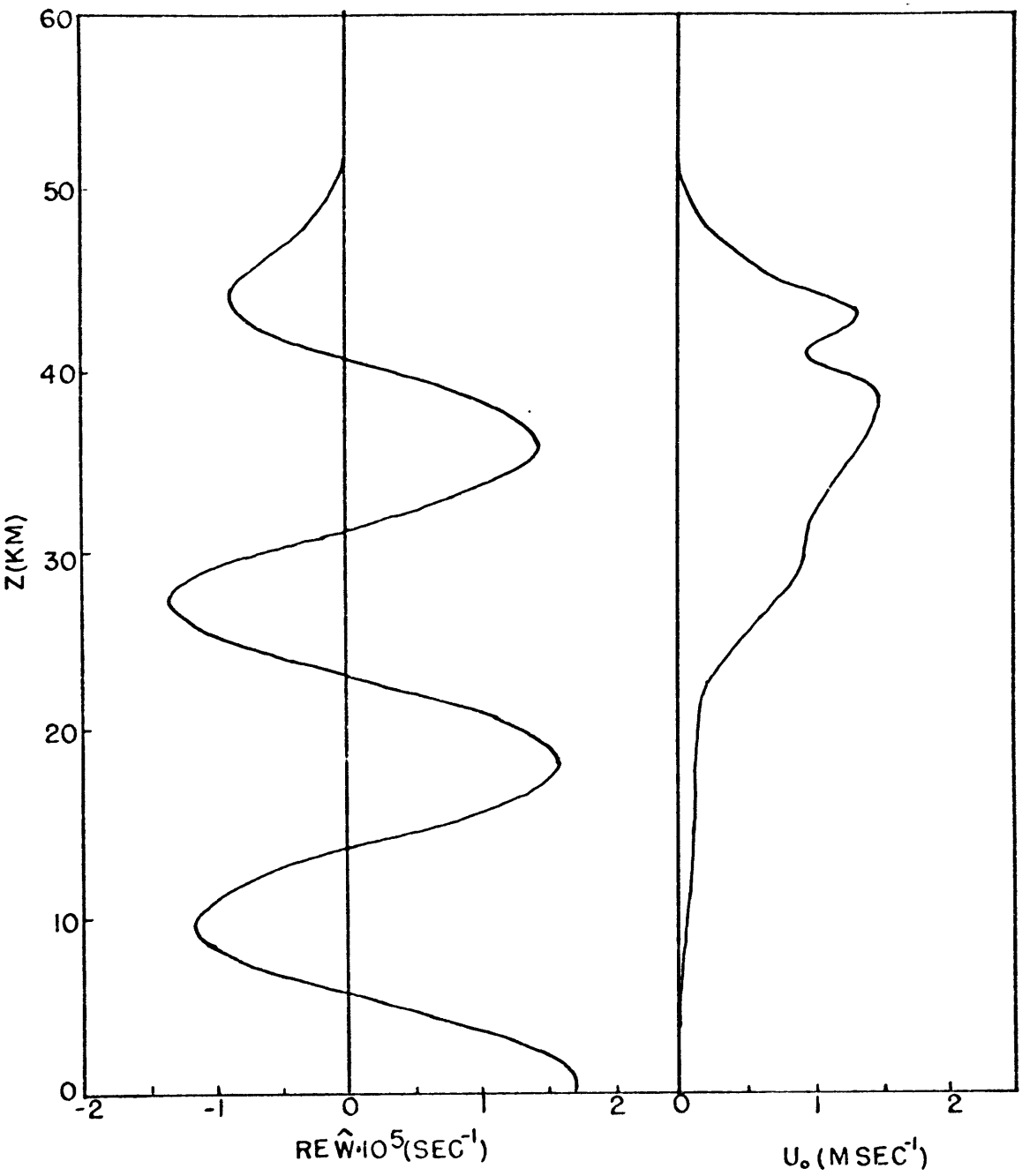

Figure 2.9: The vertical profile of the vertical component $Re\,\hat{\omega}$ of the wave motions and of the mean wind u_0 at three hours.

ii) The graph of u_0 shows induced velocities with a maximum magnitude of about 1.5 m/sec. This is a consequence of the gradient of momentum flux of the waves as they propagate upwards from the lower boundary. The equation for u_0 ,

$$u_{0t} = -2\rho^{-1} \mathrm{Re}\,(\rho u_1 w_1^*) \tag{45}$$

shows this dependence. The induced motions are larger at higher altitudes because of the decrease of density with height.

iii) The mean motion in the dissipative region above 40 km shows an increase in amplitude followed by a decrease to zero. The increase is the result of the gradient of momentum flux of the waves caused by the damping. This acceleration of u_0 is counteracted by the direct linear frictional damping only at higher levels in the damping region. An effect of this nature can occur in the real atmosphere where the waves are dissipated by viscosity, turbulence, or non-adiabatic effects. Bretherton (1969) discusses the effect of turbulent dissipation on mountain waves.

This effect is partially suppressed in the remaining calculations by increasing the amplitude of α to 0.02 in the dissipation term for the mean flow. As very little momentum reaches the damping region in subsequent calculations these considerations are not of great importance.

Case II, Linear mean wind with critical level.

The region of integration was 35 km in the vertical with the upper 10 km acting as the damping region. The damping parameter for the wave motions was

$$\alpha = \begin{cases} 0.002\left(e^{0.74(z_0 - z)} - 1\right) \text{ sec}^{-1}, & z > z_0 \\ 0, & z < z_0 \end{cases}$$

where z_0 is at 25 km. For the mean wind the value of α = 0.02 sec^{-1} was chosen. As relatively little energy propagates into the damping region in this calculation the damping conditions are not of great importance.

The mean wind was initially a linear function of height. The value of u_0 at three hour intervals is shown in Figs. (2.10). The graphs of $\text{Re}\, \frac{1}{2}\hat{u}_1\hat{w}_1^*$ and $\text{Re}\, \hat{u}_1$ are given in Figs. (2.11, 2.12).

The motions were forced at the lower boundary as usual. The amplitude of the vertical velocity at the lower boundary was given by $\hat{w}_1 = 0.1\left(1 - e^{-\beta t}\right)$ m/sec for $\beta = 1/(3 \text{ hrs})$.

In this case the forced motions propagate upward through the region of wind shear towards a critical level at 20 km where $u_0 = 55.5$ m/sec. The wave motions will interact with the mean wind and the change of the mean wind will alter the propagation characteristic of the waves and so on. The rate of change of u_0 depends on the momentum flux gradient as pointed out in the previous case (equation 45).

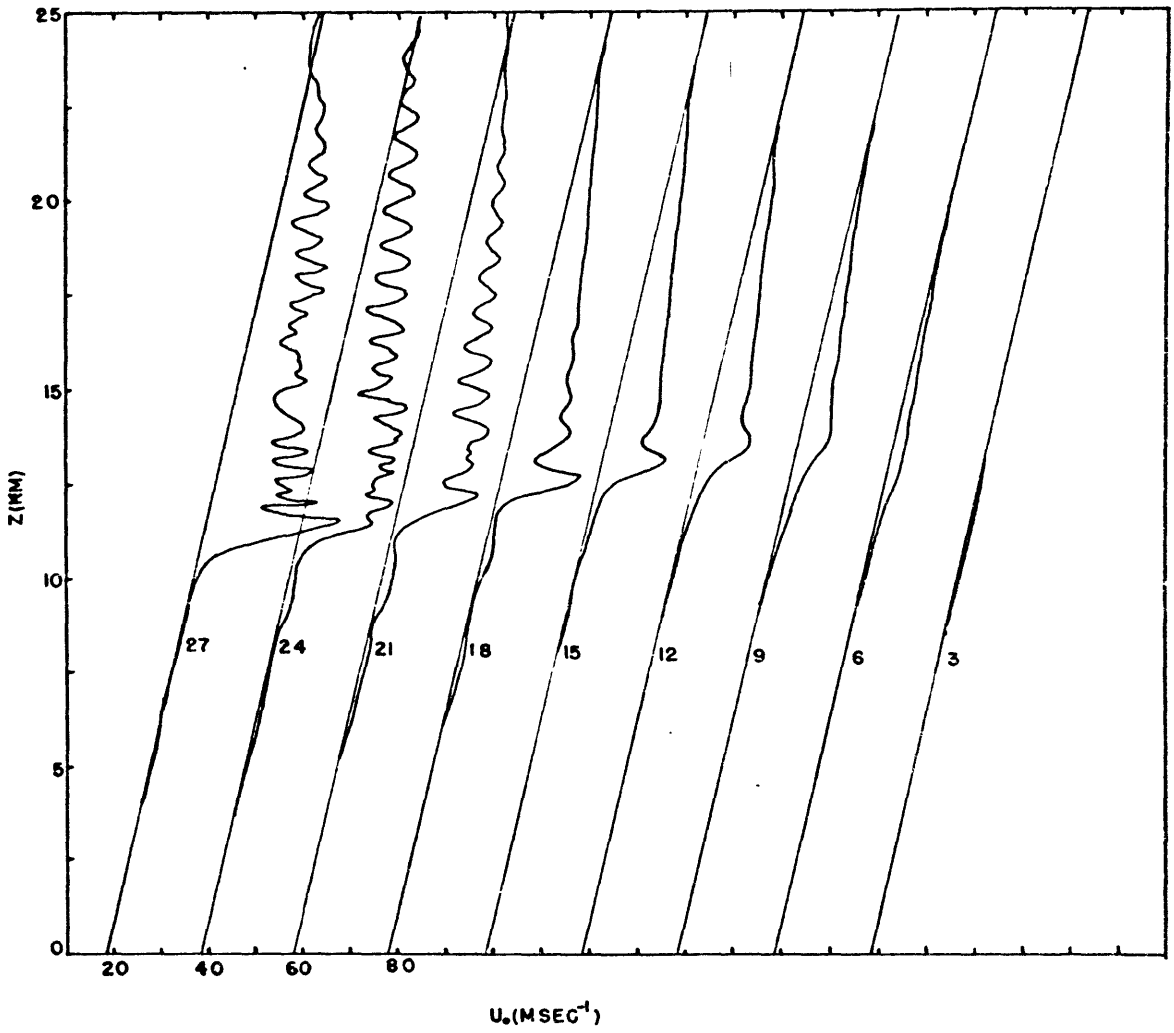

Figure 2.10: The vertical profile of the mean wind U_o at three hour intervals from 3 to 27 hours. The straight lines show the linear profile of the wind at time zero. The profiles have been displaced by an amount corresponding to 20 m/sec to facilitate comparison.

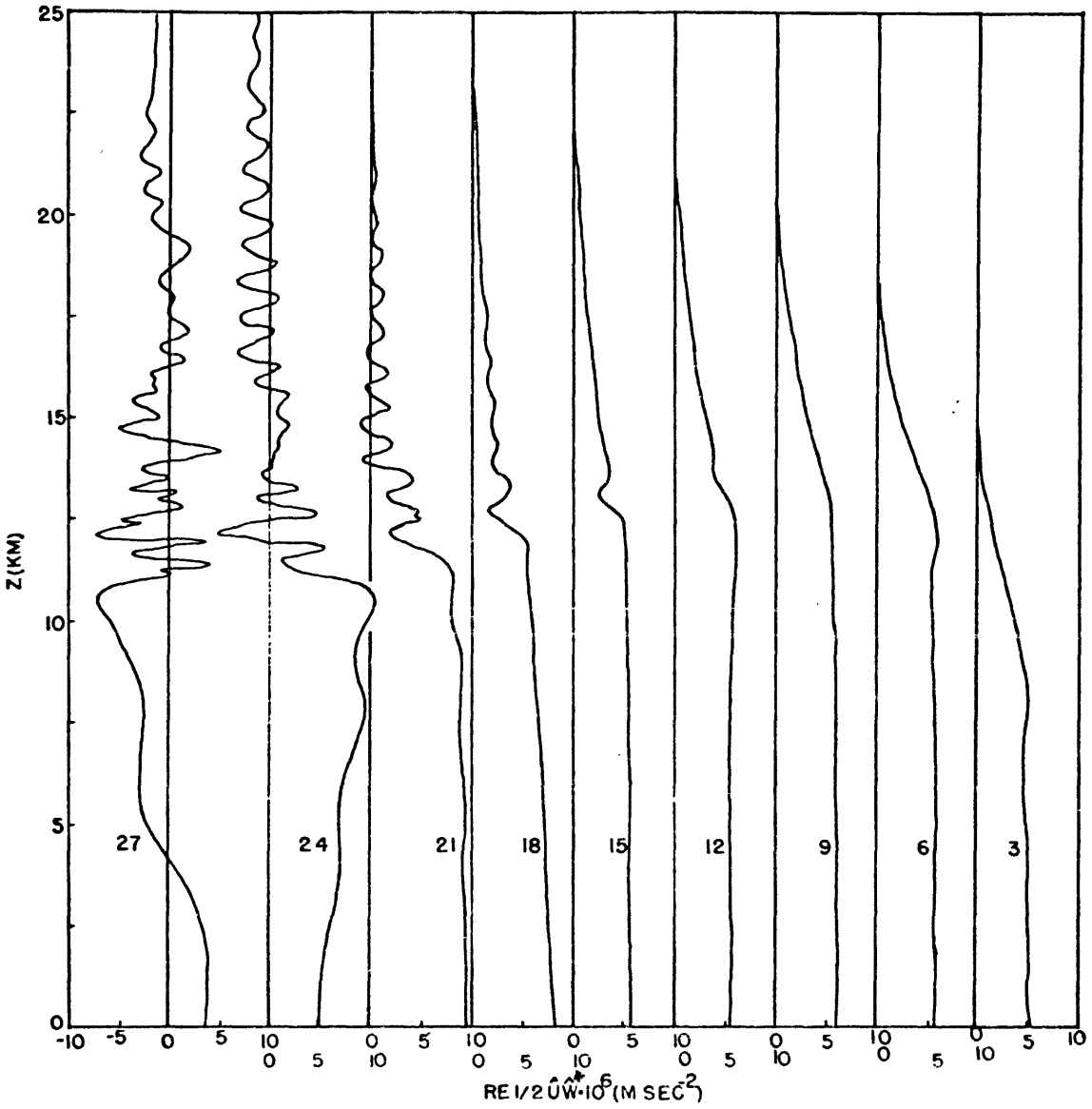

Figure 2.11: The vertical profiles of the momentum flux term $R_e \frac{1}{2} \hat{u}\hat{\omega}^*$ at three hour intervals from 3 to 27 hours.

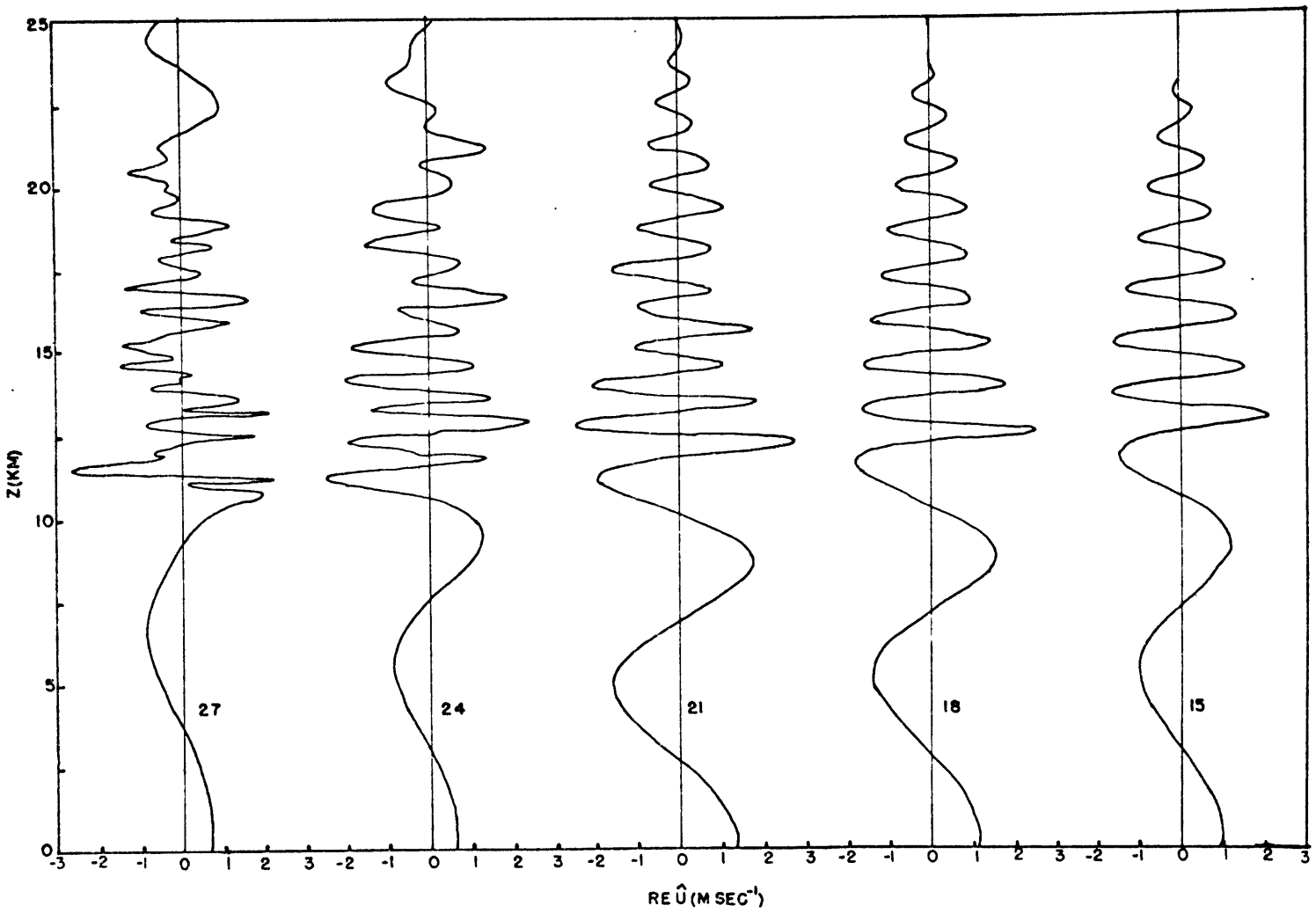

Figure 2.12: The vertical profiles of the horizontal component $Re\,\hat{u}$ of the wave motions at three hour intervals from 15 to 27 hours.

The first effect of note is the acceleration of u_0 in a region well below the critical level during the early stages of the calculation. This is not a critical level interaction but is a consequence of the momentum flux gradient set up by the propagation of the waves into the region of wind shear. Such accelerations were obtained in the previous case where $u_0 = 0$ initially. The form of u_0 at $t = 0$ will determine the importance of this effect.

The acceleration of u_0 continues as time goes on and leads to the formation of a region of shear in u_0 at the base of a region of accelerated motion. The profile of u_0 develops a "nose" with a region of positive u_{0z} below and negative u_{0z} above. The shears grow in magnitude with time and the base of the accelerated region descends. After 15 hours a wave like structure appears in the vertical profile of u_0 which grows in amplitude and is established at higher levels as time goes on. At 18 hours the value of the Richardson number, $R_i = S_0 / u_{0z}^2$ at the base of the nose in u_0 is approximately 1/4 while in the region of negative shear above the nose, $R_i > 1/4$. After 18 hours irregular small scale features appear in the profile of u_0 and become established at higher levels with time.

The graphs of the momentum flux show corresponding features. Up to 12 hours, the propagation of the wave motions from the lower boundary establishes a region of constant flux in the lower levels and a gradient of flux which penetrates to higher levels with time. This serves to accelerate u_0 over the broad region below the critical level. After 12 hours a "inverse nose" is established in the flux

profile where the regions of positive and negative gradient imply the acceleration and decelleration of u_o which causes the "nose" in the wind profile. The profile of the momentum flux mirrors the behavior of the mean flow as would be expected. After 18 hours the irregular small scale vertical structure appears in the profile of the flux. The flux below the region of maximum gradient is no longer linear with z. The value of the flux with time in this region shows on oscillatory behavior. At upper levels a negative momentum flux becomes established.

The profiles of $Re\ \hat{u}$ to 15 hours show the existence of the wave motions through most of the region with reduced vertical wavelengths in the accelerated region. After 18 hours the vertical profiles also show the irregular small scale structure seen in the other variables.

The behavior of the flow with time may be interpreted in terms of the mechanisms discussed in the linear calculations and several interesting points may be noted:

The acceleration of the mean flow in the early stages of the calculation as a consequence of the penetration of the region by the wave motions has been mentioned above. The effect of this is to move the region of primary interaction of the wave and the mean flow away from the position of the "initial" critical level at 20 km. It also points out the ambiguity of defining a critical level in terms of the forcing frequency and the value of u_o (i.e., $\sigma = \nu - k u_o = 0$). The acceleration of u_o by the waves alters the local value of the frequency of the waves as pointed out in the linear calculation for σ

and the interaction need not occur near the "initial" critical level. This also shows that the mean wind need not have a critical level initially for interaction to occur but that the penetration of the region by the wave may set up the conditions for interaction.

The interaction of the wave and the mean flow at 12 and 15 hours results in the "nose" in u_0 and subsequently in a regular variation of the profile with height which becomes established at higher levels with time. This is a consequence of the mutual interaction of the wave and the mean flow in a manner similar to that discussed in the linear case for $u_0 = u_0(z,t)$. The features show oscillatory behavior in time with a period of several hours.

At 18 hours the shears in u_0 have increased and violated the Richardson stability condition. The motions show irregular small-scale structure in the vertical at later times. This is likely the result of instability of the flow. The numerical model cannot, however, adequately model this phenomenon as a fixed horizontal wavelength is assumed. Another effect which appears to be active is that of over-reflection which was discussed for the linear case. There is the oscillatory momentum flux with time in the region below the shear level as was found in the linear case. No irregular vertical structure has appeared in this lower region as it does in the accelerated region.

The increase in u_{0z} results in the decrease of the attenuation factor $\exp(-2\pi\sqrt{Ri-1/4})$ of linear theory. The application to the non-linear case is not direct but the momentum flux does show an increasingly

negative momentum flux in the accelerated region. This may be a consequence of both the increased penetration of momentum across the shear zone and instabilities.

The upshot of this is that energy is being transmitted both upward and downward out of the accelerated region. The motions also exhibit irregular small-scale structure which suggests that turbulent motions would occur in the real atmosphere. The lower boundary of the accelerated region continues to descend with time. The importance of the critical level interaction as both a sink and a source of wave motions is obvious. The transmission and reflection of wave energy in a region with variable u_0 is essentially a non-linear process. Linear estimates will be inherently ambiguous. The results depend on the original distribution of u_0, the amplitude of the wave motion, and the length of time for which the wave motions continue.

The possibility of regions of turbulent motions extending over appreciable extent in the vertical is also of importance. The character of the interaction may again change if turbulent dissipation becomes of importance and enhanced turbulence will have an effect on the diffusion processes operating in the region.

The results of the calculation, as discussed above, must also be considered in the light of the following considerations:

i) The calculation models the interaction of a wave with a well defined frequency and wavelength propagating into the region of wind shear. Wave motions in the atmosphere have a distribution of

frequencies and wavelengths. The single component may not be too bad an approximation for certain cases in the atmosphere however as it is possible that particular sources of wave motion will dominate the spectrum at certain times and produce a peak in the spectrum. The spectral analysis of a set of ROBIN soundings of the atmosphere in terms of vertical wavelength is discussed in a later section and shows a fairly concentrated peak. The presence of other components of the wavemotions would alter the interaction of the waves with the mean flow depending on the distribution of phase speeds of the waves. The finite differencing in the calculation will smear out the interaction of the wave and the mean flow.

ii) The effect of viscosity and heat conduction in the region of a critical level might be expected to become intense due to the short vertical wave lengths predicted by linear theory. Hazel (1969) investigated this problem and found that even in the linear case the effect is negligible. This may become more important, however, if enhanced turbulent motions develop as a consequence of the interaction.

iii) The calculation has been performed for a long period of time. The existence of reasonably consistent trains of waves in the atmosphere for times of the order of a day is implied. The amplitude of the wave motion at the lower boundary is not inconsistent with the amplitude observed at the peak in the spectrum of the observed motions discussed in a later section. The amplitudes are larger in the region of interaction of course. The observations do not apply to waves for which critical level interactions are occurring.

iv) The calculation allows only a single horizontal wavelength for the motions. The model does not admit of harmonics (in x) of the forced wave motion due to non-linear interactions. Possible instability due to the violation of the Richardson stability condition or to other conditions can be manifest only for motions with the given horizontal wavelength.

Case III, Jet in the mean wind

The calculation proceeds exactly as before, the only difference being the initial form of u_o which has the jet-like structure shown in Fig. (2.13). Figs. (2.14, 2.15) display the momentum flux term $Re\,\frac{1}{2}\hat{u}\hat{w}^*$ and $Re\hat{u}$ . .

There are two critical levels in the mean flow at $\Delta t = 0$ where $u_o = 55.5$ both above and below the maximum velocity in the jet-like structure of the mean wind. In this case the initial form of u_o is such that the wave motions undergo interaction with the mean flow much nearer the critical level than was the case for the linear wind profile. This is the result of the concentrated shear region in $u_o(t=0)$. It requires much less time, in this case, to develop the accentuated shear in u_o which is a consequence of the interaction. From 6 hours onward, there exist regions of both positive and negative u_{oz} for which $R_i < 1/4$. The momentum flux and u_o again develop small irregular vertical wavelengths in their profiles in the region of interaction and below this region the momentum flux varies in an oscillatory manner. The profile of $Re\,\hat{u}$ also changes dramatically. The lower

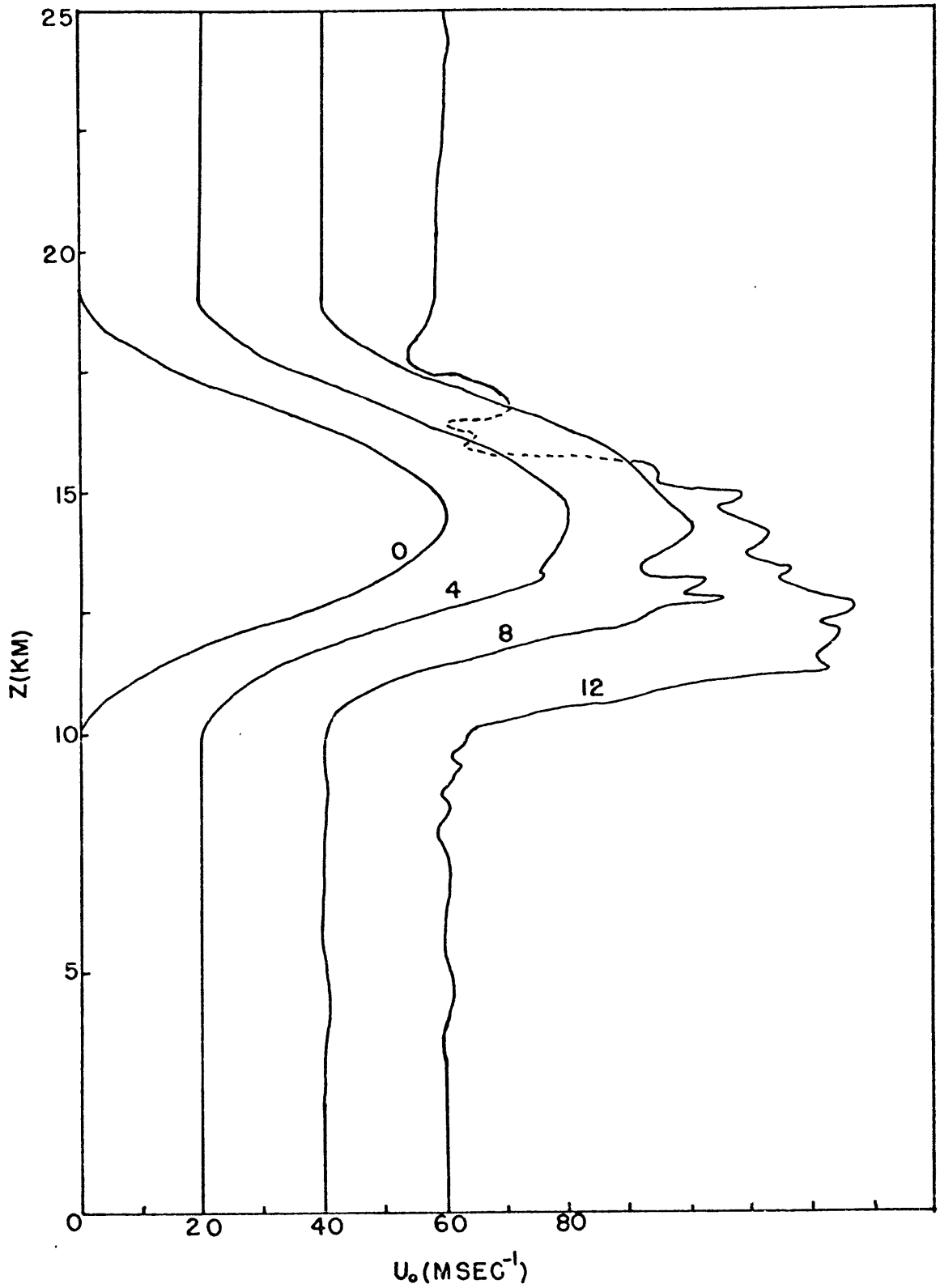

Figure 2.13: The vertical profiles of the mean wind u_o at four hour intervals from 0 to 12 hours. The profiles have been displaced by an amount corresponding to 20 m/sec to facititate comparison.

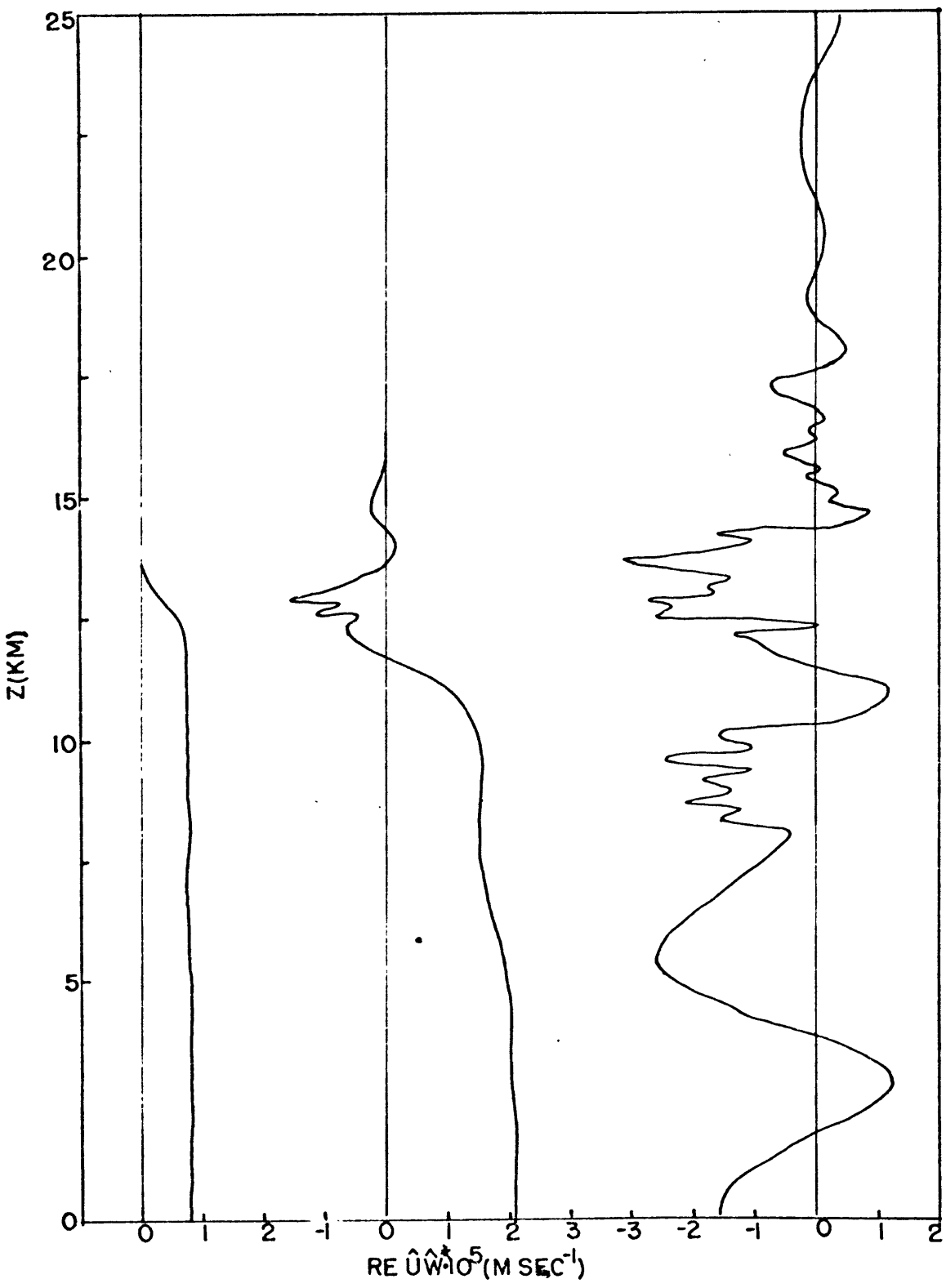

Figure 2.14: The vertical profiles of the momentum flux term $Re\frac{1}{2}\hat{u}\hat{w}^*$ for the wave motions at 4,8 and 12 hours.

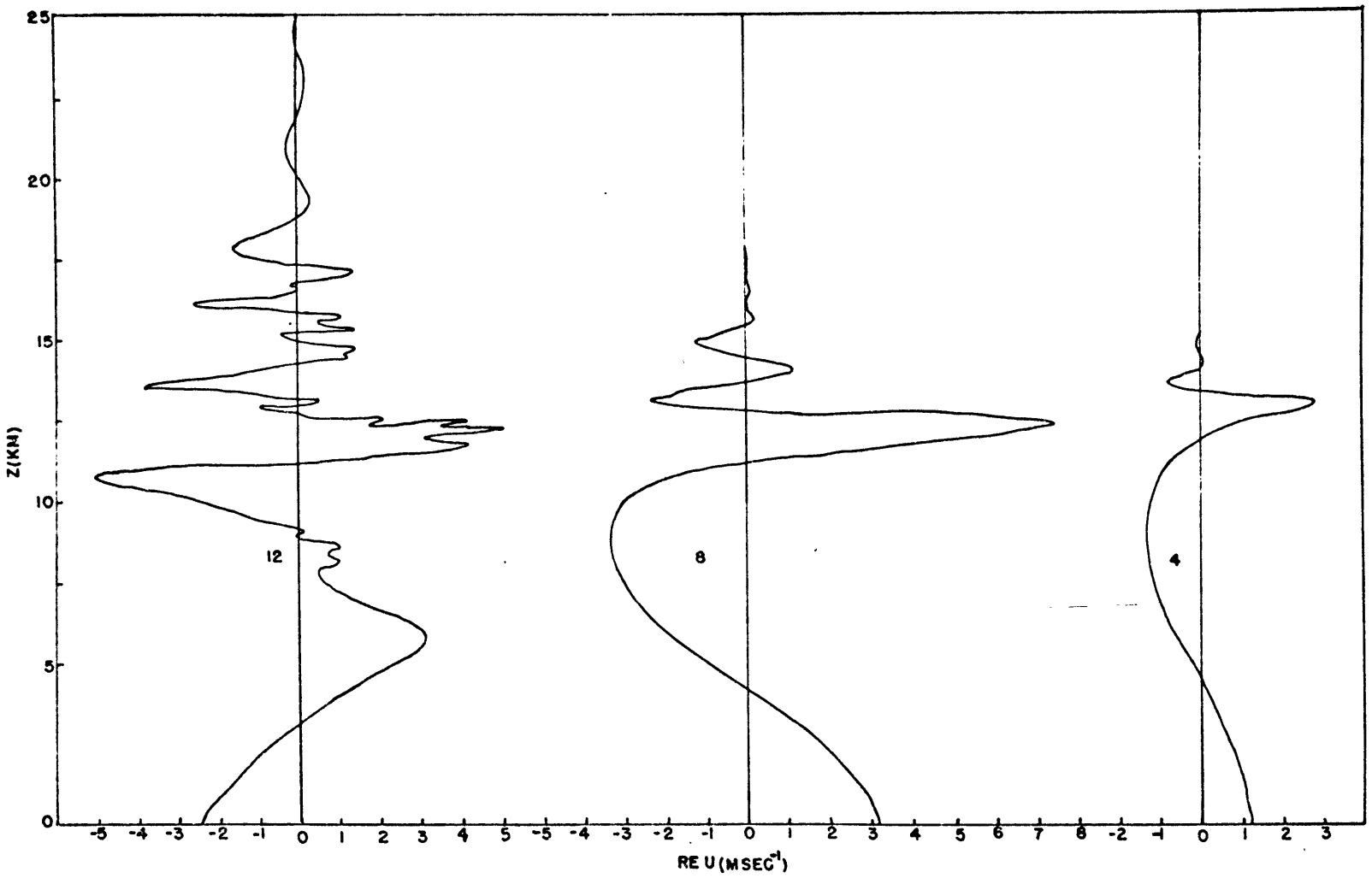

Figure 2.15: The vertical profiles of the horizontal component $\mathrm{Re}\hat{u}$ of the wave motions at 4, 8 and 12 hours.

shear layer continues to descend throughout.

From 8 hours onward it is apparent that the upper shear level in u_{0z} is also undergoing interaction with the wave motions and here the mean flow is decelerated. Regions of negative u_{0z} are developed for which $Ri < 1/4$ and the momentum flux and mean wind develop irregular small scale vertical structure here as well. Wave motions and momentum penetrate the region.

The results of this calculation are similar in many respects to the calculation for the previous case. The additional points of note are:

i) The initial form of u_0 is such that the interaction occurs much nearer the "initial" critical level than the previous case.

ii) The upper region of shear, which also has a critical level, is decelerated by the interaction with the wave motions which penetrate and perhaps are generated at the lower shear level. Both the upper and lower shearing regions descend with time.

iii) Another effect, which occurs for the previous case as well, is the increase in the momentum flux in the region below the level of interaction before the oscillatory behavior associated with over-reflection has begun. Thus at 4 and 8 hours the momentum flux is nearly linear with height but increases in magnitude. The linear calculation (Fig. 2.7a) for the same initial distribution of u_0 has a momentum flux which is rapidly established at a constant value in both height and time in this region. One might expect behavior opposite to that

observed in the non-linear case. Thus one might expect increased partial reflections as the shear of the mean wind increases and a decrease with time in the magnitude of the momentum flux. The reason for the observed behavior is not clear but appears to be associated with a value of $\overline{u}_{oz}$ such that $Ri \lesssim 1/4$. This is perhaps clearer in Fig. (2.11) for the previous case where the flux in the lower region increases after 15 hours. The value of $Re\,\hat{u}$ at 8 hours reflects the growth of $|\hat{u}|$ at this time.

iv) Again the generation of other scales of motion is restricted by the single horizontal wavelength of the model. The interaction of the wave motion with the lower shear layer and the subsequent effect on the upper shear level may be responsible for an important source of energy capable of propagating in the vertical. The source and/or sink aspect of the critical levels is again of great importance.

In general, the interaction of the waves and the mean wind causes a region of accelerated mean motion. The lower boundary of the region descends with time and the value of $\overline{u}_{oz}$ increases until the stability condition is violated. Energy of the motions penetrates the shear level, is generated in the over-reflection of the waves, and is most likely produced by the growth of unstable modes. The critical level operates as a complicated source-sink region under these conditions. Calculations such as those of Hines and Reddy (1967) which implicitly assume the complete absorption of the wave motions will be applicable only in the early stages of the interaction. The shear zone continues to descend with time in the calculations and no approach to steady state condition is apparent.

3.0 Observations of gravity waves in the upper atmosphere

The problem of measuring gravity waves in the atmosphere is a very difficult one. The difficulty becomes apparent when the characteristics of gravity waves are considered. The simple theory of the previous section provides only a frequency relation between the period and the horizontal and vertical wavelengths of the motion. Aside from the upper bound of the Brunt frequency for the gravity wave spectrum there is virtually no further bounds on the scales of motion. Furthermore, the results of the previous section show some of the consequences of gravity-wave interactions and show that the form of the gravity wave can vary considerably depending on the interactions occurring.

The complete identification of gravity wave motions in the upper atmosphere would involve the measurement of the wind, temperature, pressure and density fields with sufficient accuracy and resolution to permit the identification and separation of waves with different frequencies and wavelengths and to permit the testing of the relations that theory gives between the fields. Such complete measurements are not possible at present and more restricted areas of the problem must be identified.

If the source mechanisms of gravity waves were known and could be measured, it would be possible to calculate the expected parameters of the wave motions in different regions of the atmosphere and to attempt to verify these predictions. This would simplify

the identification problem tremendously. The only success with such methods has been in conjunction with nuclear explosions (e.g., Harkrider (1964), Hines (1967), Row (1967)). In the absence of known natural sources, a different problem presents itself. Is there a dominant scale to the motions in the different regions of the atmosphere and are these dominant scales compatible with gravity wave motions?

Measurements of small scale motions in the upper atmosphere have been made by several methods, many of which are height dependent. The prominent methods are meteor radar, rocket grenade, ionospheric measurements, vapor trails, falling spheres, parachute sondes, and radar tracked chaff (see e.g., Craig (1965), Georges (1968)). The rocket based measurements are notorious in lacking horizontal and time resolution, mainly because of practical difficulties with multiple shots and horizontal range restrictions, while the methods depending on naturally occurring tracers apply mostly to the atmosphere above 80 km.

It is the purpose of this section to describe two methods for measuring the wind structure in the 30-60 km region of the atmosphere, to attempt to determine dominant scales of motion and compare them with gravity wave behavior and to discuss the place of such methods in the general problem of the identification and measurement of gravity waves in the atmosphere.

3.1 The ROBIN experiment

The experiment consisted of the launching of eighteen ARCAS-ROBIN sensors over a six-hour time period from White Sands Missile Range, New Mexico on March 6, 1965.

The ROBIN sensor is a spherical, one meter, 1/2 mil, mylar plastic, inflatable balloon. The balloon contains a six-point, 1/4 mil, mylar, corner reflector coated with aluminum and is inflated, after ejection from the rocket, by vaporization of isopentane to a superpressure of approximately 10 mb. The total weight of balloon and reflector is about 115 gm.

The ROBIN balloon is boosted to 70-90 km, depending on slant range, by an ARCAS rocket which has a solid propellent, end burning, 4.5 inch rocket motor. After ejection and inflation, the ROBIN balloon is tracked with an FPS-16, precision, 10 cm radar which automatically records on magnetic tape the range, azimuth and elevation coordinates of the balloon at the rate of 10 points per second.

The experiment consisted of the launching of nine pairs of ROBIN balloons, a pair being launched on the hour and one minute past the hour from 0900 to 1500 MST (1600-2200 GMT) with two additional pairs launched at 1130 and 1230 MST. The data obtained consisted of seventeen soundings of the atmosphere, at time intervals ranging from one half to six hours and horizontal separations ranging from less than 7 to more than 50 kilometers.

TABLE 3.1

Details of ARCAS-ROBIN experiments at WSMR, March 6, 1965

Time MST	Rocket Number	Radar Number	Maximum Altitude of data (km)	Minimum Altitude of data (km)
0900	749	1	93	37
		3	92	45
0901	755	2	90	30
		4	93	36
1000	887	1	94	21
		3	94	42
1001	751	2	73	22
		4	73	37
1100	748	1	89	28
		3	89	44
1101	924	2	76	28
		4	--	--
1130	922	1	92	31
		3	92	45
1131	888	2	95	34
		4	95	47
1200	930	1	95	29
		3	96	45
1201	923	(no data)		
1230	752	1	87	34
		3	--	--
1231	883	2	77	29
		4	76	39
1300	756	1	94	23
		3	94	41
1301	638	2	77	22
		4	77	41
1400	921	1	95	25
		3	--	--
1401	892	2	79	22
		4	76	42
1500	933	1	95	21
		3	95	40
1501	935	2	70	20
		4	72	39

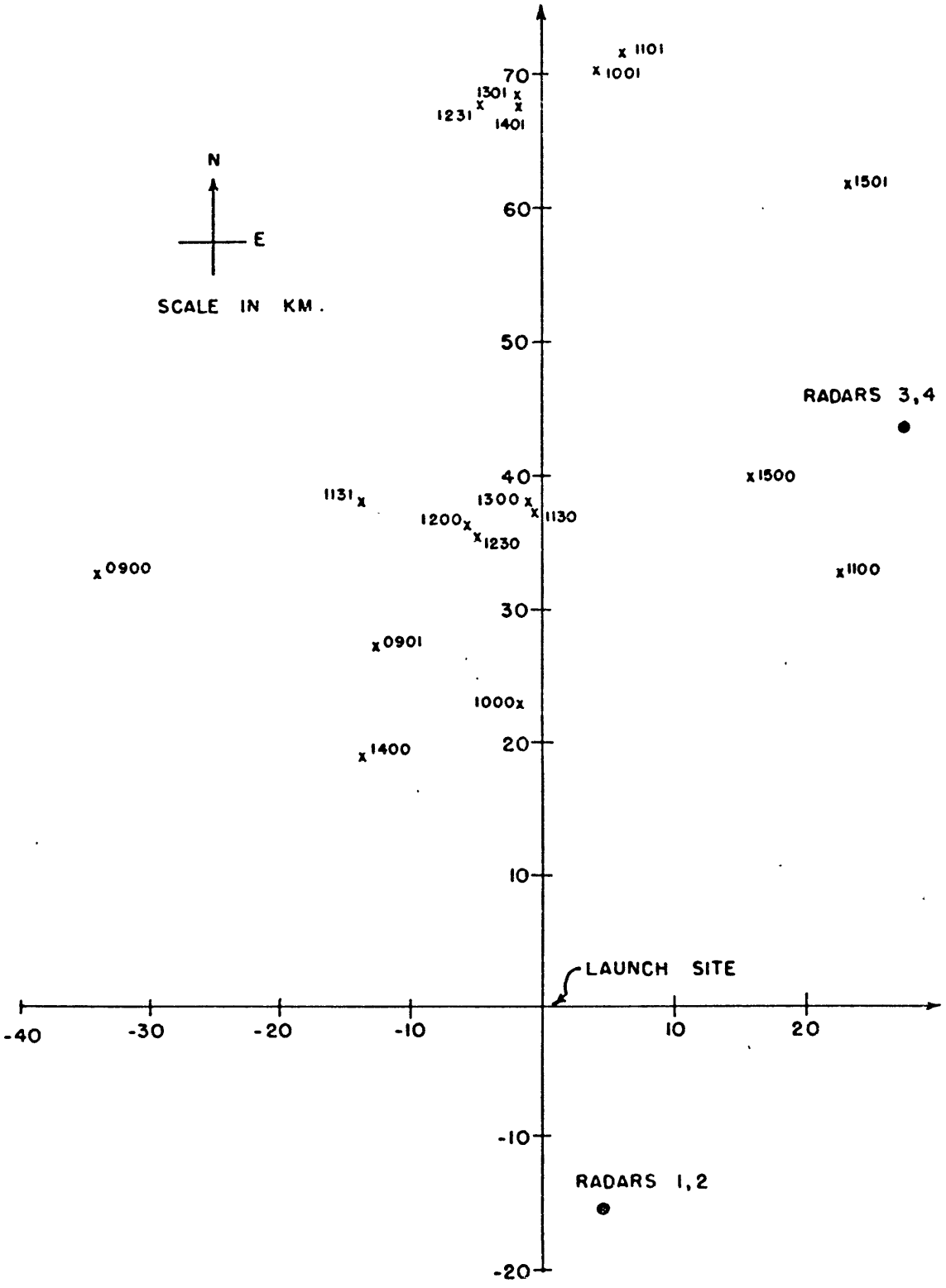

Figure 3.1: Plan view of balloon positions at 50 km and of radars. The balloons are identified by launch time (MST).

Four FPS-16 radars were used to track the pairs of balloons, two radars following each balloon. Two of the radars were located at Holloman Air Force Base about 52 kilometers north-northeast of the launch site and the remaining two were located about 15 kilometers south-southeast of the launch site. One radar from each site was used to track each balloon.

The positions of the balloons as they passed through 50 km are shown in Fig. 3.1 together with the relative positions of launch site and radars. The radars are referred to by number hereafter. Table 3.1 identifies the balloons by time of launch and rocket number and gives the number of the tracking radars together with the data acquired. In what follows, the data between 30 and 60 km is used.

3.1.1 Data reduction

By means of a computer program, the basic (r, θ, ϕ, t) radar data are transformed into the usual meteorological (x, y, z, t) data. These data are then transformed into u and v components of velocity and various smoothing procedures are used in an attempt to eliminate radar and computational noise while retaining small-scale information.

In a complete treatment of the motion of a falling balloon in a variable wind field, the effect of buoyancy, coriolis, and hydrodynamical forces must be considered. Neglecting buoyancy forces, which are negligible for the 30-60 km height range, and coriolis forces, the equations for the wind velocities in terms of balloon motions may be written after Engler (1965) as

$$u = \dot{x} - \frac{\ddot{x}\dot{z}}{\ddot{z}-g}$$

$$v = \dot{y} - \frac{\ddot{y}\dot{z}}{\ddot{z}-g}$$

where x, y, z are the balloon coordinates and dots indicate time differentiation.

3.1.2 Calculation of smoothed velocities

The simplest estimate of velocities and that which was used here results from dropping the terms with second derivatives. The velocities calculated are then simply the balloon velocities.

Smoothed velocities were calculated at standard 50 m height intervals from the raw data as follows. For a smoothing interval ($2\Delta H$) all balloon position data (x, y, z, t) with z-coordinates in the interval $z_o - \Delta H < z \leq z_o + \Delta H$, centered about the standard level z_o were selected. The best straight line, in the least squares sense, was then fitted in (x,t), (y,t), and (z,t) space and the slope of these lines taken as the x, y, and z velocities at the midpoint z_o. Four values of ΔH, namely 50, 100, 150, 250 meters were used so that the effect of increased smoothing could be considered. Fig. 3.2 gives a typical sounding for each of the four smoothings.

This method of obtaining smoothed velocity profiles differs from that previously employed on ROBIN data by Engler (1965) where the data is smoothed over equal time intervals. Because of the much larger fall speeds at higher levels, the balloon will traverse a much

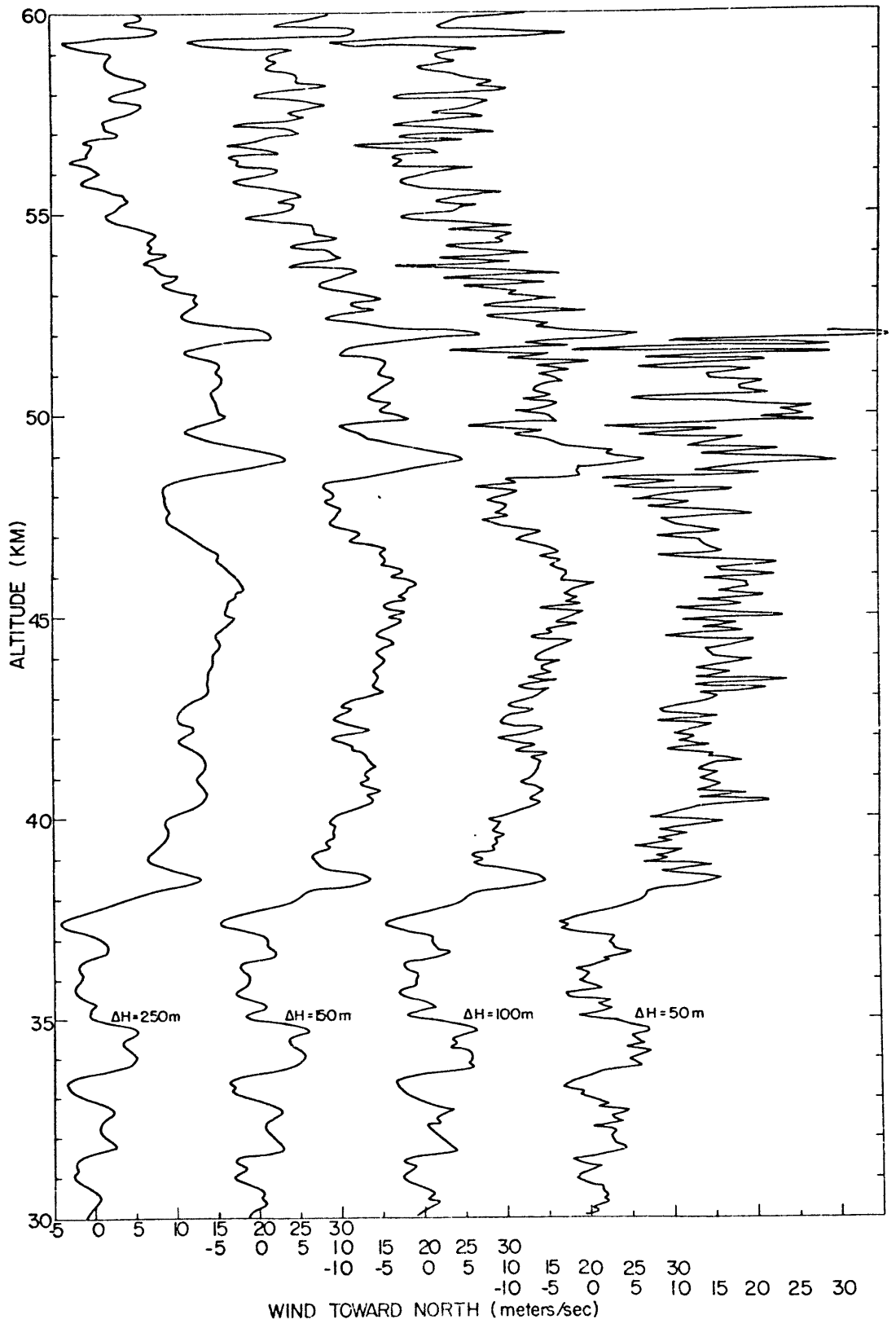

Figure 3.2: Velocity profiles for the balloon launched at 1000MST and tracked by radar 1. The smoothing interval used is shown on the diagram.

greater vertical distance in a given time interval at higher altitudes. Thus in terms of space scales, smoothing over a constant time interval will correspond to smoothing over large space intervals at the top of soundings and much smaller space intervals at the bottom of soundings. The method of smoothing used here avoids this complication in that the same space interval is used for smoothing at all levels of the sounding. The compensatory disadvantage is that fewer data values will occur in a fixed height interval at higher levels of the sounding and thus a smaller number of data values will be used in obtaining velocities at higher levels. The effect of this is clearly shown for the smaller smoothings in Fig. 3.2.

The problem of obtaining wind velocities from balloon velocities can be considered in two parts, the effect of fitting a least squares line to the balloon coordinate data to obtain the time derivative and the importance of the acceleration terms in the calculation of the wind velocities.

The effect of fitting the data to obtain the first derivative is seen as follows. Assume the acceleration terms are negligible and $u = \dot{x} = A\cos(mz)$ is the known form of the wind field. Assume also that $\dot{z}$, the vertical balloon velocity, is constant. Then the least squares fit of the line $x = a + bt$ to the data over the height interval $(-\Delta H, \Delta H)$ is obtained for

$$\int_{-\Delta H}^{\Delta H} (a + bt - x)^2 \qquad \text{a minimum}$$

Substituting entirely in terms of z, differentiating by a and b and solving for b gives $b = \frac{3A}{m^3\Delta H^3}\left[\sin(m\Delta H) - m\Delta H\cos(m\Delta H)\right]$ as the least squares approximation to the velocity. The response function of the smoothing as a function of vertical wavenumber is then

$$R(m) = \frac{3}{(m\Delta H)^3}\left[\sin(m\Delta H) - m\Delta H\cos(m\Delta H)\right]$$

This is an acceptable response to the smoothing involved in obtaining the velocities. It is of the same form as that obtained by Luers and Engler (1967) who obtained it for fitting over equal time intervals. Their result in terms of the time interval $(-\Delta t,\Delta t)$ can be written

$$R(m) = \frac{3}{(m\dot{z}\Delta t)^3}\left[\sin(m\dot{z}\Delta t) - m\dot{z}\Delta t\cos(m\dot{z}\Delta t)\right]$$

It is apparent that the response changes for different levels of the sounding as $\dot{z}$ changes. The choice of the fitting over constant height intervals rather than time intervals is clearly preferable, other things being equal.

The second problem in obtaining wind velocities from the balloon motions is that of the evaluation of the acceleration terms $\dot{z}\ddot{x}/(\ddot{z}-g)$, $\dot{z}\ddot{y}/(\ddot{z}-g)$. These terms are important in the upper portions of the soundings. They are, however, sensitive to error as they involve the second derivatives of the balloon position data. An attempt was made to include these terms in the velocity calculations and it was found

that the effect was small in general below 55 km but above this height the correction could be quite large. The large correction was manifested in the smaller scales as would be expected. Introducing the acceleration corrections into the velocity profiles was found to be questionable as the resulting corrections differed for the measurements of the same profile by two radars as well as giving amplitudes which were unrealistic at certain points in the soundings. Because of the sensitivity of the term to error and the resultant difference in profiles due to measurements of different radars, the accelerations were not included in the calculation of velocities.

This reflects the general difficulty involved in measurements by means of the ROBIN system and the difference in the averaging over time and space to obtain velocities. Averaging over equal time intervals may allow a better estimate of the acceleration terms at the top of the soundings but the averaging has a response that depletes the terms most affected by the inclusion of the acceleration terms. The equal height interval smoothing guarantees that there is the same response at all levels of the sounding but the lack of what is felt to be an acceptable method of obtaining acceleration terms results in the attenuation of smaller scales at the top of the soundings for which the acceleration terms are important. The method used here should result in a good representation of the wind field below about 55 km with a less accurate representation above this height.

3.1.3 Smoothing and the accuracy of soundings

In the present experiment an estimate of the error can be found over some height interval of the sounding by comparing the velocities as obtained by two radars measuring the motions of the same balloon.

If u_1, u_2 are the velocities as obtained from two radars on the same balloon, the calculated mean square velocity difference between the radars over some altitude band (for the u component say) is

$$\overline{E_u^2} = \sum_{i=1}^{m} \frac{(u_{1i} - u_{2i})^2}{m}$$

where the m values of u_1 and u_2 are specified at 50 m height intervals. The r.m.s. velocity difference for the height interval is then $\sqrt{\overline{E_u^2}}$.

Table 3.2 gives the r.m.s. velocity differences as averaged over all soundings for the 60-50 km and 50-40 km altitude ranges. Individual contributions from each sounding with paired radar coverage were averaged to give the result.

The values of r.m.s. velocity difference decrease for lower levels in the atmosphere. Also, the increased smoothing interval is effective in removing r.m.s. velocity difference. Excessive smoothing will reduce both "real" and error variance and will force the soundings to agree.

TABLE 3.2

Average calculated RMS velocity differences

Height Interval (km)	Smoothing Interval ΔH(m)	No. of Paired Measurements	Mean RMS velocity differences (m/sec) $\sqrt{E_v^2}$	$\sqrt{E_u^2}$
60-50	50	14	20.4	23.8
	100	14	8.9	9.9
	150	13	4.8	5.2
	250	14	2.4	2.4
50-40	50	10	7.6	8.7
	100	10	2.8	3.3
	150	9	1.4	1.6
	250	10	0.7	0.9

3.1.4 Smoothing and the variance of soundings

Table (3.3) gives the variances obtained for two regions of the soundings and for different smoothing intervals. Several results are apparent.

i. There is a systematic difference in the variances obtained from the two radars of each pair. The expected difference in variance due to the distance from the radar to the balloon is not found in the case of radars 1 and 3 but rather the reverse relation as the balloon-radar distance is greater for radar 1 than radar 3. It is apparent that the specific operating characteristics of the radars are not uniform and that the smoothing procedure must counteract this possibility.

ii. The variances of the soundings differ markedly for the

TABLE 3.3

Variances

Height Interval (km)	Smoothing ΔH(m)	No. Paired Measurements	Mean Var. R. 1 (m^2/sec^2)	Mean Var. R. 3 (m^2/sec^2)	No. Paired Measurements	Mean Var. R. 2 (m^2/sec^2)	Mean Var. R. 4 (m^2/sec^2)
	v component						
60-50	50	7	135.0	291.7	7	491.2	123.8
	100	7	54.1	79.2	7	157.9	73.8
	150	6	41.3	45.1	7	87.5	66.0
	250	7	36.0	35.4	7	66.2	61.0
50-40	50	5	36.5	49.8	6	69.5	43.3
	100	5	25.2	28.3	6	36.6	33.0
	150	4	22.5	22.8	6	31.3	30.5
		5	16.7	17.7	6	28.4	28.1
	u component						
60-50	50	7	185.5	339.9	7	491.2	123.4
	100	7	71.5	89.5	7	151.9	73.8
	150	6	47.1	53.5	7	87.5	66.0
	250	7	39.2	41.2	7	66.1	61.0
50-40	50	5	44.9	47.8	6	69.7	43.3
	100	5	19.8	21.4	6	36.6	33.0
	150	4	17.9	19.1	6	31.3	30.5
	250	5	14.9	16.1	6	28.4	28.1

smaller smoothings. This difference becomes much smaller at the largest smoothing used where effective agreement is reached between radars.

3.1.5 Smoothing and correlation

The correlation coefficient is the measure of the 'goodness' of the linear relationship between two quantities. For the case of two radars on the same target consider $u_1 = U + e_1$, $u_2 = U + e_2$ where u_1, u_2 are the velocities measured by the two radars, U is the 'real' velocity and e_1, e_2 are the error terms. The square of the correlation coefficient is then

$$r^2 = \overline{(U'^2 + U'(e_1+e_2) + e_1e_2)}^2 \Big/ \overline{(U'^2+U'e_1+e_1^2)}\,\overline{(U'^2+U'e_2+e_2^2)}$$

Assuming the errors to be independent, random, with mean zero and the same variance the correlation coefficient is approximately,

$r \sim \sigma_U^2/(\sigma_U^2+\sigma_e^2)$ which is a rough estimate of the real to the real plus error variance of the sounding. Further the ratio of the error to real variance is approximated by $\sigma_e^2/\sigma_U^2 \sim \frac{1-r}{r}$ Table (3.4) gives the average values of the correlation coefficient for the radar pairs for the various smoothings together with the variance ratio.

The correlation coefficients increase with increased smoothing. At larger smoothing intervals the increase in correlation is small and further smoothing of the soundings will increase the correlation only slightly while reducing the real variance of the soundings. Fig. (3.3) gives the behavior of the correlation coefficient with smoothing interval.

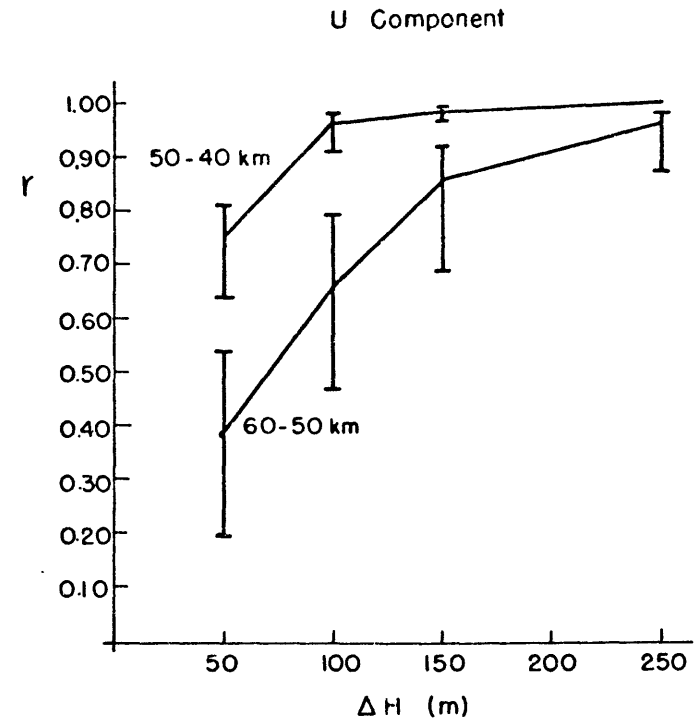

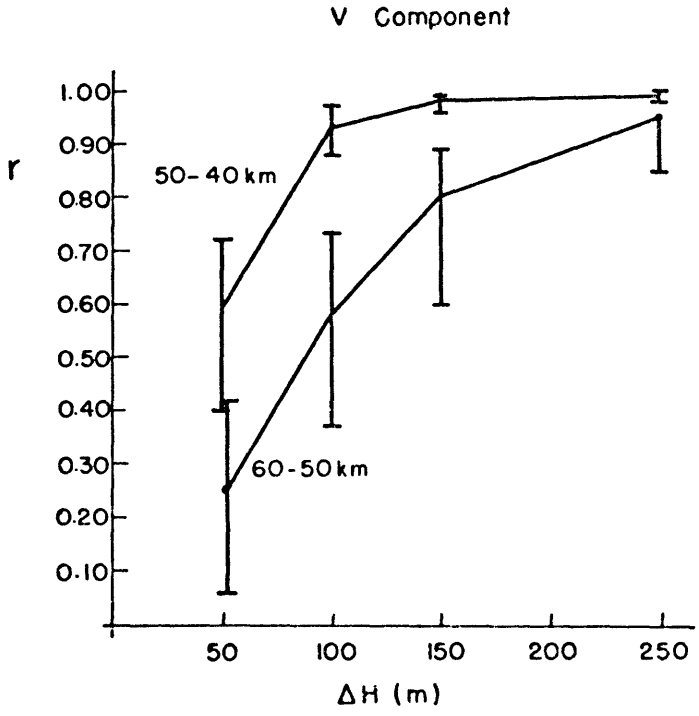

Figure 3.3: Variation with smoothing interval ΔH of the correlation coefficient r between winds measured by two radars on the same balloon for the altitude bands 60-50 and 50-40 km. Five per cent confidence intervals for r are shown. Time of sounding 0900 MST.

TABLE 3.4

Comparison of correlations for double radar coverage

Component	Height Interval (km)	ΔH (m)	Mean r radars 1,3	Mean r radars 2,4	σ_e^2/σ_v^2 radars 1,3	σ_e^2/σ_u^2 radars 2,4
V	60-50	50	0.20	0.27	4.00	2.70
		100	0.51	0.62	0.96	0.61
		150	0.77	0.82	0.29	0.22
		250	0.92	0.93	0.09	0.08
	50-40	50	0.44	0.61	1.27	0.64
		100	0.69	0.89	0.45	0.12
		150	0.89	0.96	0.12	0.04
		250	0.98	0.99	0.02	0.01
U	60-50	50	0.18	0.14	4.55	6.14
		100	0.49	0.41	1.04	1.44
		150	0.74	0.70	0.35	0.43
		250	0.93	0.89	0.08	0.12
	50-40	50	0.47	0.48	1.13	1.08
		100	0.82	0.81	0.22	0.23
		150	0.95	0.94	0.05	0.06
		250	0.98	0.98	0.02	0.02

To summarize, the redundant radar coverage permits the calculation of statistical measures of the error in the soundings as well as allowing a rational choice of smoothing interval. The smoothing interval $\Delta H = 250$ gives good agreement between measurements as shown by the r.m.s. velocity difference, variances and correlation coefficients. Further smoothing will improve this agreement only slightly while removing the real variance of the soundings. Fig. (3.4) gives examples of the resulting velocity profiles for soundings separated in time by one hour but not coincident in space.

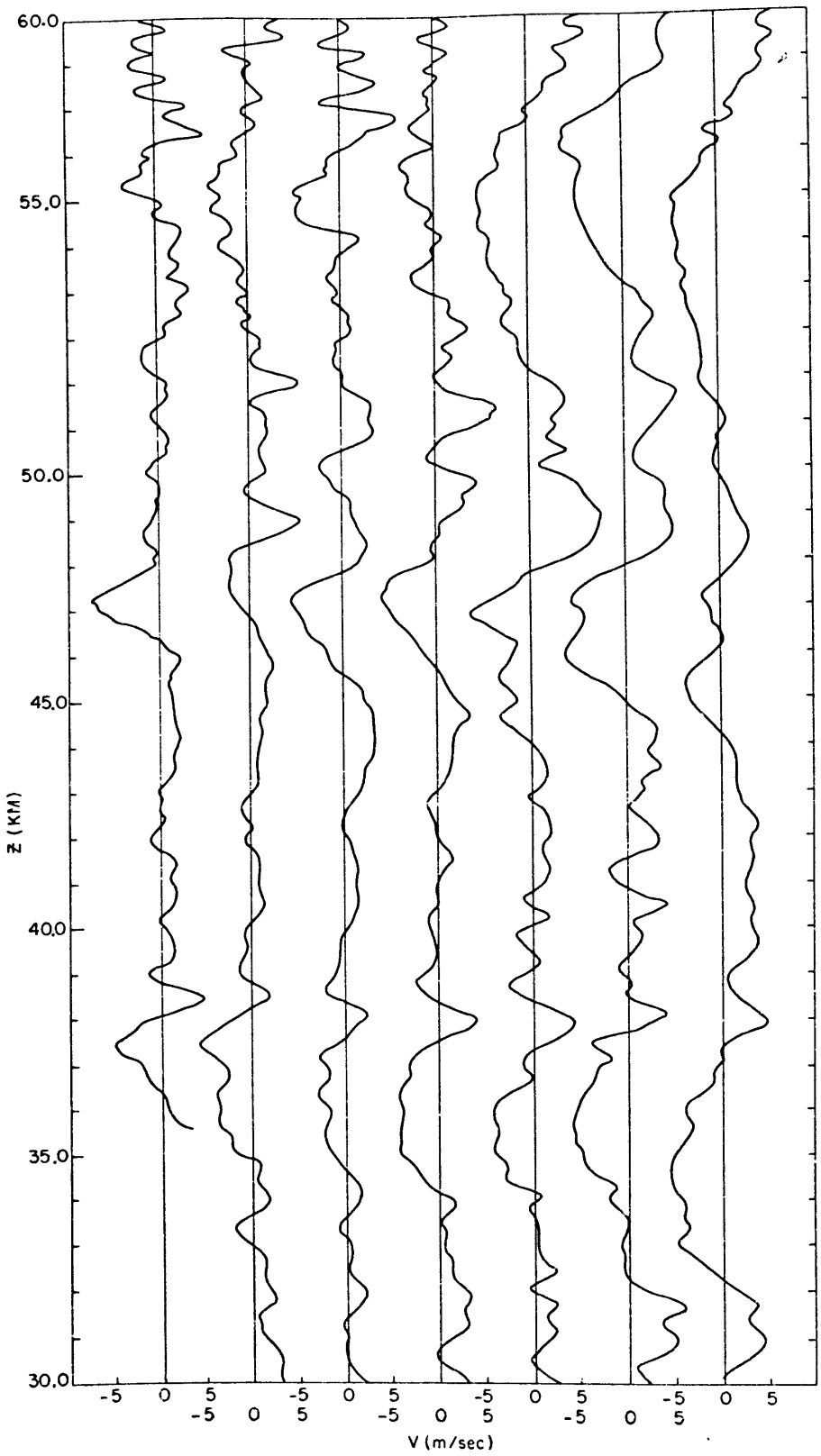

Figure 3.4: Velocity profiles for the v component from which the mean wind has been removed. The profiles from left to right in the diagram were obtained at one hour intervals from 0900 to 1500 MST but were not concident in space.

3.1.6 Spectra and the vertical scale of the motions

The spectra of the u and v components of velocity were obtained by removing quadratic trend from the soundings and subjecting the result to spectral analysis by way of the fast Fourier transform. Fig. (3.5) gives the spectra obtained by averaging over all soundings in the experiment. The points of note are:

i. For the spectrum of the v component of velocity a peak exists in the 8-9 km vertical wavelength region with a subsequent rapid fall off therefrom. In the region from 8 to 3 km the slope of the spectrum in this log-log scale is -2 while below 3 km the slope is -3. Some indication of peaking of the spectrum near 3 km and 1.5 km exists but these are not significant. The sharp drop in values at 500 m is a result of the smoothing applied to the sounding.

ii. The spectrum of the u velocities displays somewhat different characteristics. There is a broad peak in the spectrum in the 8-12 km region followed by a small gap near 5 km with the subsequent fall off as -2.

iii. In either case the fall off of the spectra with wavelength is rapid and there is little evidence to suggest a 'dominant' scale at wavelengths less than the peak values.

iv. The smooth fall off of the spectra do not suggest that there exists a naturally occurring feature of the spectra which would permit the separation of motions into various scales according to vertical wavelength.

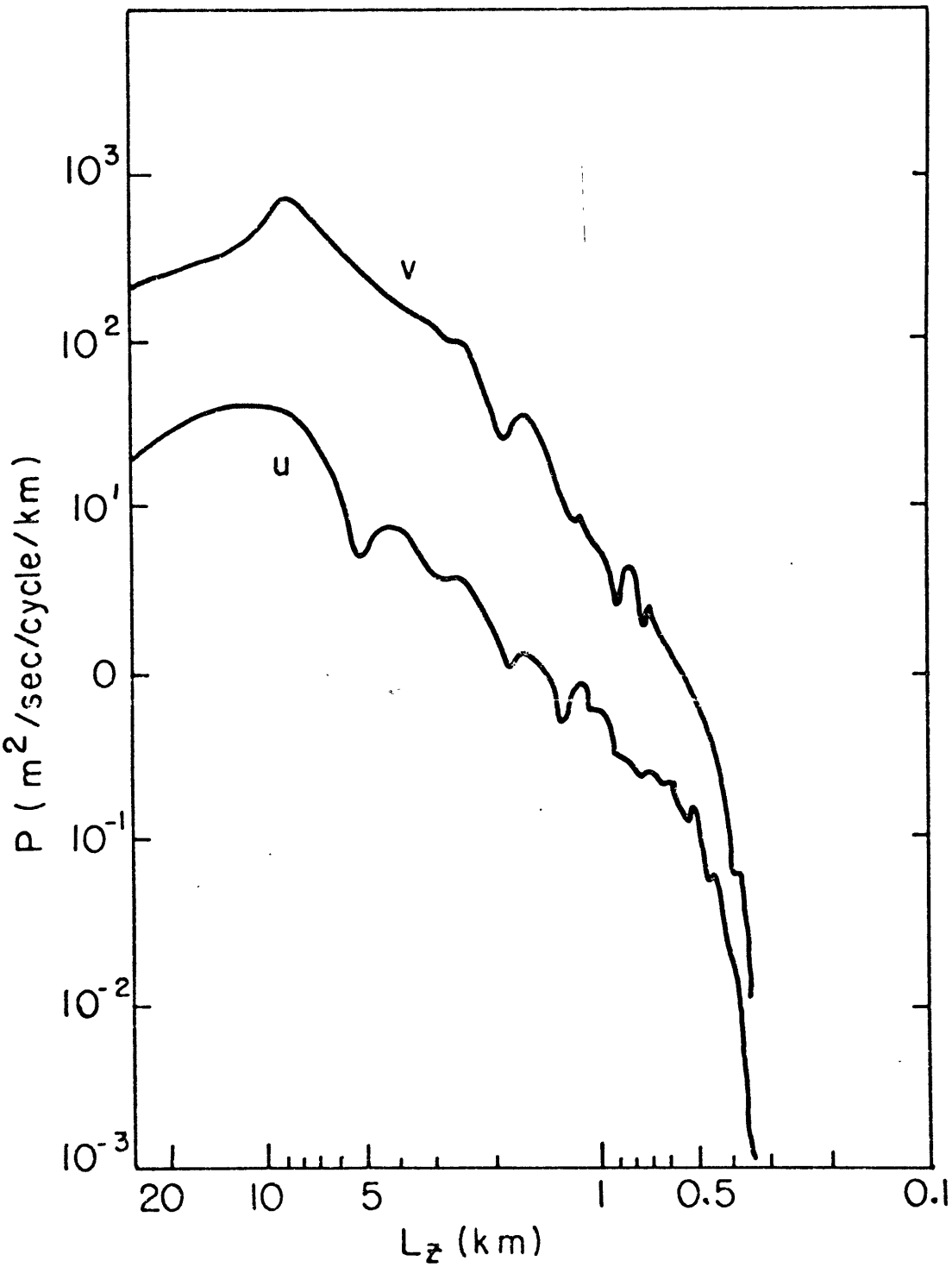

Figure 3.5: The spectra of the u and v components of velocity obtained by averaging over all soundings. The graph of the spectrum for the v component has been displaced one interval in the vertical.

A similar study in the lower 20 km of the atmosphere from rising balloon measurements Endlich et al., (1969) found spectral slopes of -3 in two cases and -2.5 in a third. Considerable theoretical and experimental work has been done on the spectra along horizontal lines in the lower levels in the atmosphere in turbulence studies, (Rieter and Burns (1968). Theoretically it is suggested that the spectral densities of turbulent motions should drop off with slopes between -1 and -4 (Justus, 1969). The region away from the peak in the spectrum then satisfies this rough criterion.

3.1.7 The horizontal scale of the motions

The estimation of the horizontal scale of the motions proceeds by relating the fall off of the correlation coefficient between soundings with spatial but not temporal separation. The correlation coefficient will be dominated by the vertical scales which contain the maximum variance in the spectra. The analysis makes use of the analogy with a sinusoid

$$u = A\cos(mz+\phi) \quad , \phi = kx+ly-\nu t$$

The correlation of two different soundings over a region assumed approximately an integral number of wavelengths in the vertical is then $r \sim \cos(k\Delta x + l\Delta y - \nu\Delta t)$. The argument of the cosine is the phase $\Delta\phi$ and relates the fall off of correlation to the structure of the phase of a plane wave. The value of the correlation coefficient for this model will depend on the orientation of the lines of constant phase and on the positions of the two soundings entering the correlation.

A simpler model which ignores phase structure relates the fall-off of correlation directly to the linear distance ΔR between soundings.

For the first case the wavenumbers k and ℓ may be related to one another using simple gravity wave theory* with $|\hat{u}|^2/|\hat{v}|^2 = k^2/\ell^2$ where $\hat{u}$ and $\hat{v}$ are the amplitudes of the u and v components of the wave. Thus $\ell = \pm \frac{|\hat{u}|}{|\hat{v}|} k$ and from the spectra of Fig. (3.5), the ratio of amplitudes is somewhat greater than one; however, for simplicity the value of one is taken. The correlation may then be written as $r \sim \cos(k(\Delta x \pm \Delta y) - \nu \Delta t)$. For $\Delta t = 0$, $r \sim \cos(k|\Delta x \pm \Delta y|)$ and that value of $|\Delta x \pm \Delta y|$ for which $r = 0$ is taken as one quarter of the horizontal wavelength. A simpler symmetric fall-off of correlation with linear separation ΔR may be assumed in the form $r \sim \cos(k\Delta R)$. Table 3.5 gives the data concerning the balloon pairs launched at the same time for the three measures of separation, ΔR, $|\Delta x + \Delta y|, |\Delta x - \Delta y|$, together with the horizontal wavelength. One quarter wavelength is identified with the intersection of the regression lines of the correlation measures $(r_u + r_v)/2$ and $(r_u^2 + r_v^2)/2$ with the axis for each of the levels 50-40 km and 60-50 km. The table shows a considerable difference in the deduced horizontal wavelength. A reasonable average value is 450 km. The lack of intersections for the parameter $|\Delta x + \Delta y|$ indicates that this is not a good choice for separation parameter and a better choice is $|\Delta x - \Delta y|$.

---

*The neglect of the effects of rotation is discussed in Appendix I.

TABLE 3.5

Data for balloons launched simultaneously

Time (EDT)	Rocket Pair		ΔR (km)	$\Delta x + \Delta y$ (km)	$\Delta x - \Delta y$ (km)
0900	749	755	12.1	16.5	4.5
1000	887	751	47.8	53.3	41.5
1100	748	924	42.3	23.4	55.0
1130	922	888	11.8	10.7	12.8
1200	No data				
1230	752	883	31.6	30.4	33.8
1300	756	638	31.3	33.7	28.0
1400	921	892	50.1	60.3	37.3
1500	933	935	23.4	30.4	13.2

Wavelengths deduced by linear regression

Level (km)	Correlation Measure	Separation Parameter (km)	Wavelength (km)
60-50	$(r_x+r_y)/2$	ΔR	384
		$\Delta x + \Delta y$	No intersection
		$\Delta x - \Delta y$	566
	$(r_x^2+r_y^2)/2$	ΔR	300
		$\Delta x + \Delta y$	No intersection
		$\Delta x - \Delta y$	405
50-40	$(r_x+r_y)/2$	ΔR	588
		$\Delta x + \Delta y$	576
		$\Delta x - \Delta y$	528
	$(r_x^2+r_y^2)/2$	ΔR	388
		$\Delta x + \Delta y$	420
		$\Delta x - \Delta y$	413

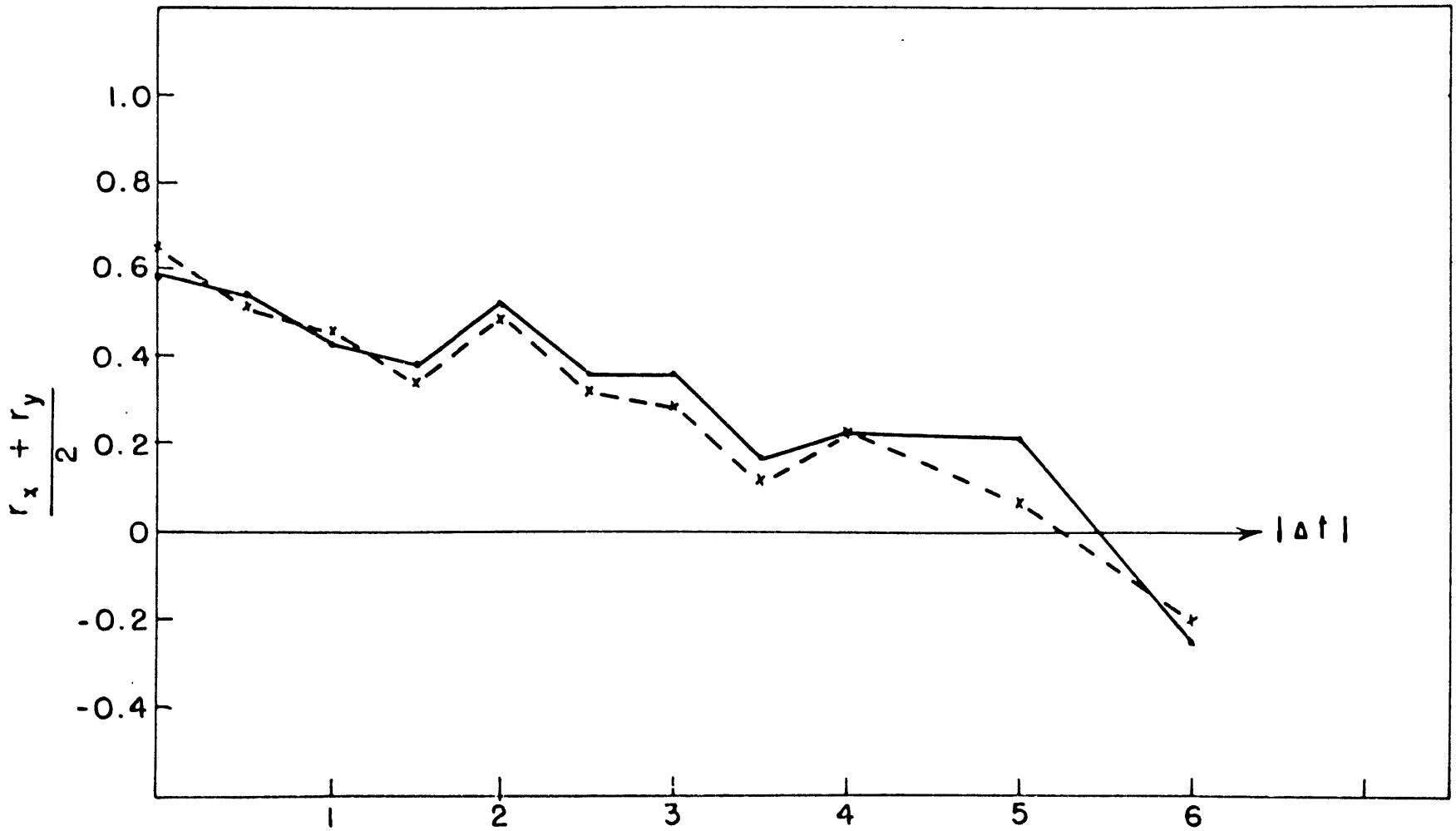

Figure 3.6: Decay of correlation measure with time separation in hours for soundings with horizontal space separation parameter less than 20 km. The dashed line corresponds to the horizontal separation parameter Δx-Δy and the solid to ΔR.

3.1.8 Time scale of the motions

The estimation of the time scale of the motions proceeds in a similar manner by means of correlation analysis. The time scale is difficult to separate from the horizontal scales as there are no pairs of soundings separated in time but at the same position in space. The method used here is to form the correlations of all soundings for which the horizontal separation is less than 20 km so that the effect of the decay of correlation with separation is small considering the large horizontal scale deduced. The approximate time scale is then obtained by averaging the correlations for these cases. Fig. (3.6) shows the behavior of the correlation measure with time separation. The figure shows an overall decay of correlations with resultant time scale in the neighborhood of 22 hours.

3.1.9 Relation of deduced scales and theoretical frequency equation

The frequency relation for gravity waves in the usual coordinate system is

$$(\nu - k u_0 - l v_0)^2 = (k^2 + l^2) S_0 / (m^2 + 1/4)$$

The spectra show that $|\hat{u}| / |\hat{v}| \sim 1$ approximately and the regressions of Table (3.5) indicate that the opposite choice of signs for the wave numbers is more likely to be correct. The deduced scales of motion may be used in the frequency equation to see if they are

consistent with the simple gravity wave model. The background wind U_o and V_o is obtained from the data as approximately 40 m sec and 10 m sec respectively. The term $1/4$ may be neglected to give

$$m^2 = \frac{(\nu - k u_o - l v_o)^2}{(k^2+l^2) S_o}$$

Introducing $k = -|k|$, $l = |k|$ and the deduced time and horizontal scale

$$L_z \sim 7 \text{ km.}$$

This is reasonably close to the 8.5 km vertical wavelength deduced from the spectra considering the crude nature of the deduced time and horizontal space scales.

Although the deduced parameters agree reasonably well with the simple frequency relation, it is conceivable that the tides in this region could have a significant influence on the deduced scales. The time scale of 22 hours lends credence to this possibility. Recently Lenhard (1966), Reed et al. (1966a,b), Beyers et al. (1966) and Groves and Makarious (1968) have investigated the tides in the 30-60 km region, principally for summer. A dominant diurnal tide is found. The vertical scale of the tidal motions is not well defined but could be of the order of the vertical scale found here. It is certainly impossible with the data available from this experiment to remove tidal motions from the soundings.

On the other hand, the deduced horizontal scale and vertical scales are certainly consistent with the gravity wave interpretation

and the long time scale can be explained in terms of the propagation direction of the wave in opposition to the mean wind. A mechanism that could give rise to such a situation is that of the waves propating away from an unsteady flow over a surface corregation. The wave motion set up in the flow over an obstacle has phase speed in opposition to the mean flow and in unsteady conditions can propagate upward to give the observed situation. Such a condition is not, therefore, inherently unlikely.

3.1.10 Summary of the results

This experiment is one of the few designed to have a reasonable chance of measuring the three parameters necessary to identify the presence of gravity waves in the upper atmosphere. The 30-60 km region is especially difficult to measure as no naturally occurring tracers are available there. This rocket experiment is novel in that the sensors are tracked with paired radars to allow estimation of measurement error and that the experiment includes soundings separated in time and in the horizontal which allow estimates of these scales of motion. The deduced scales of motion are found to be consistent with gravity wave motions although a question remains as to the influence of the tides in this region. The results indicate some of the difficulties involved in the measurement of gravity waves in the atmosphere and point out again the importance of the relation between observation and theory in that a thorough knowledge of the sources and propagation characteristics of gravity waves would allow a much simpler experiment for the verification of a predicted state than the necessity of

attempting to identify the presence of gravity waves in the entire spectrum of possible waves.

3.2 The measurement of velocities in the 30-60 km region by means of smoke trails

3.2.1 The smoke-trail system

The winds are measured by observing photographically a trail of trimethylaluminum (TMA) as it deforms with time. Two cannisters of TMA form the payload of a Nike-Iroquois two stage rocket. One cannister of TMA is deposited on the upward trajectory of the rocket and the second on the downward trajectory. Two such rockets are fired simultaneously giving four trails in all. Each trail is observed from three separate camera sites using K-46 cameras with 7 inch focal lengths. The cameras use plus X, 5 inch film, are synchronized in time and operate on a 0.7, 1.5, and 3.0 second exposure sequence on a 15 second cycle. The F stops are changed at predetermined times into the flight. The orientation of the cameras is obtained by calibration on the star field. To achieve the necessary contrast and lighting of the trail the experiment can be performed only at sunrise or sunset.

The smoke trail experiment discussed here consisted of a sunset launching of two rockets, each of which produced two smoke trails. The experiment was performed over the western Florida Gulf Coast on December 9, 1968. Fig. (3.7) shows the relative positions of the launch sites, camera sites, and smoke trails. The camera sites which

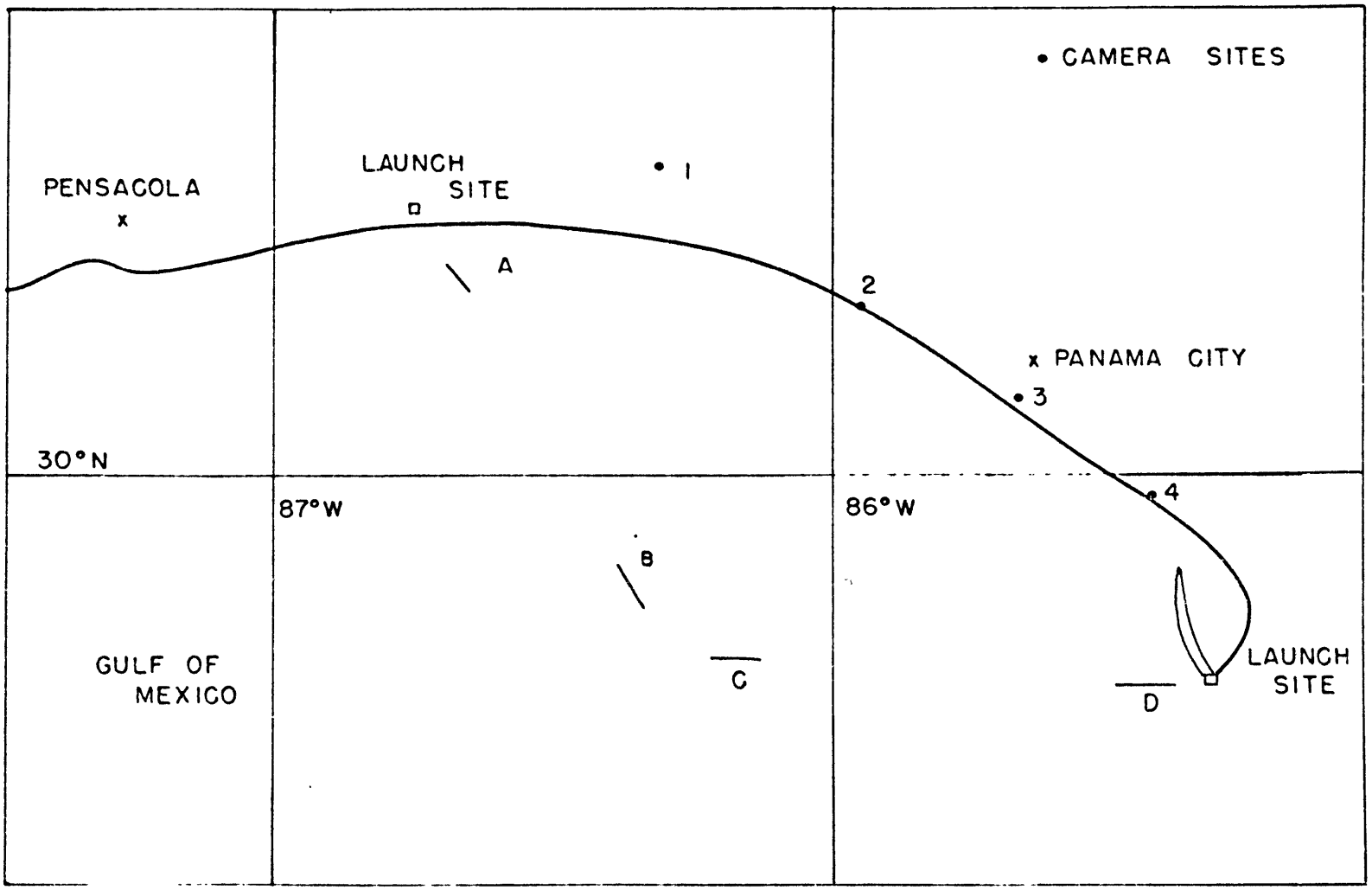

Figure 3.7: Positions of the launch sites, camera sites, and the smoke trails labeled A,B,C and D.

had cameras focused on each trail are given in table (3.6). Usable data was obtained for three of the four trails. Data for trail B was not usable.

3.2.2 Data reduction procedure

The data reduction scheme calculates the position in space of points along the smoke trail from data read from the films. The scheme was designed to permit automatic numerical calculation of trail position. To this end, the data from three camera sites are used to solve for position points of the trail in space, the intent being to remove ambiguities inherent in a two-station solution and to permit the evaluation of a maximum-likelihood solution with attendant error statistics.

The photographs from three camera sites are synchronized in time and the position of points along the trail are read in terms of a coordinate system superimposed on the plane of the film. These points are converted into azimuth and elevation angles in terms of a common coordinate system. The azimuth and elevation of the center of each frame and the tilt angle are calculated from calibration on the star field.

One station is then chosen as the lead station. A particular ray from this station is matched with the rays from the other two stations to look for triplets of rays which intersect or come near intersection at a point in space. Ray triplets which come near enough to intersection, as established by certain tolerances, go into the maximum-likelihood solution to produce a position point of the trail in space. Error measures are produced which can be used to accept or reject the

TABLE 3.6

Orientation of cameras at camera sites

Camera site	Trails observed
1	A, B, C
2	A, B, D
3	A, C, D
4	B, C, D

TABLE 3.7

Summary of reduced trail position data

Trail	Time after Launch (sec)	Lowest Point (km)	Highest Point (km)
A	40	32.4	40.4
	70	38.8	44.4
	100	32.2	44.4
	130	32.2	44.2
	160	32.4	46.6
	190	32.4	46.4
C	310	33.8	56.8
	370	33.8	61.4
	400	33.6	61.4
D	46	31.2	42.0
	76	31.4	48.4
	106	31.4	54.2
	166	31.6	48.8
	226	31.4	48.2

solution point. The data were read from the film and processed by means of this reduction scheme at the University of Dayton Research Institute. A description of the reduction procedure is given by Boehmer (1970). Fig. (3.8) shows a tracing of the reduced trail position for trail D as it changes with time. The trail positions were obtained at 30 second intervals in general. Table (3.7) gives a summary of the reduced data available for the different trails.

The trail positions of Fig. (3.8) are the result of considerable hand editing of the data as the data reduction suffered from several difficulties. One of the main difficulties was the lack of film reading equipment at the University of Dayton capable of reading the film under suitable magnification and therefore with suitable accuracy. A second major difficulty arose because of the experiment site along the western Florida Gulf coast which constrained camera positioning. Camera sites which were almost colinear, as can be seen from Fig. (3.7), were chosen and this reduces the resolving power of the reduction method. A final difficulty involved the lack of accuracy of the star calibrations used to obtain the orientation of the cameras.

The upshot of these difficulties is the inability of the reduction scheme to resolve the 'correct' solution from among a group of possible solutions. This made it necessary to hand edit the output which required a considerable amount of extra effort. The basic reduction procedure appears to have promise however if the difficulties mentioned above can be overcome. Despite this, the velocity profiles are obtained with reasonable accuracy as is shown in the next section.

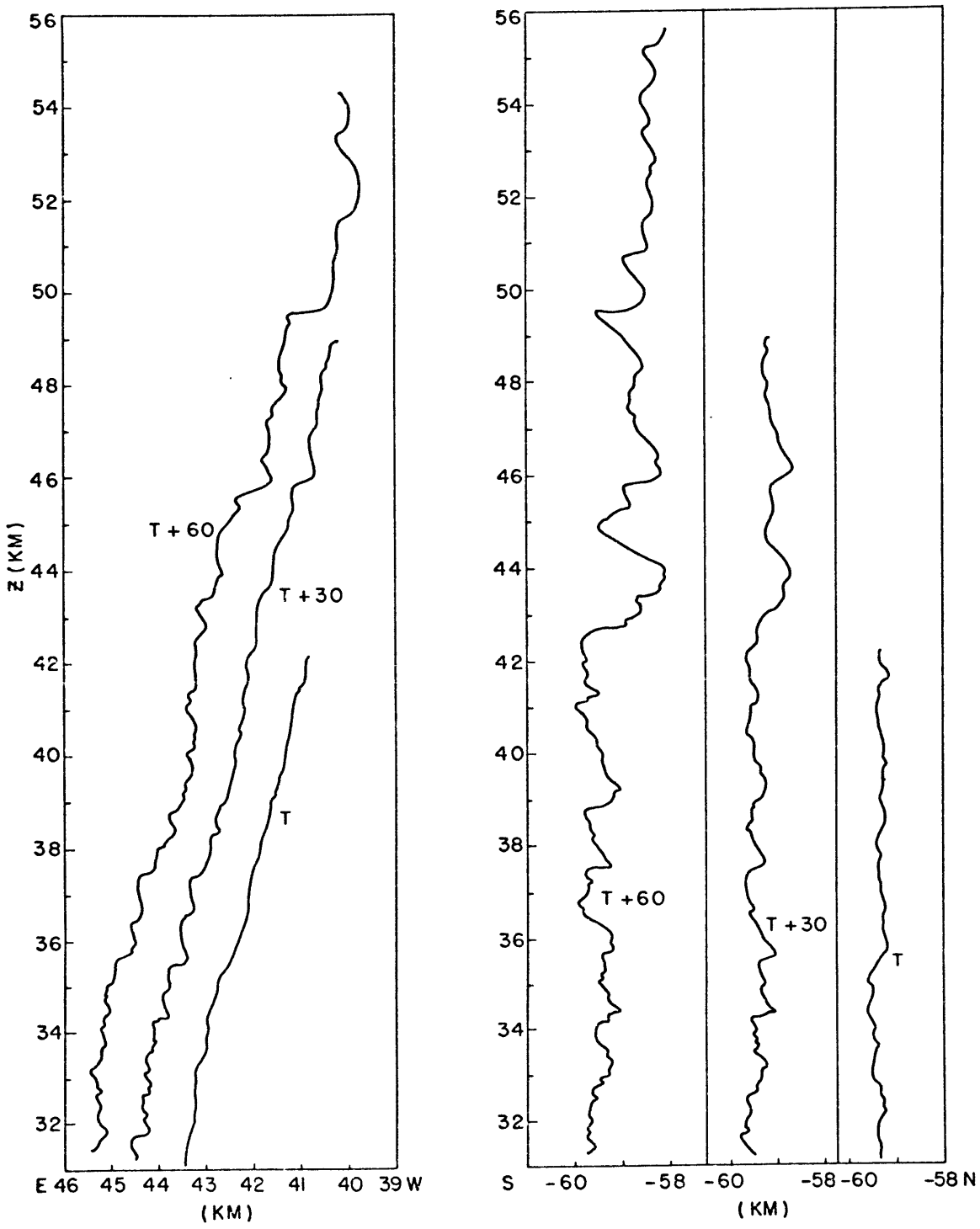

Figure 3.8: Position data for smoke trail D obtained by reduction of photographic data and subsequent editing. The trail positions are obtained at 30 second intervals.

3.2.3 Velocity profiles

The velocity profiles are obtained from the trail positions by differentiating with time. There are basically two methods by which this may be done. The first fits a least squares line to the trail positions in (x,t) and (y,t) space at a given height and takes the slope of the line as the velocity at that height. The second uses the fact that the trail deformation at any time is the integrated effect of the motions over the entire time from the first appearance of the trail. Dividing this displacement by the appropriate time interval gives the velocity.

The choice of the second method is made here to overcome some of the data difficulties mentioned in the previous section. The use of the least squares method is not feasible here as trail C has only three sets of position data and trail A exhibits a change of rate of progression of the position of the trail after three sets of data, due to apparent camera difficulties. Use of a least squares fit with three time points is equivalent to subtracting the first trail position from the last trail position. Fig. (3.8) shows the difficulty in this course. Although the shape of the trails is very similar there are regions in the trail where the deviations are displaced somewhat in the vertical. Even such a small effect will have a large effect on the velocities as obtained by differencing.

The shape of the trail is seen to be considerably more accurately defined than the relative trail positions at a point. The shape of the trail also contains the basic data of the wind field in terms

of the amplitudes and scales of motion. For these reasons the velocity profiles were calculated by reading trail positions at 200 m intervals in the vertical, removing the quadratic trend from the position data and dividing by the time of release of the smoke from the rocket at each level. This variable divisor is important as the rocket takes about thirty seconds to traverse the thirty kilometers of interest. The result of such a calculation is shown in Fig. (3.9) where all but the first of the trail positions have been transformed into velocity profiles. These velocities are now the deviation from the mean velocity and posses the additional virtue that the entire length of the trail gives rise to a velocity profile while a differencing method would produce a velocity profile only of the length of the shortest trail.

The velocity profiles are smoothed by repeated application of a smoothing with weights 1/4, 1/2, 1/4. The several velocity profiles calculated from the same smoke trail permit an estimation of the error of the profiles and the least amount of smoothing that will promote good agreement between the measurements. Table (3.8) gives the values of the rms error difference and the correlation coefficient for both components of velocity between the different determinations of the velocity profile for the same trail. The rms error difference is given as in the discussion for the ROBIN error analysis. It is apparent from this table that the correlation between the profiles of times 106 and 166 are consistently the highest and that the rms error is smallest. Further, smoothing more than twice

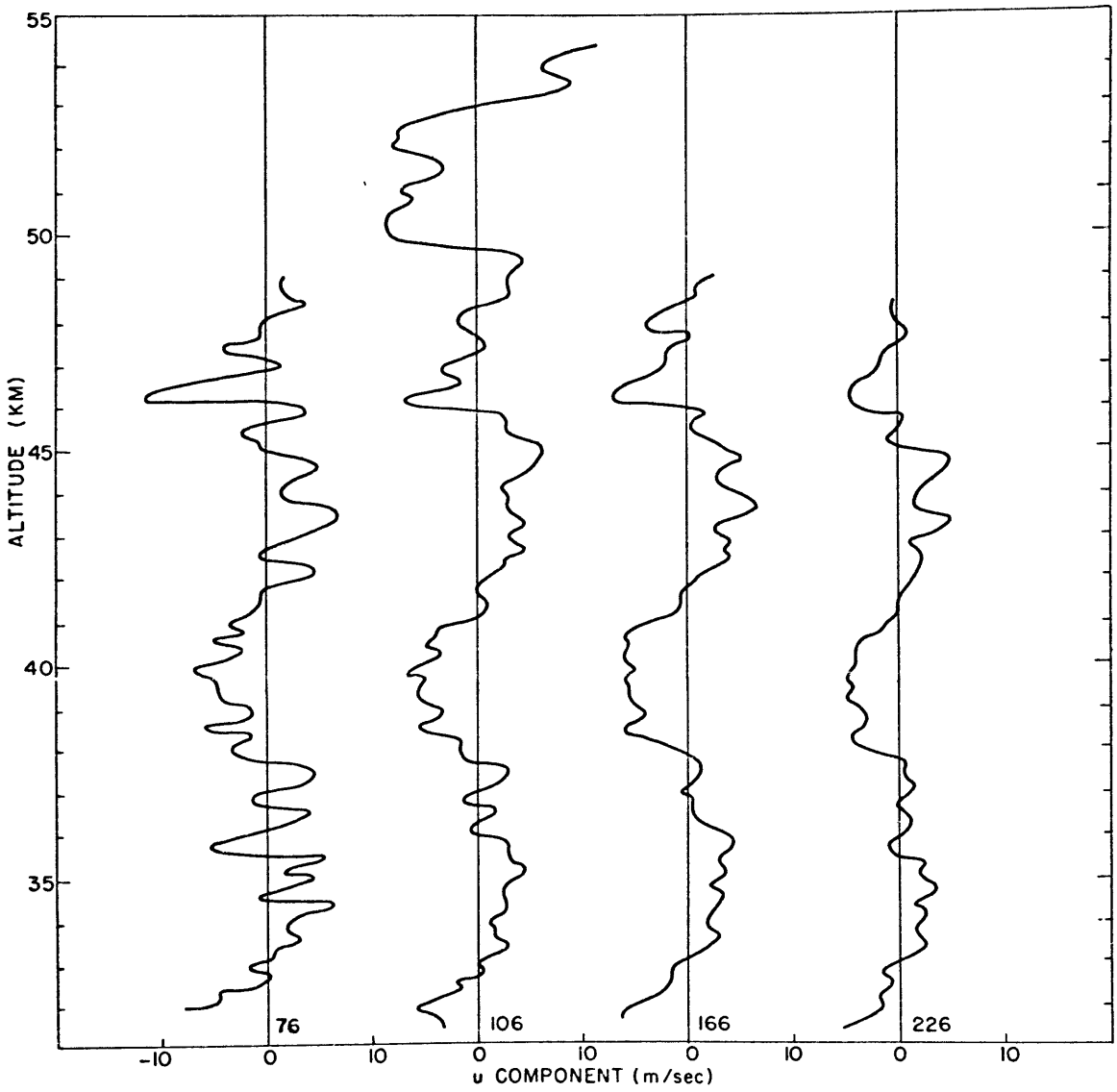

Figure 3.9: Velocity profiles calculated from the trail position data for trail D at 76,106,166 and 226 seconds after launch.

TABLE 3.8

Correlation and rms error values between velocity profiles of trail D, smoothing with simple 1/4, 1/2, 1/4 weights. Results for the v component appear above the diagonal and for u below the diagonal

Times	76		106		166		226		
	Correlation Coeff.	rms error (m/sec)	Correlation Coeff.	rms error (m/sec)	Correlation Coeff.	rms error (m/sec)	Correlation Coeff.	rms error (m/sec)	No. of Smoothings
			0.80	4.22	0.84	3.80	0.74	4.60	0
76			0.83	3.60	0.87	3.18	0.79	3.89	1
			0.84	3.38	0.88	2.98	0.81	3.62	2
			0.85	3.17	0.89	2.79	0.83	3.30	4
	0.72	2.68			0.86	3.17	0.74	4.28	0
106	0.83	1.18			0.89	2.76	0.77	3.83	1
	0.87	1.60			0.89	2.62	0.78	3.62	2
	0.91	1.31			0.89	2.46	0.79	3.34	4
	0.74	2.61	0.92	1.47			0.67	4.22	0
166	0.85	1.81	0.95	1.15			0.73	3.59	1
	0.89	1.53	0.96	1.05			0.75	3.27	2
	0.93	1.25	0.96	0.96			0.78	2.87	4
	0.69	2.67	0.87	1.72	0.88	1.78			0
226	0.85	1.66	0.92	1.36	0.92	1.52			1
	0.90	1.30	0.94	1.23	0.94	1.42			2
	0.94	0.95	0.95	1.13	0.95	1.31			4

has little effect in increasing the correlation of the profiles while smoothing out the smaller vertical scales. This reasoning is applied to all three trails and the maximum correlation and minimum rms error are chosen in each case. The results are given in Table (3.9) for the case of two smoothings. The longest velocity profile of each pair is then chosen. The rms values give an estimate of the error for the chosen trail while the statistic $\frac{1-r}{r} \sim \frac{\sigma_e^2}{\sigma_u^2}$ approximates the ratio of error to real variance as in the case of the ROBIN data. The maximum possible error is considerably greater and the choice of profile by this method permits the minimization of this error. The errors are fairly large but not extreme considering the difficulties in the reduction mentioned above. The shape of the trails are well represented. The velocity profiles are given in Fig. (3.10).

TABLE 3.9

Maximum correlation and minimum rms error pairs after smoothing twice

TRAIL	TIMES	Velocity component	Correlation Coefficient	rms error (m/sec)	$\frac{\sigma_e^2}{\sigma_v^2}$
A	100,130	u	0.95	1.46	0.05
		v	0.95	1.50	0.05
C	370,400	u	0.91	1.81	0.10
		v	0.94	2.13	0.06
D	106,166	u	0.96	1.05	0.04
		v	0.89	2.62	0.12

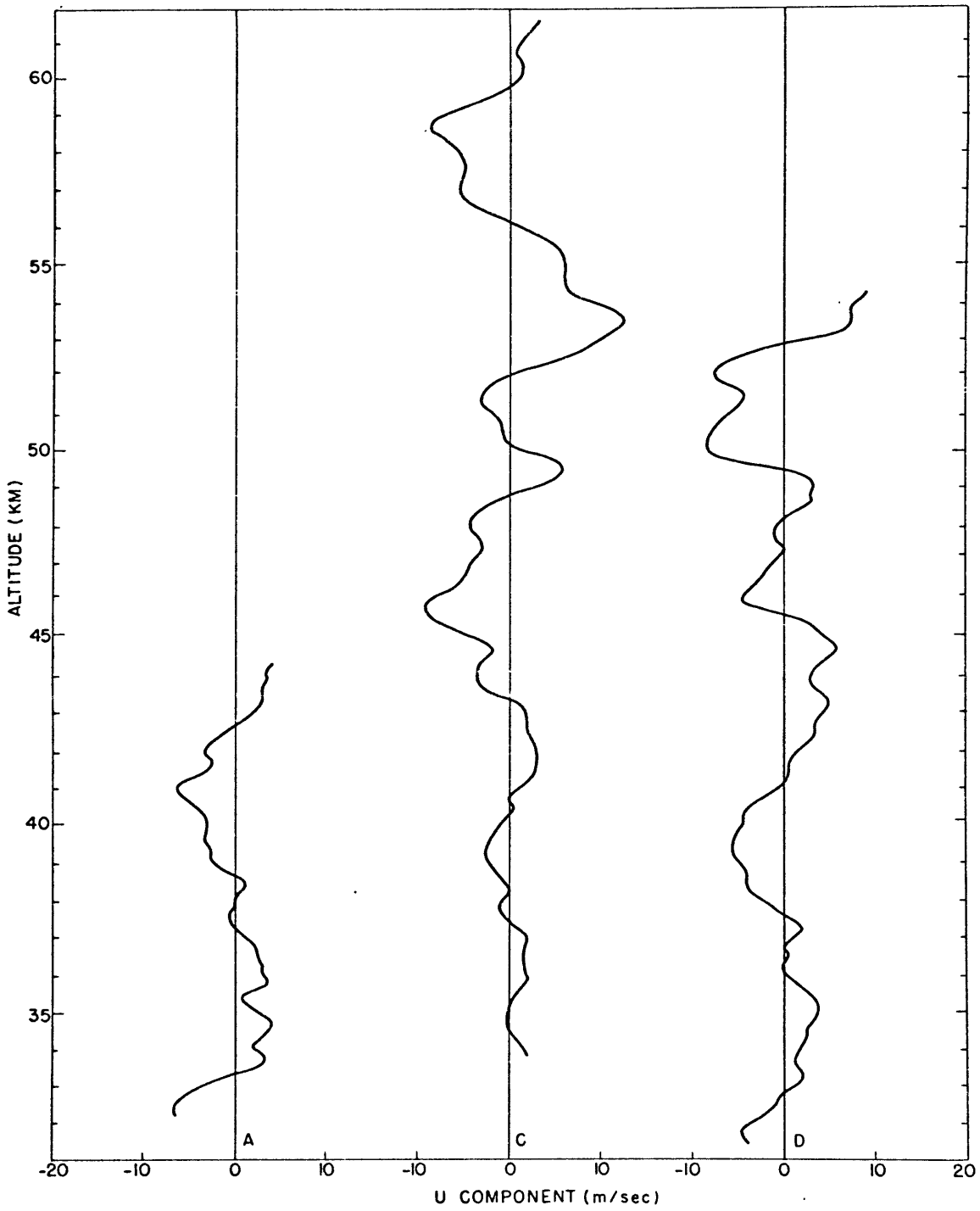

Figure 3,10a: Smoothed vertical profiles of the u component of velocity obtained from smoke trail position data.

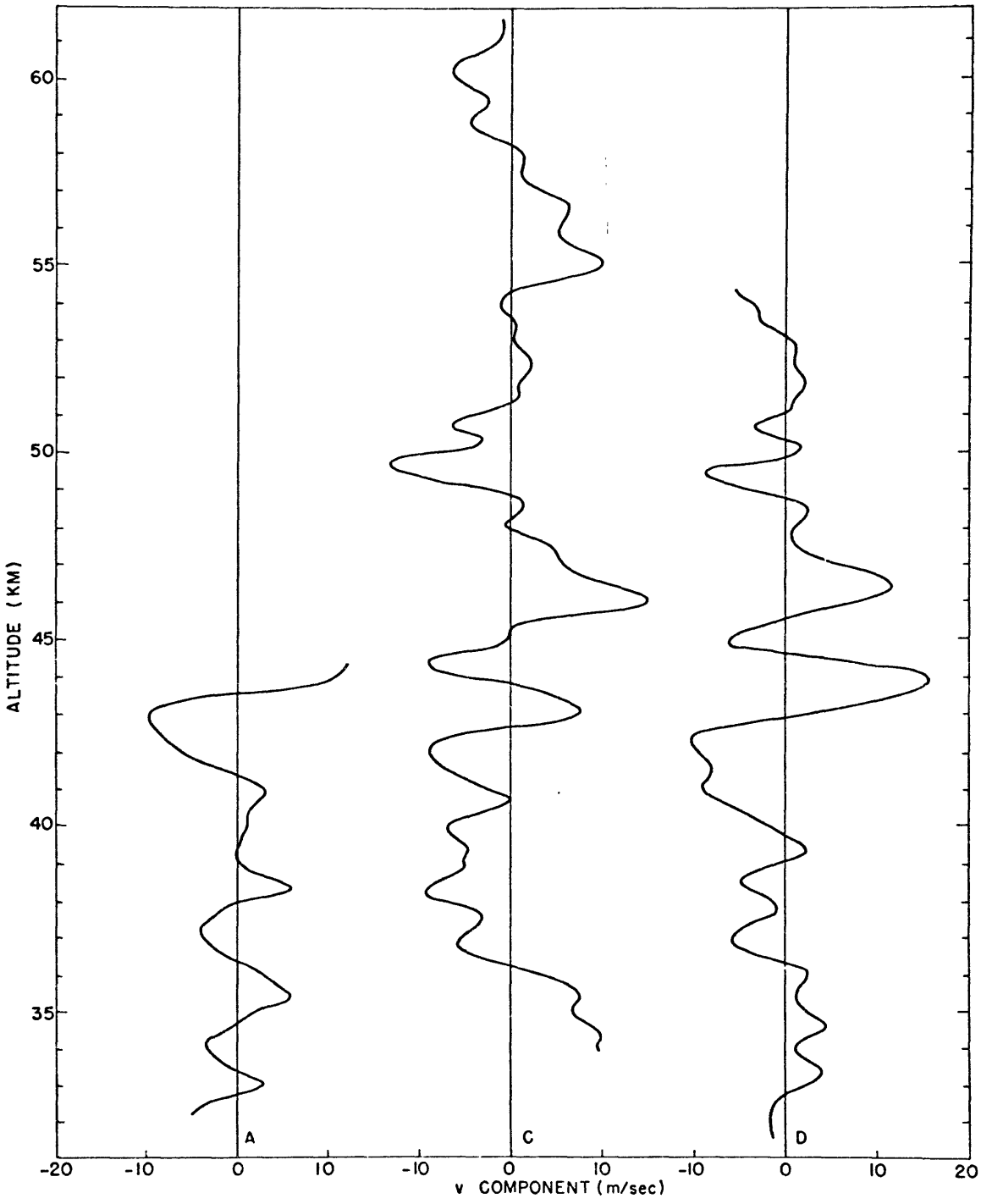

Figure 3.10b: Smoothed vertical profiles of the v component of velocity obtained from smoke trail position data.

3.2.4 Analysis of the velocity profiles

The velocity profiles are given in Fig. (3.10). The trails are, unfortunately, of three different lengths which makes comparison rather difficult. The general appearance of the profiles is believable, there is an obvious relation between the excursions of the various trails in a general sense, and the trails do exhibit a wave-like appearance.

The spectra of the velocity components for the three soundings are given in Fig. (3.11). The spectra differ somewhat from those obtained in the ROBIN experiment but in general possess a broad peak followed by a general decline with decreasing wavelength. The sharp decline in spectral density for wavelengths of less than a kilometer is due to the smoothing applied to the original data. The behavior of the spectra for the u component appears somewhat different from that of the v component with the u component comprising a broad peak with subsequent fall off with slope between -2 and -3 as previously. The v spectrum however maintains a much broader area at large wavelengths with power extending to smaller wavelengths before a sharp drop off of the spectrum is noted. Fig. (3.12) gives the graphs of the spectra where the ordinate is in a linear rather than a log scale. The spectra for the u component exhibit a broad peak in the region of 8-12 km without subsequent peaks of note. The spectra for the v component display somewhat different characteristics. The two longer trails are analysed with fundamental period of 25.6 km while the shorter trail has a fundamental period of one half this. The

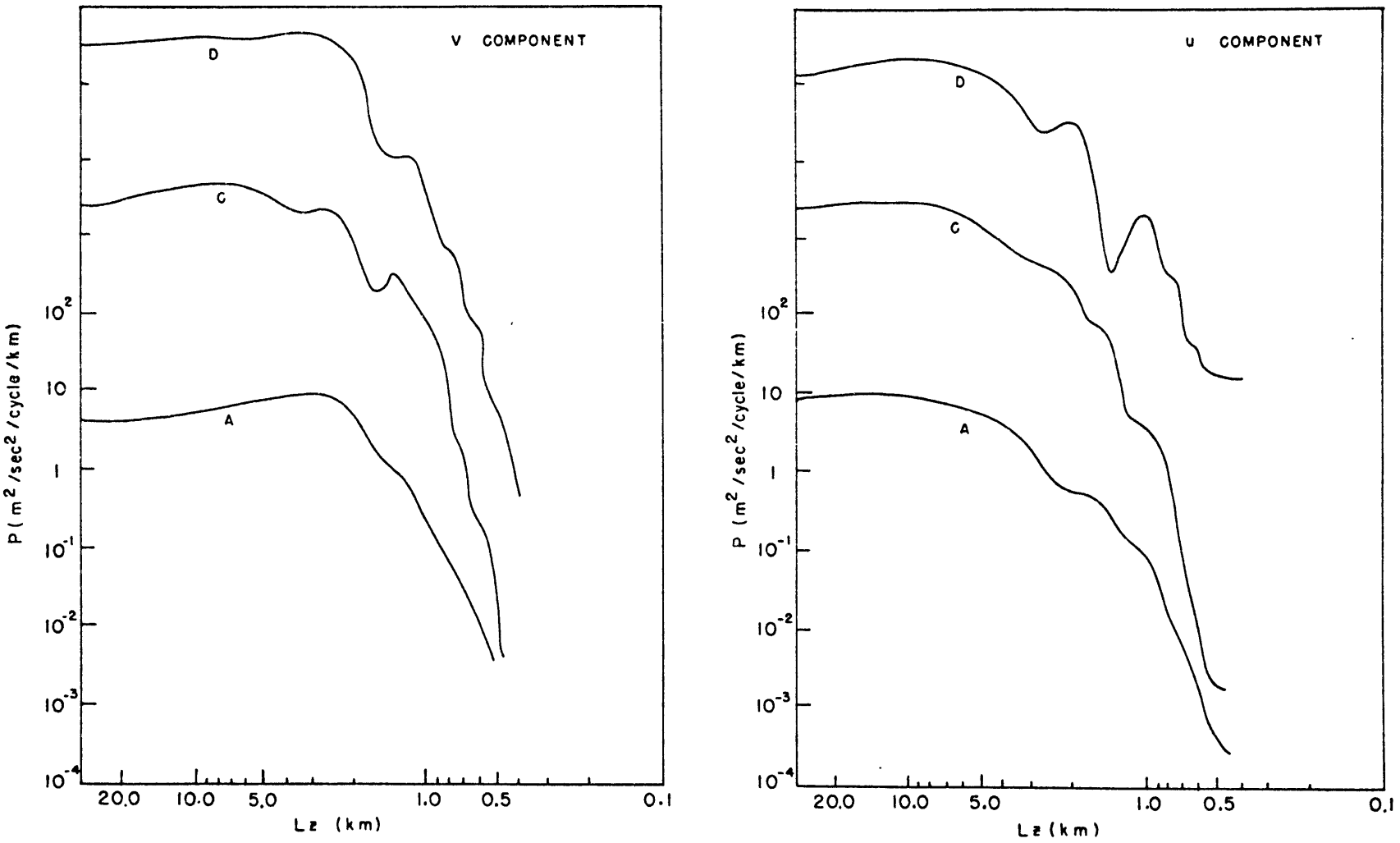

Figure 3.11: The spectra of the smoothed velocity profiles on a log-log scale. The graphs of the spectra are displaced two intervals in the vertical on the diagram.

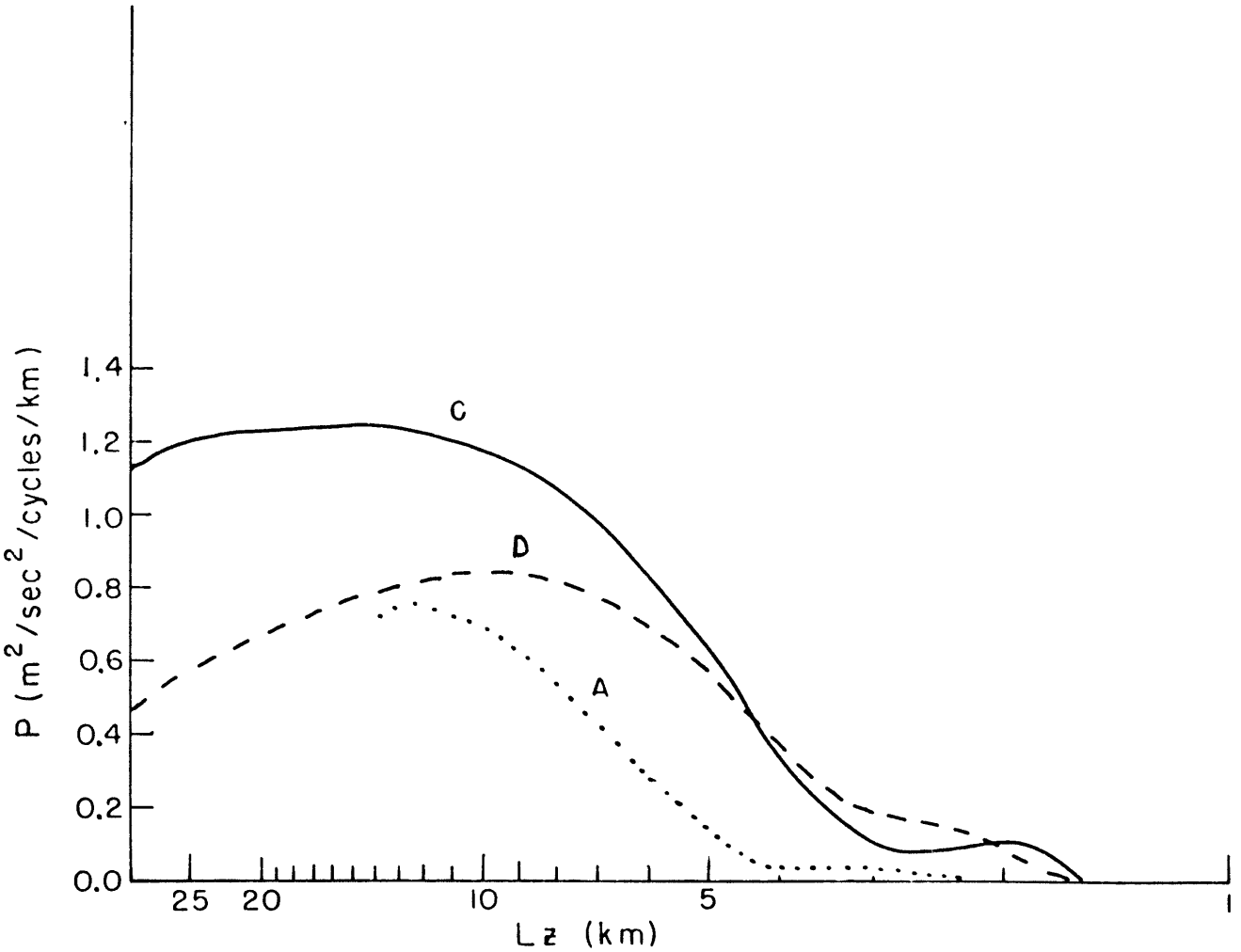

Figure 3.12a: The spectra of the smoothed velocity profiles for the u component. The ordinate is linear rather than logarithmic in this case.

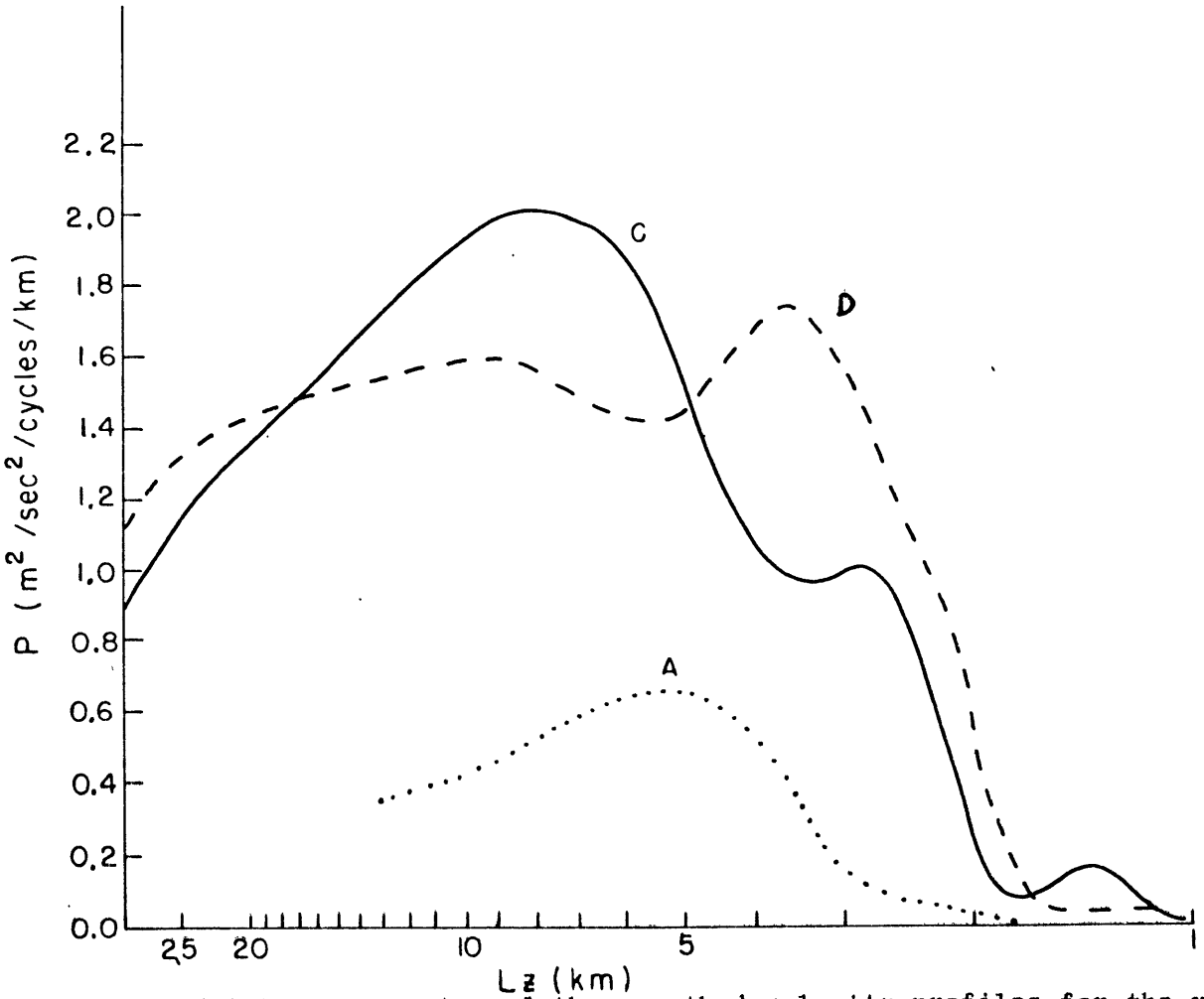

Figure 3.12b: The spectra of the smoothed velocity profiles for the v component. The ordinate is linear rather than logarithmic in this case.

longer trails exhibit a broad peak in the 8 km region with a further peak of some note in the region of 3-4 km. The spectrum for trail A however shows a quite different result.

The spectra for these trails have been calculated from relatively little data and this is particularly the case in trail A. The smaller variance and different shape for the v spectrum of trail A is due to the fact that it lacks the upper portion of the sounding which contains a large proportion of the variance of the sounding and further, the top of the trail occurs at a large excursion which will have an effect on the calculated spectrum. Trails C and D give spectra which do not suffer such difficulties. The results do not have the stability of those obtained by averaging over all ROBIN soundings.

Table (3.10) gives the correlation coefficients between that portion of the soundings common to all trails and the horizontal distances between trails. Again, the shortness of trail A makes comparison between trails less exact than would be expected if the upper portions, which possess a considerable proportion of the variance of the longer soundings, were included. There is very little data to provide a horizontal scale for the motions. A crude estimate may be made by assuming a simple plane wave which gives a decay of correlation with horizontal separation in the form of a cosine

$r \sim \cos(k\Delta x + l\Delta y)$ or $r \sim \cos\left(\frac{2\pi}{L}\Delta R\right)$ where L is the wavelength and ΔR the distance perpendicular to the phase lines. The wavelength may be determined geometrically by finding the value of L

TABLE 3.10

Correlation between trails separated in the horizontal

TRAIL	A	C	D	Horizontal separations (km)
A		-0.09	0.44	AD = 148
C	-0.07		0.46	AC = 86
D	0.53	0.34		CD = 72

Values above the diagonal apply to the v component and those below apply to the u component.

TABLE 3.11

Estimate of phase angle and horizontal wavelength from correlation results

Correlation pairs	Angle of phase lines with E-Waxis	Deduced horizontal wavelength (km)
AD, CD	160^{o}	105
AC, AD	163^{o}	76
CD, AC	161^{o}	124

and the orientation of the lines of constant phase which will give the observed decay of correlation between a given trail and the other two trails. This may be calculated three different ways using each of the three trails. The results are given in Table (3.11).

The orientation of the phase lines can also be estimated from the simple gravity wave theory which gives the relation between the square of the amplitudes and the wavenumbers as $|\hat{u}|^2/|\hat{v}|^2 \sim k^2/\ell^2$ whence for ψ the angle of the phase with the x axis $\tan\psi = k/\ell = |\hat{u}|/|\hat{v}|$. For the broad peak in the spectrum for longer vertical wavelengths trails C and D give respectively $\psi = 143^\circ, 144^\circ$. For the secondary peaks the phase orientation is $\psi = 157^\circ, 159^\circ$. The results for trail A are not consistent for the reasons given in the discussion of the spectra.

Considering the crude methods used, the results are in reasonable agreement.

3.2.5 Summary of results

i. The experiment demonstrates the feasibility of using the smoke trail method in the 30-60 km region. Previous use of this method has been confined mainly to higher altitudes and larger scales of motion, e.g. Zimmerman (1964), Kochanski (1964), Rosenberg and Edwards (1964).

ii. The reduction method using three or more camera sites to permit automatic data reduction of trail positions appears to have promise if it is possible to obtain sufficiently accurate film reading,

calibration data, and optimum camera placement.

iii. Despite the considerable effort of hand editing the data and the effect of the error remaining in the data, it is possible to calculate reasonably accurate velocity profiles by the method used here. The internal comparison of profiles allows the estimation of the error and permits the choice of a profile with the least error.

iv. The velocity profiles give a dominant vertical scale of 8-12 km with a secondary scale of motion in the 3-4 km region. The crude analysis of horizontal scale gives a wavelength of one to two hundred kilometers. The lines of constant phase are roughly in a NE-SW direction.

3.3 Comparison of methods and the problem of gravity wave measurement

The ROBIN and the smoke trail methods each have their advantages and disadvantages for measuring the motions in the 30-60 km region. The advantages of the ROBIN system are:

i. It is a relatively simple system in terms of rocket, payload, and radar system.

ii. The data are recorded automatically in a form suitable for computer reduction.

iii. The system can be used at any time of the day and in most weather conditions.

The disadvantages of the ROBIN system are:

i. The reduction of the radar data to wind velocities is difficult in terms of the dynamics of the balloon and the effect of the radar characteristics.

ii. The method in not capable, in general, of measuring vertical velocities.

iii. The collapse of the balloon may result in unknown lift forces coming into play.

The smoke trail method also has its compensating advantages and disadvantages.

The advantages are:

i. The smoke moves with the wind and no dynamical problems are involved.

ii. The possibility of observing vertical motions exists.

The disadvantages are:

i. The experiment is complicated in terms of the camera equipment and sites necessary.

ii. The primary photographic data must be read before numerical reduction can be effected and the reduction procedure is sensitive to the accuracy of film reading, and of site position.

iii. Adequate photographic conditions are obtained only at sunrise and sunset and in fine weather.

It is apparent that the measurement of gravity waves in the atmosphere is a difficult task. Not only is the possible behavior of the waves complex, as seen from previous results, the methods of measurement have characteristic difficulties. Basically, the measurement of gravity waves must be attacked in a much more comprehensive manner than has been done in the past. There must be an effort to identify and measure sources of waves in the atmosphere in order that the experiments may be designed to verify a predicted situation rather than to identify completely the existing motions. Such sources as the flow over surface features may be a possibility here. Furthermore the experiments must be designed to permit the measurement of vertical, horizontal, and time scales of the motions not just one or two of these. The statistics of gravity wave motions, if sufficient data is included to give stability, are themselves important in terms of such problems as energy transport as well as suggesting mechanisms of gravity wave production and transmission.

The ROBIN experiment was a step in the right direction in attempting to deduce the scales of motions of the waves. Better coverage in the horizontal and time would have been an asset. The smoke trail method provides a measurement system with a highly desirable sensor of atmospheric motions but it is greatly hampered by the photographic conditions required. The method is likely to be of use in conjunction with other measuring systems which allow a measure of the time scale of the motions.

4.0 Concluding remarks

Two topics relating to gravity wave motion in the atmosphere have been investigated. The theoretical aspect of the study concerned the critical level interaction. After a brief review of simple linear theory and some remarks on ray tracing in the atmosphere, a numerical model was devised for linear motions with a given periodicity in the horizontal. The model was of second order accuracy in truncation error and was stable for time-steps of 30-60 seconds. Calculations were performed to illustrate the time dependent behavior of wave motions at a critical level for a linear and time-dependent mean wind and for shear layers for which $Ri > 1/4$ and for which $Ri < 1/4$ (for which over-reflection occurred).

Some simple non-linear aspects of the waves were investigated. Unlike the internal gravity waves in the ocean, simple plane waves in the atmosphere do not satisfy the complete equations of motion nor do they satisfy a resonant interaction condition (except approximately for small vertical wavelengths). Interactions between waves at the second order of perturbation magnitude thus give rise to second order motions bounded in time.

The numerical model was extended to include the interaction of the wave and the mean flow. Calculations showed that the interaction of the wave and the mean flow could occur in regions well away from the initial critical level. A region of accelerated mean motion was induced which descended with time. The magnitude of u_{0z} increased

with time until the Richardson stability condition was violated. Irregular small scale variations in the vertical profile appeared suggesting the growth of unstable modes although the numerical model is not able to represent this process well. With the increase of U_{0z}, wave energy penetrated the critical level, was over-reflected, and unstable modes apparently grew. The source-sink role of the critical level is the most dramatic and important aspect of the results of the calculations.

Future investigations of this problem must concentrate on including adequate specification of the horizontal variation of the motions which will permit interaction between waves and the growth of unstable modes. An attempt to extend the calculation to many Fourier components proved to be extremely expensive in computer time.

The second topic which was investigated was the measurement of gravity wave motions in the 30-60 km region of the atmosphere. An experiment which was performed using the ROBIN sounding system was analysed. The data reduction technique, which was different than that usually used for this system, was analyzed. Double radar coverage permitted a more extensive investigation of the accuracy and resolution of the data than hitherto. The experiment was also one of the few which permitted an estimation of the horizontal, vertical and time scales of the motions. The deduced values of 450 km, 8.5 km, and 22 hours were in reasonable agreement with the relation predicted by simple linear theory.

A 'smoke trail' experiment for measuring small scale motions in the 30-60 km region was also analysed. This is the first time this

technique has been used at these heights. Despite difficulties with the data reduction procedure, it was possible to obtain wind profiles and to estimate the accuracy of measurement. Spectral analysis of the profiles showed a long vertical wavelength component of the motions at 8-10 km plus a shorter wavelength component at about 3 km. Horizontal scales were estimated as about 100 km.

The difficulty of measuring gravity waves in the atmosphere is great. The choice appears to be between identifying sources of wave motions and designing experiments to verify predicted conditions or of making a large number of measurements with good time and space resolution. The latter choice will be extremely expensive unless remote sensing techniques can be used and future observational work must lean toward the first choice.

The observation of a region in the atmosphere where critical level interaction is occurring would be of great interest. If sources of wave motions could be identified reasonably well it would be possible to determine the expected behavior of the waves as they propagate through the atmosphere using the numerical model (or preferably a more complicated model) and to make observations to verify the predicted results.

Appendix I: Neglect of rotation for gravity wave motions

The linearized equations for three-dimensional inviscid, adiabatic motions where rotation has been retained and where u_o, v_o, ϕ_{oz}, are constant are;

$$u_t + u_o u_x + v_o u_y - fv + \phi_x = 0$$
$$v_t + u_o v_x + v_o v_y + fu + \phi_y = 0$$
$$w_z - w + u_x + v_y = 0$$
$$\phi_{zt} + u_o \phi_{zx} + v_o \phi_{zy} + w S_o = 0$$

Introducing simple plane wave solutions

$$(u, w, \phi) = Re\,(\tilde{u}, \tilde{w}, \tilde{\phi})\, e^{z/2}\, e^{i(kx + ly + mz - \nu t)}$$

the equations may be written as

$$\begin{pmatrix} -i\sigma & -f & 0 & ik \\ f & -i\sigma & 0 & il \\ ik & il & im - 1/2 & 0 \\ 0 & 0 & S_o & -i\sigma(im + 1/2) \end{pmatrix} \begin{pmatrix} \hat{u} \\ \hat{v} \\ \hat{w} \\ \hat{\phi} \end{pmatrix} = 0$$

where $\sigma = \nu - ku_o - lv_o$

The frequency relation is

$$\sigma^2 = f^2 + \frac{(k^2 + l^2) S_o}{m^2 + 1/4} = f^2 + A^2$$

and the relation between $\hat{u}$ and $\hat{v}$ involves f as well.

The effect of rotation will depend on the relative importance of the terms f^2 and A^2. For $f^2/A^2 \ll 1$ the rotation will be unimportant. In terms of the horizontal and vertical wavelengths

$$A^2 = \frac{(k^2+l^2)S_0}{m^2+1/4} \propto \frac{L_z^2}{L_H^2}$$

The estimation of the horizontal wavelength from the decay of correlation between soundings involves an estimation of the orientation of the lines of constant phase. The maximum decay of correlation will occur for soundings which are separated by a line perpendicular to the lines of constant phase. The deduced wavelength along any other line, assumed to be perpendicular to the lines of constant phase, will be larger than the true value. The estimation of the horizontal wavelength in section (3.1.7) will be, at worst, an over estimation of L_H. Thus the value of A^2 obtained by inserting the estimated values of the wavelengths will, at worst, be smaller than the true value.

Thus if $f^2/A^2 \ll 1$, the rotation can be neglected and the relation between $\hat{u}$, $\hat{v}$ given by $|\hat{u}|^2/|\hat{v}|^2 = k^2/l^2$ which was used in section (3.1.7) will be appropriate.

Introducing the estimated values gives

$$A^2 \sim \frac{(2)(8.5)^2(4\times10^{-4})}{(4.5\times10^2)^2} \sim 2.9\times10^{-7}\ \text{sec}^{-2}$$

$$f^2 \sim (7.3\times10^{-5})^2 \sim 5.3\times10^{-9} \quad (\text{at } 30^\circ\text{N})$$

The $f/A \sim 0.13$ and the Coriolis term is an order of magnitude smaller

than the other terms and can be neglected. It is the intrinsic or doppler shifted frequency which must be compared with the Coriolis frequency to determine the importance of rotation, not the observed frequency.

Bibliography & References

Beyers, N.J., Miers, B.T. and Reed, R.J., 1966: Diurnal tidal motions near the stratopause during 48 hours at White Sands Missile Range, J. Atmos. Sci., 23, 325-333.

Boehmer, R.P., 1970: A three station method to acquire smoke trail position, Air Force Cambridge Research Laboratories, Report No. AFCRL-70-0262.

Boer, G.J. and Mahoney, R.R., 1968: Further results on the velocity structure in the 30-60 km region deduced from paired ROBIN soundings, Air Force Cambridge Research Laboratories Report No. AFCRL-68-0559.

Booker, J.R. and Bretherton, F.P., 1967: The critical layer for internal gravity waves in shear flow, J. Fluid Mech., 27, 513-539.

Breeding, R.J., 1970: A nonlinear investigation of singular levels for internal atmospheric gravity waves, Ph.D. Thesis, Department of Earth and Planetary Sciences, Massachusetts Institute of Technology.

Bretherton, F.P., 1966: The propagation of groups of internal gravity waves in shear flow, Quart. J. Roy. Meteor. Soc., 92, 466-480.

Bretherton, F.P. and Garrett, C.J.R., 1968: Wave trains in inhomogenous moving media, Proc. Roy. Soc., London A302(1471), 529-554.

Bretherton, F.P., 1969: On the mean motion induced by internal gravity waves, J. Fluid Mech., 36, 785-805.

Bretherton, F.P., 1969: Momentum transport by gravity waves, Quart. J. Roy. Meteor. Soc., 95, 213-243.

Chimonas, G., 1968: The launching of low frequency travelling disturbances by auroral currents, Proc. ESSA/ARPA acoustic-gravity wave symposium, T.M. Georges (ed.), U.S. Gov't Printing Office, p. 101-107.

Craig, R.A., 1965: The upper atmosphere, Academic Press, New York.

Craik, A.D., 1968: Resonant gravity-wave interactions in a shear flow. J. Fluid Mech., 34, 531-549.

Eckart, C., 1960: Hydrodynamics of oceans and atmospheres, Pergamon Press, New York.

Einaudi, F., 1968: Higher order approximation in the theory of acoustic-gravity waves, Proc. ESSA/ARPA acoustic-gravity wave symposium, T.M. Georges (ed.), U.S. Gov't Printing Office, p. 343-348.

Engler, N.A., 1965: Development of methods to determine winds, density, pressure, and temperature from the ROBIN falling balloon, AFCRL Report No. AF19(604)-7450.

Flock, W.L. and Hunsucker, F.D., 1968: The auroral zone as a source of travelling ionospheric disturbances, Proc. ESSA/ARPA acoustic-gravity wave symposium, T.M. Georges (ed.), U.S. Gov't Printing Office, p. 159-170.

Foldvik, A. and Wurtele, M.G., 1967: The computation of the transient gravity wave, Geophys., J.R. Astr. Soc., 13, 167-185.

Friedman, J.P., 1966: Propagation of internal gravity waves in a thermally stratified atmosphere, J. Geophys. Res., 71, 1033-1954.

Georges, T.M., 1967: Ionospheric effects of atmospheric waves, ESSA Tech. Rep. TER-57/ITSA-54, U.S. Gov't Printing Office.

Georges, T.M. (ed.), 1968: Acoustic-gravity waves in the atmosphere, Proc. ESSA/ARPA symposium, U.S. Gov't Printing Office.

Gossard, E.E., 1962: Vertical flux of energy into the lower ionosphere from internal gravity waves generated in the troposphere, J. Geophys. Res., 64, 2129-2133.

Graves, G.V. and Markarious, S.H., 1968: Diurnal S-N wind components below 60 km derived from rocket observations for various seasons and latitudes, Space Res. VIII, North-Holland, Amsterdam, p. 857-864.

Greenhow, J.S. and Neufeld, E.L., 1959: Measurements of turbulence in the 80 to 100 km region from radio echo observations of meteors, J. Geophys. Res., 64, 2129-2133.

Harkrider, D.G., 1964: Theoretical and observed acoustic-gravity waves from explosive sources in the atmosphere, J. Geophys. Res., 69, 5295-5321.

Hazel, P., 1967: The effect of viscosity and heat conduction on internal gravity waves at a critical level, J. Fluid Mech., 30, 775-783.

Hess, S.L., 1959: Introduction to theoretical meteorology, Holt and Co., New York.

Hines, C.O., 1960: Internal gravity waves at ionospheric heights, Can. J. Phys., 38, 1441-1487.

Hines, C.O., 1963: The upper atmosphere in motion, Quart. J. Roy. Meteor. Soc., 89, 1-42.

Hines, C.O., 1964: Minimum vertical scale in the wind structure above 100 km, J. Geophys. Res., 69, 2847-2848.

Hines, C.O., 1965: Dynamical heating of the upper atmosphere, J. Geophys. Res., 70, 177-183.

Hines, C.O. and Reddy, C.A., 1967: On the propagation of atmospheric gravity waves through regions of wind shear, J. Geophys. Res., 72. 1015-1034.

Hines, C.O., 1967: On the nature of travelling ionospheric disturbances launched by nuclear explosions, J. Geophys. Res., 72, 1877-1882.

Hines, C.O., 1968: A possible source of waves in noctilucent clouds, J. Atmos. Sci., 25, 937-942.

Hines, C.O., 1969: Second order perturbations; energy density and energy flux, NCAR Tech Note, NCAR-TN-43, 67-76.

Houghton, D.C. and Jones, W.L., Gravity wave propagation with a time dependent critical level, Proc. ESSA/ARPA acoustic-gravity wave symposium, T.M. Georges (ed.). U.S. Gov't Printing Office, p. 241-248.

Jones, W.L., 1969: Reflection and stability of waves in stably stratified fluids with shear flow: A numerical study, J. Fluid Mech., 34, 609-624.

Jones, W.L., 1969: Ray tracing for internal gravity waves, J. Geophys. Res., 74, 2028-2033.

Kochanski, A., 1964: Atmospheric motions from sodium cloud drifts, J. Geophys. Res., 69, 3651-3662.

Krishnamurti, T.N., 1964: Theory of two-dimensional mountain waves, Reviews of Geophysics, Vol. 2, No. 4, 593-624.

Lamb, H., 1945: Hydrodynamics, Dover, New York.

Lenhard, R.W., 1963: Variation of hourly winds at 35-65 km during one day at Eglin Air Force Base, Florida, J. Geophys. Res., 68, 227-235.

Lettau, B., 1966: Persistence of small-scale features in the mesospheric wind field, Air Force Cambridge Research Laboratories Report No. AFCRL-66-371.

Liller, B. and Whipple, F.L., 1954: High-altitude winds by meteor photography, Rocket Exploration of the Upper Atmosphere, R.L.F. Bayd and M.J. Seaton (eds.), Pergamon Press, London, 112-150.

Lindzen, R.S., 1968: Data necessary for the detection and description of tides and gravity waves in the upper atmosphere, J. Atmos. Terr. Phys., 31, 449-456.

Lindzen, R.S., 1968: Some speculations on the roles of critical level interactions between internal gravity waves and mean flows, Proc. ESSA/ARPA acoustic-gravity wave symposium, T.M. Georges (ed.), U.S. Gov't Printing Office, p. 231-240.

Lorenz, E.N., 1967: The nature and theory of the general circulation of the atmosphere, World Meteorological Organization, Geneva.

Luers, J. and Engler, N., 1967: On optimum methods for obtaining wind data from balloon sensors, J. Appl. Meteor., 6(5), 816-834.

Madden, T.R. and Claerbout, J.F., 1968: Jet stream associated gravity waves and implications concerning associated jet stream stability, Proc. ESSA/ARPA acoustic-gravity wave symposium, T.M. Georges (ed.), U.S., Gov't Printing Office, p. 121-134.

Mahoney, J.R. and Boer, G.J., 1967: Small scale velocity structure in the 30-60 km region deduced from paired ROBIN soundings, Air Force Cambridge Research Laboratories Report No. ARCRL-67-0263.

Martyn, D.F., 1950: Cellular atmospheric waves in the ionosphere and troposphere, Proc. Roy. Soc. London, Ser. A., 201, 216-233.

Midgley, J.E. and Liemohn, H.B., 1966: Gravity waves in a realistic atmosphere, J. Geophys. Res., 71, 3729-3748.

Morse, P.M. and Feshback, H., 1953: Methods of theoretical physics, McGraw Hill Book Co., New York.

Munro, G.H., 1950: Travelling disturbances in the ionosphere, Proc. Roy. Soc. London, Ser. A., 202, 216-234.

Pierce, A.D., 1963: Propagation of acoustic-gravity waves from a small source above the ground in an isothermal atmosphere, J. Acoust. Soc. Am., 35, 1798-1807.

Pierce, A.D., 1965: Propagation of acoustic-gravity waves in a temperature and wind stratified atmosphere, J. Acoust. Soc. Am., 37, 218-227.

Pitteway, M.L.V. and Hines, C.O., 1963: The viscous damping of atmospheric gravity waves, Can. J. Phys., 41, 1935-1948.

Pitteway, M.L.V. and Hines, C.O., 1965: The reflection and ducting of atmospheric acoustic-gravity waves, Can. J. Phys., 43, 2222-2243.

Phillips, N.A., 1963: Geostrophic Motion, Reviews of Geophysics, 123-176.

Phillips, O.M., 1966: The dynamics of the upper ocean, Cambridge Univ. Press, Cambridge.

Press, F. and Harkrider, D., 1962: Propagation of acoustic-gravity waves in the atmosphere, J. Geophys. Res., 67, 3889-3908.

Queney, P., Corbey, A., Gerbier, N., Koschmieder, A. and Zierep, J., 1960: The airflow over mountains, Tech. Rep., 34, W.M.O., Geneva.

Reed, R.J., McKenzie, D.J. and Vyverberg, J.C., 1966: Further evidence of enhanced diurnal tidal motions near the stratopause, J. Atmos. Sci., 23, 247-251.

Reed, R.J., McKenzie, D.J., and Vyverberg, J.C., 1966: Diurnal tidal motions between 30- and 60 km in summer, J. Atmos. Sci., 23, 416-423.

Revah, I., 1969: Etude des vents de petite échelle observés au moyen des trainées météoriques, Ann. Geophys., 25, 1-45.

Richtmyer, R.D. and Morton, K.W., 1967: Difference methods for initial-value problems, second ed., Interscience, New York.

Rosenberg, N.W. and Edwards, H.D., 1964: Observations of ionospheric wind patterns through the night, J. Geophys. Res. 69, 2819-2826.

Row, R.V., 1967: Acoustic-gravity waves in the upper atmosphere due to a nuclear detonation and an earthquake, J. Geophys. Res., 72, 1599-1610.

Spizzichino, A., 1969: Generation of gravity waves in the higher atmosphere by non-linear effects, Department 'Recherches Spatiales' radioelectriques', Tech Note EST/RST/45.

Thorpe, A., 1966: On wave interaction in a stratified fluid, J. Fluid Mech., 24, 737-748.

Witt, G., 1962: Height structure and displacements of noctilucent clouds, Tellus, 14, 1-18.

Wickersham, A.F., 1968: The diurnal source and nature of gravity waves ducted in the lower thermosphere, Proc. ESSA/ARPA acoustic-gravity wave symposium, T.M. Georges (ed.), U.S. Gov't Printing Office, p. 325-336.

Yanowitch, M., 1967: Effect of viscosity on gravity waves and the upper boundary condition, J. Fluid Mech., 29(2), 209-231.

Zimmerman, S.P., 1964: Small-scale wind structure above 100 km, J. Geophys. Res., 69, 784-785.

Biographical Note

George J. Boer was born in Edmonton, Alberta on October 12, 1941. He received a B.Sc. from the University of British Columbia in 1963 and an M.A. degree from the University of Toronto in 1965. He then worked as a forecaster for the Meteorological Branch of the Canadian Department of Transport in Montreal, P.Q. until awarded a research assistantship at M.I.T. He is married to the former Barbara Jean Macintosh of Halifax, N.S.